Analysis of subcarrier multiplexing signals in optical fibre communication

Cheng, Linghao

2006

Cheng, L. (2006). Analysis of subcarrier multiplexing signals in optical fibre communication. Doctoral thesis, Nanyang Technological University, Singapore.

https://hdl.handle.net/10356/3582

https://doi.org/10.32657/10356/3582

Nanyang Technological University

Analysis of Subcarrier Multiplexing Signals in Optical Fibre Communication

Cheng Linghao

School of Electrical and Electronic Engineering

A thesis submitted to the Nanyang Technological University
in fulfilment of the requirement for the degree of
Doctor of Philosophy

2006

Acknowledgement

I would like to express my deepest gratitude to my supervisor, Associate Professor Sheel Aditya, for his invaluable guidance and unwavering support throughout my study at the Nanyang Technological University. Without his encouragement and patience, this work could not have been completed.

I also wish to express my most sincere appreciation to Mr. Li Zhaohui, Mr. Ning Guoxiang and Mr. Liu Ning for their valuable discussions, suggestions and help in the experiments. Their insight, expertise and wealth of knowledge are invaluable for me. I would like to thank my roommates, Mr. Ma Tingquan, Mr. Huang Mingda and Mr. Shao Yu for their consistent support from the very beginning.

My gratitude also goes to other members in Infocomm Institute for Research and in Positioning and Wireless Technology Center. In particular, I would like to thank Dr. Lu Chao, Dr. Wang Yixing, Mr. Zhang Zhen, Mr. Liang Bin, Ms. Chai Ooy Mei and Mr. Ng Teng Kwee for their friendly help and support.

Last but not least, I would like to express my appreciation to those who have helped me during this period directly or indirectly. I wish to extend my

utmost gratitude to my family and friends for their consistent understanding and encouragement.

Summary

The increasing demand of bandwidth in the recent years has made broadband access networks more and more important. Because of its potential advantages in realizing low cost broadband access networks, subcarrier multiplexing (SCM) with the help of lightwave techniques continues to be an area of active research. However, in such systems, nonlinear distortions are also introduced by the lightwave components and fibre. This thesis aims to provide a comprehensive analysis of the nonlinear distortion in SCM optical communication systems. After the basic introduction to subcarrier multiplexed optical communication systems, the three most significant types of nonlinear distortions are analyzed:

- Nonlinear distortion due to dual-drive Mach-Zehnder modulator (DD-MZM);
- Nonlinear distortion due to stimulated inelastic scattering, including stimulated Brillouin scattering (SBS) and stimulated Raman scattering (SRS);
- Nonlinear distortion due to nonlinear refraction of fibres, including self-phase modulation (SPM) and cross-phase modulation (XPM).

For each type of nonlinear distortion, an analytical model is presented and verified by numerical simulations and experiments. These analytical models result in many new closed-form expressions. Therefore, the analytical models enable one to get a better physical insight into the nonlinear distortion phenomena and help one to evaluate the impact of these distortions quickly. Hence, these analytical models can facilitate the task of system design greatly. The thesis concludes by mentioning the major conclusions and achievements of the work presented here and the proposed future work.

Contents

List of Figures

List of Tables

List of Acronyms and Symbols

Abbreviations	**Full Expressions**
CATV	Cable Television
CSO	Composite Second-Order
CTB	Composite Triple-Order
CW	Continuous Wave
DD-MZM	Dual-Drive Mach Zehnder Modulator
EDFA	Erbium Doped Fibre Amplifier
FWM	Four-Wave Mixing
GVD	Group-Velocity Dispersion
HFC	Hybrid Fibre Coax
IIP3	The Input Third-order Intercept Point
IM/DD	Intensity Modulation/Direct Detection
IMP	Intermodulation Products
LAN	Local Area Network
LD	Laser Diode
LO	Local Oscillator
EAM	Electro-Absorption Modulator
IMP	Intermodulation Products
NIMP	IMP through Fibre Nonlinearity
NLSE	Nonlinear Schrödinger Equation

ODSB	Optical Double Side Band
OIP3	The Output Third-order Intercept Point
OSSB	Optical Single Side Band
OTDM	Optical Time Division Multiplexing
RIN	Relative Intensity Noise
RoF	Radio-over-Fibre
SBS	Stimulated Brillouin Scattering
SCM	Sub-Carrier Multiplexing
SFDR	Spur-Free Dynamic Range
SNR	Signal-to-Noise Ratio
SPM	Self-Phase Modulation
SRS	Stimulated Raman Scattering
SSF	Split-Step Fourier
WDM	Wavelength Division Multiplexing
XPM	Cross-Phase Modulation

Mathematical Symbols

g	standard Raman gain coefficient divided by the fibre effective area
j	imaginary unit
m	modulation index
n_2	the nonlinear index coefficient of a fibre
t	the physical time
v_g	the group velocity at the central wavelength
z	the fibre coordinate and the direction of propagation
A	the slowly varying envelope of the electric field

$\tilde{A}$	the Fourier transform of A
A_{eff}	the effective core area of fibre
D	the fibre dispersion parameter
P	the intensity of the electric field
$\tilde{P}$	the Fourier transform of P
T	the reference time of a frame moving with the pulse at v_g
α	the fibre loss coefficient
β_2	the second order propagation constant
γ	the fibre nonlinear coefficient
δ	Dirac's delta function
λ	the optical wavelength
ω	angular frequency

Chapter 1

Introduction

Over the past 30 years, the enormous progress realized in optical fibre communication field has been leading us to a world of broadband network. Nowadays, the bit rate-distance product of modern optical fibre communication systems can exceed by a factor of 10^7 compared with the first-generation optical fibre communication systems, reaching about $10^7\,\text{Gbps} \cdot \text{km}$. Therefore optical fibre communication systems have been deployed worldwide over years for long-haul communications [1].

The great success of optical fibre communication systems for long-haul communications comes from the extremely low loss and large bandwidth of fibre. The low attenuation windows of fibre at $1.3\,\mu m$ and $1.55\,\mu m$ have bandwidths of about 30,000 GHz. In contrast to the huge capacity of fibre-optic systems, in electronic systems even with carrier frequencies of many gigahertz (GHz), bandwidths are limited to a few GHz at most. This mismatch between the bandwidth of fibre-optic systems and electronic systems results in two major issues. The first one is the well known "electronic bottleneck": how can the optical bandwidth be exploited when the bandwidth of electronics driving the optical devices is so limited? The other one is how

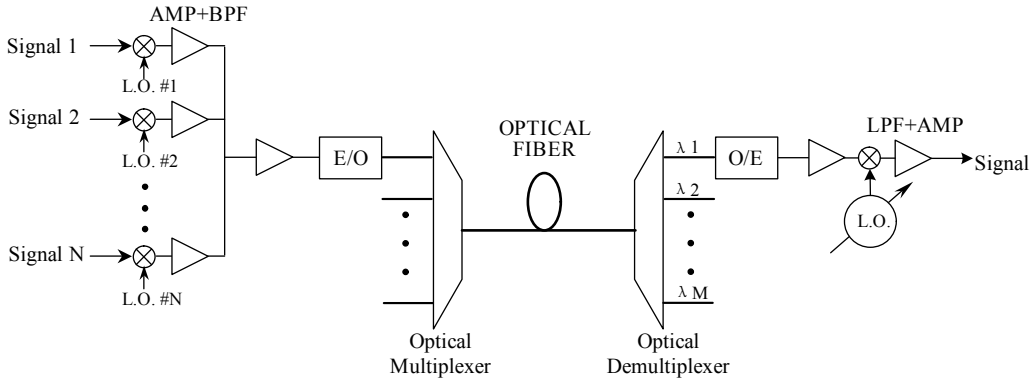

Figure 1.1: Subcarrier multiplexing system configuration with wavelength division multiplexing technique. AMP: Amplifier; BPF: Bandpass filter; LPF: Low pass filter; L.O.: Local oscillator; E/O: Electronic-to-optical conversion; O/E: Optical-to-electronic conversion.

to group a number of various types of low data-rate traffics in electronic systems to form a high data-rate traffic for transmission in fibre-optic systems. These two issues are especially prominent when one wants to interface the fibre-optic systems with electronic systems to realize a broadband access network because traditionally the access network is dominated by electronic systems and provides different services over a distribution network [2, 3].

Many approaches to solve these problems have been suggested, including optical time division multiplexing (OTDM) and wavelength division multiplexing (WDM). In this dissertation, we will consider a simple, cost-effective and promising alternative approach known as subcarrier multiplexing (SCM) [2–12].

1.1 Subcarrier Multiplexing (SCM)

The principle of SCM is reasonably straightforward and it is an easy technique to employ in practice. As shown in Figure 1.1, a number of base-band

analogue and/or digital signals are first modulated onto different radio frequencies by using local oscillators (LO), which are the so-called sub-carriers, in contrast to the optical carrier frequencies. The up-converted signals are then combined to drive a high-speed light source, typically a laser diode (LD), and then transmitted over fibres. The modulation of optical carriers can be achieved by direct modulation of LDs or by using external modulators. In both cases, typically, current limits to modulation rates are less than 20 GHz. To exploit the bandwidth of fibre more fully, it is necessary to combine SCM with other more broadband methods of dividing the optical spectrum such as WDM. Therefore, several optical channels centred at different wavelengths with SCM signals can be multiplexed together optically and transmitted in the same fibre. At the receiver site, after optical demultiplexing and converting the optical signals to electrical signals, a user can receive any one of the sub-carrier channels by tuning a local oscillator and down-convert the RF or microwave signals to base-band or IF frequencies, similar to the way we tune in radio or TV channels.

1.2 Applications of SCM

SCM is a very good interface between fibre-optic systems and electronic systems. Therefore, it can be used for a very wide range of applications. Its potential application areas include: microwave and millimetre-wave signal distribution for antenna remoting or fibre radio applications; replacement of coaxial cable systems for cable TV (CATV); telephony; data transmission and local area networks (LANs). It is also used for chromatic dispersion monitoring in long-haul optical digital communication systems. In this section, we introduce 3 typical systems using SCM: hybrid fibre coax (HFC) CATV

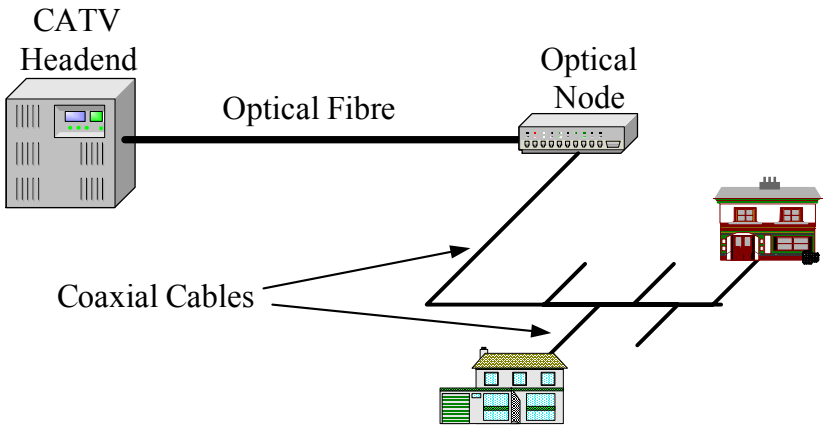

Figure 1.2: A HFC CATV network.

system, radio-over-fibre (RoF) system and microwave/millimetre wave fibre-optic system.

1.2.1 HFC CATV System

Optical fibre links were widely deployed from the late 1980s to work as fibre trunk lines in coaxial cable-based CATV networks. Nowadays, almost all CATV services over the world are carried by such HFC CATV networks. A typical HFC CATV network is shown in Figure 1.2, which consists of a fibre trunk and a coaxial distribution network. Traditionally, CATV networks provide the multichannel services over a wide spectrum, typically spanning about 1 GHz. For example, in North America, the networks provide amplitude modulated-vestigial sideband (AM-VSB) modulation over the frequency range from 50 to 88 MHz and from 120 to 550 MHz, whilst the band from 88 to 120 MHz is reserved for frequency modulated (FM) radio broadcast. Each AM-VSB channel occupies a bandwidth of 6 MHz and the networks can provide about 80 channels simultaneously. Currently, HFC CATV networks are required to provide digital services and the band between 550 MHz and 1 GHz is utilized for these services. Because so many

channels are multiplexed, the modulation index of each subcarrier during the translation to optical frequency domain is very small, typically only 4%. Besides, due to the wide spectrum width of CATV systems, the 2nd order intermodulation products (IMPs) ($f_i \pm f_j$) can also fall in this spectrum range. Therefore, both the 2nd order IMPs and the 3rd order IMPs ($f_i \pm f_j \pm f_k$) are important nonlinear distortions in CATV systems [2, 13].

In summary, the characteristics of HFC CATV networks are:

- A large number of subcarriers;
- Subcarrier frequencies are typically less than 1 GHz;
- Very small modulation index for each subcarrier;
- Both the 2nd and the 3rd order IMPs are important nonlinear distortions. These IMPs may result from modulation, fibre nonlinearity, etc.;
- Fibre dispersion also leads to IMPs and some other nonlinear distortions.

1.2.2 RoF System

RoF systems were first developed in the early 1980s in the Unites States for military applications to place the radar emitters (dish) far from the control electronics and personnel due to the development of radar-seeking missiles (antiradiation missiles). More recently, with the quick development and wide deployment of mobile communication systems, RoF technology has received more and more attention in solving problems for these systems. The next generation of mobile communications systems will make extensive use of microcells. This will permit a large increase in the numbers of users and will

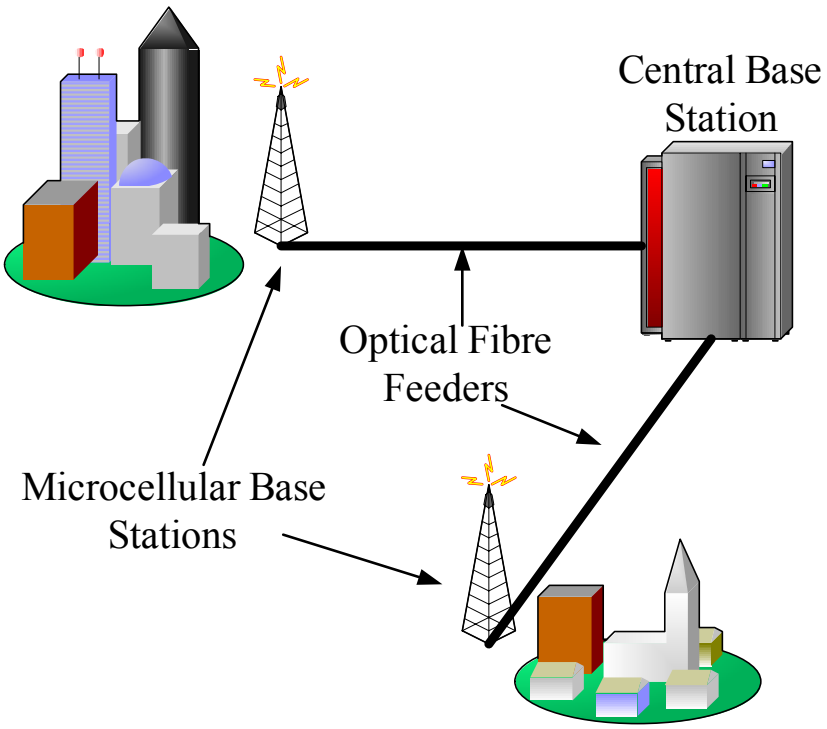

Figure 1.3: A radio-over-fibre network.

also allow a significant increase in the available channel bandwidth, so that broadband services can be offered, in addition to the voiceband services offered with current systems. The introduction of large numbers of microcells will result in the need to interconnect huge numbers of cells and microcells, and this can be carried out effectively using optical fibre, which offers a high transmission capacity at low cost. As shown in Figure 1.3, the transmission of radio signals over fibre, with simple optical-to-electrical conversion, followed by radiation at remote antennas, which are connected to a central station, has been proposed as a method of minimizing costs.

Depending on the application of mobile communication systems, the subcarrier frequency in RoF systems is typically above 1 GHz. Table 1.1 shows the frequency bands used or proposed for some services. Different from HFC CATV systems, the occupied bandwidth of subcarriers in RoF systems

Services	Frequency Allocation
Mobile Phone	1.8 or 1.9 GHz
Wireless LAN	2.4 or 5.1 GHz
MVDDS and DBS	12.2 $\sim$ 12.7 GHz
W-ATM	5.2 or 17 GHz
W-B-ISDN	19 GHz
LMDS	27.5 $\sim$ 31.3 GHz
MBS	40 GHz
HS-WLAN	60 GH

Table 1.1: Proposed frequency allocations for some services. MVDDS: Multichannel Video Distribution and Data Service; DBS: Direct Broadcast Satellite; W-ATM: Wireless Asynchronous Transfer Mode; W-B-ISDN: Wireless Broadband Integrated Services Digital Network; LMDS: Local Multipoint Distribution System; MBS: Mobile Broadband Services; HS-WLAN: High-Speed Wireless LAN.

is very small, typically at the level of tens of MHz. Therefore, the dominant nonlinear distortion in RoF is the 3rd order IMPs [6, 14, 15].

In summary, the characteristics of RoF systems are:

- A central station supports a large number of remote antenna sites;
- Subcarrier frequencies are typically above 1 GHz;
- Fibre dispersion may lead to RF power fading.
- The 3rd order IMPs are the dominant nonlinear distortions.

1.2.3 Microwave/Millimetre Wave Fibre-Optic System

The idea of RoF systems can be extended to microwave and millimetre wave bands. The primary reason to use these bands is to meet the increasing demand to provide broadband data services such as image-based services. Due to the congestion of conventional frequency bands, many microwave

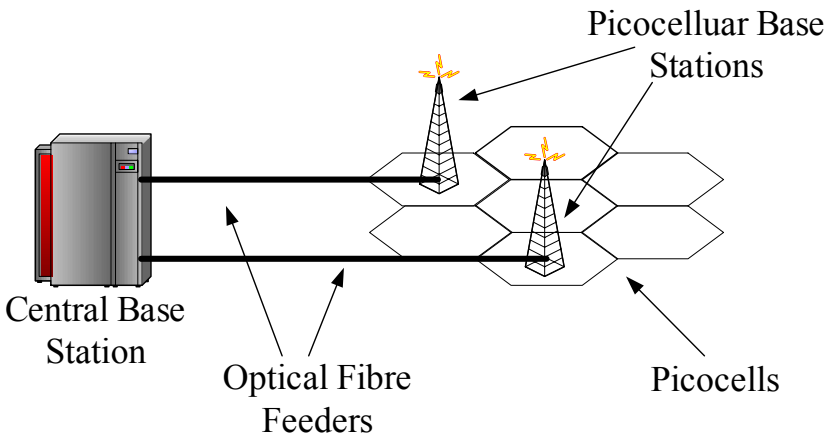

Figure 1.4: A microwave/millimetre wave fibre-optic system.

and millimetre wave bands are proposed to be used for these new services, such as those in Table 1.1. Moreover, the limited propagation distances achievable at these bands also offer the advantage of efficient frequency reuse by the adoption of a pico-cellular-based architecture as shown in Figure 1.4, which reduces the total bandwidth required to obtain a given coverage. However, due to the serious bandwidth limits of electronics in these bands, the system architectures are quite different from those of RoF. The direct modulation of the laser bias level is seldom used in these systems due to the limited modulation bandwidth of lasers. External modulators, such as dual-drive Mach-Zehnder modulators (DD-MZM) and electroabsorption modulators (EAM), are widely used because of their much wider modulation bandwidth. The remote generation of microwave and millimetre wave signals is also widely used in these systems. This can be achieved through harmonic generation, electrooptical upconversion and heterodyning two correlated laser sources [16–20].

In summary, the characteristics of microwave and millimetre wave fibre-optic systems are:

- A central station supports a large number of remote antenna sites;
- Subcarrier frequency is typically above 10 GHz;
- Effect of fibre dispersion can be quite strong;
- The 3rd order IMPs are the dominant nonlinear distortions.

1.3 Advantages of SCM

SCM systems need not carry out complex digital processing when converting RF signals to optical signals and vice versa. Also, many of the components required for SCM systems are readily available. Modulators, mixers and amplifiers employed in traditional access networks can be used allowing a realistic low-cost solution to the problem of exploiting optical bandwidth. In the context of RoF systems, the reduction in cost is brought about in two ways. First, the remote antenna or radio distribution point needs to perform only simple functions, and it is small in size and low in cost. Second, the resources provided by the central stations can be shared among many antenna sites. In addition to the advantages of potential low cost, SCM has the further benefit that transferring the RF frequency allocation to a central station can allow flexible network channel allocation and rapid response to variations in traffic demand. Moreover, it has the advantage that it is very easy to mix different types of traffic on the same fibre by allocating different subcarriers to different types of traffic, providing several different services at the same time.

1.4 Noise and Distortion in SCM Systems

In SCM systems, the effects of noise and distortion are somewhat different from those in digital transmission systems where the pulses can be regenerated with a slight increase in bit error rate (BER). For SCM systems, the signals can be amplified but are not regenerated and therefore any noise or distortion added to the signal as it passes through the system appears at the output of the receiver. It is therefore very important to characterize the noise and distortion in SCM systems. The noise and distortion can come from the optoelectronic devices as well as the optical fibre links. As the noise and distortion due to the optoelectronic devices such as laser diode and photodetector have been extensively studied earlier [21–25], in this thesis we focus on noise and distortion due to external modulators and optical fibre links.

1.4.1 Noise

There are many sources of noise in an optical communication system. The optical source will usually introduce some unwanted intensity variations, caused by effects such as mode instability or spontaneous emission noise. These intensity noises are usually collected together in the term relative intensity noise (RIN) defined as the ratio of the mean square of the intensity fluctuations to the square of the mean of the intensity. It varies with frequency and for semiconductor laser diodes tends to peak near the relaxation oscillation frequency Ω_R but decreases rapidly for frequency greater than Ω_R since the laser is not able to respond to fluctuations at such high frequencies. At a given frequency, RIN decreases with an increase in the laser power as P^{-3} at low powers, but this behaviour changes to P^{-1} dependence at high powers. At power levels above a few milliwatts, the SNR, which is defined as

$\bar{P}/\sigma_p$, where $\bar{P}$ is the average optical power and σ_p is the root-mean-square (RMS) noise, exceeds 20 dB and improves linearly with the power. However, at high powers, the nonlinear gain parameter of laser plays a crucial role and leads to a saturated SNR value of about 30 dB.

The optical fibre channel is not considered to add noise to the signal but rather to degrade the signal through attenuation, dispersion and the introduction of distortion through nonlinearities. Further, the optical amplifiers used in many optical links increase the signal level but also degrade the SNR by at least 3 dB. There are several types of optical amplifiers such as Erbium-doped fibre amplifiers (EDFA), semiconductor optical amplifiers (SOA), fibre Raman amplifiers (FRA) and fibre parametric amplifiers (FPA) [26]. EDFA is the most popular amplification scheme in current optical fibre links due to its maturity and moderate cost compared to other amplification schemes. However, the noise figure of EDFA is not the best. FRA provides an amplification scheme with very low noise figure but its cost currently is quite high. SOA is a very promising scheme for integration in one chip but currently it is still noisy. FPA is still a developing technique and has attracted considerable attention in recent years. The noise due to optical amplifiers has significant impact on the performance of a system. Therefore, many efforts have been made to optimize the placement of optical amplifiers. Besides the noise due to optical amplifiers, optical fibre channel can change the distribution of noise through some nonlinearities such as those due to external modulators, self-phase modulation, cross-phase modulation, stimulated Raman scattering and parametric gain [27–34].

At the receiver the usual noise sources, including shot (quantum) noise,

photodiode dark current noise and thermal noise from the load resistor and from the voltage amplifier. In SCM systems, the optical power levels incident on the receiver photodiode are often quite high with a result that the receiver can be operating in the shot-noise-limited domain. Therefore, the emphasis tends to be on minimising the transmitter noise contribution, i.e. the RIN.

1.4.2 Distortion

The distortions in SCM systems are caused by dispersion and nonlinearities. These can be due to the laser intensity-current characteristic for direct laser bias modulation or as a result of the nonlinear transfer function of external modulator, such as the cosine transfer function of MZM. Optical fibre can also lead to nonlinear distortion due to fibre dispersion and nonlinearity. The dominant effects due to fibre nonlinearity are self-phase modulation (SPM), cross-phase modulation (XPM), stimulated Brillouin scattering (SBS) and stimulated Raman scattering (SRS). These effects are introduced in Chapter 2. Here we confine our discussion to the parameters used to quantify distortion in SCM systems.

Basically, a nonlinear transfer function can be expanded as a polynomial according to Taylor expansion and represented by the equation below:

$$V_0 = a\,V_1 + b\,V_1^2 + c\,V_1^3 + \cdots \tag{1.1}$$

where V_1 is the input signal and V_0 is the output signal. If the input is a signal at frequency f_1, then the higher order terms in Eq. (1.1) will generate harmonics at $2f_1$, $3f_1$, etc. The harmonics may fall in-band and cause distortion. If the signal contains more than one frequency, for example two

frequencies at f_1 and f_2, then mixed frequency components will occur at $f_1 + f_2$, $f_1 - f_2$, $2f_1 + f_2$, $2f_1 - f_2$ and so on. In SCM systems, some of these components will fall in-band and cause unwanted interference. The term $2f_1 - f_2$ (and $2f_2 - f_1$) commonly occurs and gives rise to the 3rd order intermodulation distortion (IMP3).

System distortion performance and limits are usually set by collecting all of the appropriate distortion components together into two agreed terms. The composite second order (CSO) and composite triple beat (CTB) levels are the ratios of the sums of the in-band second order components to carrier and third order components to carrier, respectively. A typical specification for an AM-VSB video distribution system is CSO < -55 dBc and CTB < -65 dBc.

1.4.3 Dynamic Range

While the noise floor determines the minimum RF signal detectable for a given link, nonlinearities in the system tend to limit the maximum RF signal that can be transmitted. For links transmitting a single tone where there is little concern for it interfering with other signals, the 1 dB compression point is generally used to specify the dynamic range. For links transmitting a larger number of signals, the input power at which IMP3 exceed the noise floor is frequently used to calculate the spur-free dynamic range (SFDR). These parameters are shown graphically in Figure 1.5.

The most straightforward limitation on the power of an input signal is the 1 dB compression point, P_{1dB}. At this RF input power, the output signal is 1 dB less than what would be predicted by the small signal gain of

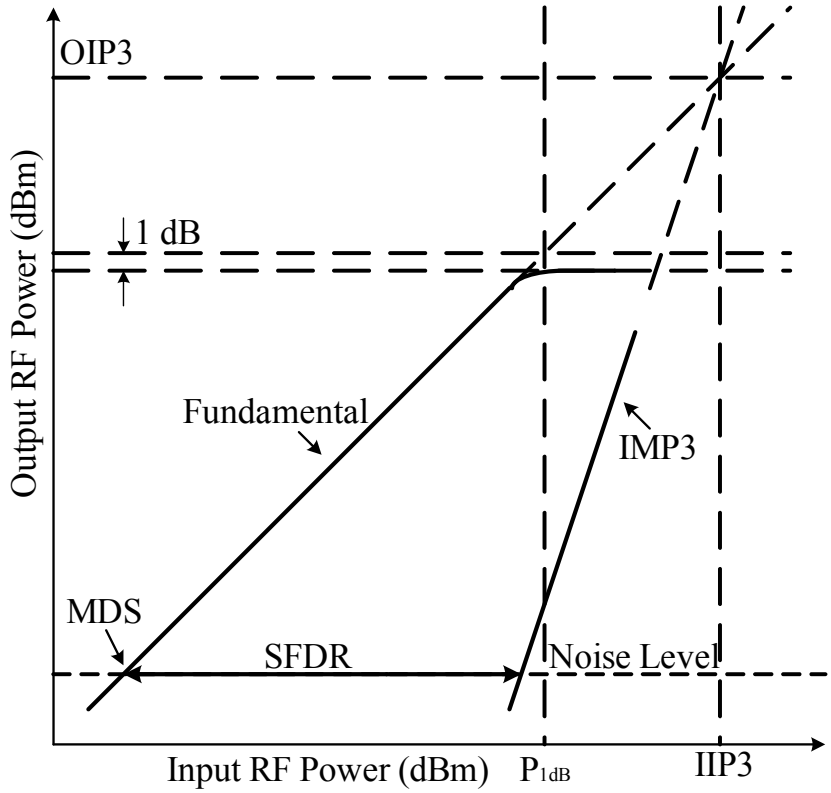

Figure 1.5: Parameters for the dynamic ranges of a system. MDS: Minimum discernible signal power; SFDR: Spur-free dynamic range; IIP3: The input 3rd-order intercept point; OIP3: The output 3rd-order intercept point; IMP3: The 3rd-order intermodulation distortion; P_{1dB}: 1-dB compression point.

the link. A more precise treatment for a large number of subcarriers uses the third-order intercept. As explained before, IMPs are generated due to interaction of subcarriers. In particular, if two equal-level sinusoidal tones at f_1 and f_2 modulate the fibre-optic link, third-order distortion products are generated at $2f_1 - f_2$ and at $2f_2 - f_1$. The magnitude of these third-order distortion products expressed in dBm has a slope of three when plotted against the input or output power level. To quantify this effect, the slopes of the output signal and distortion terms are extrapolated to higher power until they intersect. The input power corresponding to this intersection is defined as the input third-order intercept point (IIP3 or input TOI). Similarly, the output power corresponding to this intersection is defined as the output third-order intercept point (OIP3 or output TOI). Once the IIP3 is determined, the SFDR can be calculated. The SFDR corresponds to the case of a link transmitting two input signals of equal power. The SFDR is defined as the range of the two input signals in which the signals are above the noise floor and the third-order products are below the noise floor. The SFDR can be calculated by the following equation:

$$\text{SFDR} = \frac{2}{3}(\text{IIP3} - \text{MDS}) \tag{1.2}$$

1.5 Objectives of Research

The rapidly increasing demand of broadband services in the recent years has been driving optical fibre penetration into access networks deeper and deeper. In practical access networks, the cost is always the first consideration and hence distribution networks are typically designed to share the cost among many clients. Fibre provides us extremely low loss and huge bandwidth. Therefore an access network with fibre as the backbone or trunk can

support many more clients than that with coaxial cable, lowering the cost per client.

The marriage of fibre-optic communication and electronic communication in access networks makes SCM more and more attractive, providing a convenient bridge between the two communication systems. Even though the concept of SCM emerged soon after optical fibre communication began to be used, the scenarios of today's access networks are very different from those a few decades ago. To meet the requirement of current access networks, some new techniques, such as WDM, electrooptical upconversion [35,36], microwave remote generation [19, 37–39], etc., have been introduced to work together with SCM. Moreover, the subcarrier frequencies are in the range of tens of gigahertz now. Therefore, some problems that were trivial before are now important and should be studied in depth. For example, higher subcarrier frequency means serious power fading due to fibre dispersion. The nonlinear distortion due to modulators or fibres also becomes more complicated when more than one subcarriers or optical channels are used. This is especially true when we study the optical fibre communication part of access networks because traditionally the research focus was put on digital optical fibre communication systems.

The primary objective of this thesis is to study SCM signals in optical fibre communication systems in a current scenario of access networks. The focus is on some problems which have not been addressed in sufficient detail before. These problems are mainly due to nonlinearities of the systems, including the nonlinearities of fibre and modulator. Existing research work on these problem does not fully satisfy the needs of current SCM optical fibre

communication systems. For instance, some of the existing work is limited to links using small signal modulation or low subcarrier frequencies [40–44]; some of the current approaches involve time-consuming numerical analyses [5] and do not reveal much information about the physical mechanism. The final purpose of this thesis is to provide some closed-form analytical expressions to evaluate and quantify the distortion due to these nonlinear effects with adequate accuracy. Besides their accuracy, the expressions are very general and can be used in a number of current SCM optical fibre communication systems. The closed-form expressions enable us to gain better physical insight into the impact of various physical parameters and hence facilitate system design greatly.

1.6 Major Contributions

In this thesis, the nonlinear effects for SCM/WDM signals in optical fibre communication systems have been studied in detail. The nonlinear distortion in such systems arises mainly from the Dual-Drive Mach-Zehnder modulator (DD-MZM) and cross-phase modulation (XPM) in the fibre. For both types of nonlinearities, closed form expressions to study the nonlinear distortion have been developed, including the effect of fibre dispersion. For the nonlinearity due to DD-MZM, a new exact analytical model for SCM systems has been presented. For the first time, theoretical estimates for intercept points (IIPs) and 1-dB compression points have been obtained; also, it is shown that the capacity of an SCM system using DD-MZM, is limited by the nonlinearity of DD-MZM.

For the nonlinearity due to XPM, a new analytical model and new expressions have been developed and it is shown that the nonlinear crosstalk

due to XPM in fibre can be significant and may impose much lower launched optical power requirement than the threshold of SBS. Interestingly, the study also points out that the maximum nonlinear crosstalk for a higher frequency subcarrier due to XPM may be lower than that for a lower frequency subcarrier. Even though this is contrary to common belief, it is confirmed by experiments. These results should be helpful in the design and optimisation of SCM-WDM access networks.

In this thesis, analytical models have also been presented for SBS and SRS, respectively. Our analysis and experiment show that in a dispersive RoF link, when phase dithering is used to suppress SBS, besides the random noise due to phase modulation, there are discrete spectral lines spaced at dither rate in the detected signal, which may act as interference. Our analysis reveals that the sharp rising/falling edges of the phase dithering signal can cause these discrete spectral lines. We demonstrate that the low pass filtering of the phase dithering signal can suppress such noise and interference. With regard to SRS, our analysis shows the low pass character of SRS induced nonlinear distortion. Therefore the nonlinear distortion due to SRS is significant for systems that have low subcarrier frequencies and large spacing between optical channels.

1.7 Outline of the Thesis

The thesis is organized as follows:

In this chapter, a general background introduction is presented. Also presented are the research motivation, objectives, and major contributions for the work presented in the thesis.

In chapter 2, the basic theory for describing fibre dispersion and nonlinearities is given. The nonlinear propagation equation, nonlinear Schrödinger equation (NLSE), is presented as the basis of the analytical model and analysis in this thesis. The standard numerical method for the solution of NLSE, the split-step Fourier (SSF) method, is introduced together with its programming and verification, which serves as a benchmark to evaluate the accuracy of the analytical models developed in this thesis. A literature review of the past analytical approaches in this field is also given in this chapter.

In chapter 3, the nonlinear distortion due to Mach-Zehnder modulator (MZM) under dispersive transmission in fibre is studied. A new exact analytical model is presented to analyze the dispersive transmission in SCM fibre-optic links using DD-MZM. The model is very general and can be applied to almost all operating conditions of DD-MZM, such as bias point, drive level, phase shift and modulation index difference between DD-MZM drives. The model results in simple, new, closed form expressions for output power spectrum, permitting an accurate and fast analysis of such links. Two special cases, optical double sideband (ODSB) and optical single sideband (OSSB) modulation, are studied in detail. Some important system parameters, such as 1-dB compression point, the input 3rd-order intercept point (IIP3) and the system capacity, are derived theoretically for the first time.

In chapter 4, the nonlinearity due to stimulated inelastic scattering of fibre, including SBS and SRS, is studied. The low SBS threshold is shown to be a serious launch power limiting factor in SCM optical fibre communication systems. Even though phase dithering of laser diode output can

significantly increase SBS threshold, the noise floor is greatly enhanced after dispersive transmission in fibre. Besides the enhanced noise, there are discrete spectral lines spaced at dither rate in the detected signal, which may act as interference. The analysis and experiments in this chapter reveals that these discrete spectral lines are caused by sharp rising/falling edges in the PRBS used for phase dithering and can be suppressed by signal filtering. SRS is shown to lead to crosstalk among optical channels. Moreover, the analysis shows that the crosstalk due to SRS is stronger at lower frequencies and larger wavelength spacing. Therefore, SRS should be carefully treated in HFC CATV systems.

In chapter 5, the nonlinearity due to nonlinear refraction of fibre, including self-phase modulation (SPM) and XPM, is studied. A new analytical model is presented to study the nonlinear distortion due to XPM in dispersive WDM microwave fibre-optic links. The model is not based on the pump-probe approach which is widely used in the previous literature. Hence the results of our model can be used in more applications such as electrooptical upconversion systems. Our simulations and experiments show that the model predicts the nonlinear distortion due to XPM quite accurately, even when the modulating microwave frequency is in tens of gigahertz and the fibre length is in tens of kilometres. Detailed analyses of the distortion due to XPM for two commonly used modulation methods, ODSB and OSSB, are also presented. Measured results for OSSB are shown to match our theoretical predictions very well. Our results show that the nonlinear distortion due to XPM can be a limiting factor for optical launch power in WDM microwave fibre-optic links; moreover, the maximum possible nonlinear distortion level for a higher frequency may be lower than that for a lower frequency. Also

presented are some simple approximations for quick estimate of the nonlinear distortion level.

Chapter 6 summarizes and concludes this thesis.

Chapter 2

Basic Theory of Fibre Dispersion and Nonlinearity

This chapter is intended to provide an overview of the fibre dispersion and fibre nonlinearities, which are important for understanding the fibre-related distortion effects discussed in later chapters. Particular attention is paid to chromatic dispersion because of its importance in the study of nonlinear effects due to fibre. For fibre nonlinearities, brief introduction to self-phase modulation (SPM), cross-phase modulation (XPM), stimulated Brillouin scattering (SBS) and stimulated Raman scattering (SRS) is given. These four phenomena are the dominant nonlinear effects in SCM optical fibre communication systems. Nonlinear pulse propagation equation and its simplified version, nonlinear Schrödinger equation (NLSE), are then introduced in detail. The NLSE governs the wave propagation in a single mode fibre and is the starting point of the models and analyses in later chapters. This chapter also includes a review of recent literature addressing the effects of fibre dispersion and nonlinearity in SCM optical fibre communication systems.

2.1 Fibre Dispersion

When an electromagnetic wave propagates in a medium, it interacts with the bound electrons in the medium. Generally the medium response to the electromagnetic wave, which is shown as the medium absorbs the electromagnetic radiation through oscillations of the bound electrons at some characteristic resonance frequencies, is frequency dependent. This property, referred to as chromatic dispersion, manifests through the frequency dependence of the mode-propagation constant $\beta(\omega)$ [45]. Normally, $\beta(\omega)$ is not linear with frequency. Therefore, the effects of fibre dispersion are then accounted for by expanding $\beta(\omega)$ in a Taylor series about the frequency ω_0 at which the pulse spectrum is centred

$$\beta(\omega) = n(\omega)\frac{\omega}{c} = \beta_0 + \beta_1(\omega - \omega_0) + \frac{1}{2}\beta_2(\omega - \omega_0)^2 + \cdots \tag{2.1}$$

where

$$\beta_m = \left(\frac{d^m\beta}{d\omega^m}\right)_{\omega=\omega_0} \tag{2.2}$$

β_0 is the dominant mode-propagation constant at ω_0. In single mode fibres, because $\beta = \bar{n}\omega/c$ where c is the speed of light in the vacuum, the parameters β_1 and β_2 are related to the mode index $\bar{n}(\omega)$ and its derivatives through the relations

$$\beta_1 = \frac{1}{\nu_g} = \frac{\bar{n}_g}{c} = \frac{1}{c}\left(\bar{n} + \omega\frac{d\bar{n}}{d\omega}\right) \tag{2.3a}$$

$$\beta_2 = \frac{1}{c}\left(2\frac{d\bar{n}}{d\omega} + \omega\frac{d^2\bar{n}}{d\omega^2}\right) \tag{2.3b}$$

where $\bar{n}_g$ is the group index and ν_g is the group velocity. As the speed of travel of an electromagnetic wave is $c/\bar{n}$, the speed of light in a fibre is then also frequency dependent because of fibre dispersion. It means that different

spectral components associated with a pulse travel at different speeds and may lead to a change of pulse shape. Moreover, the envelope of an optical pulse moves at the group velocity while the parameter β_2 stands for dispersion of the group velocity, leading to pulse broadening. This phenomenon is known as the group-velocity dispersion (GVD) and hence β_2 is called as GVD parameter. In the fibre-optic literature, another dispersion parameter D is commonly used and is related to β_2 by the relation

$$D = \frac{d\beta_1}{d\lambda} = -\frac{2\pi c}{\lambda^2}\beta_2 \approx \frac{\lambda}{c}\frac{d^2\bar{n}}{d\lambda^2} \tag{2.4}$$

where λ stands for the wavelength of the light.

In single mode fibres, the mode index $\bar{n}$ has two contributors: one is the material refractive index; the other is due to the waveguide structure of fibres. Therefore, the fibre dispersion also has two contributions: material dispersion D_M and waveguide dispersion D_W. Consequently, D can be written as the sum of the two terms: $D = D_M + D_W$.

The origin of material dispersion is related to the characteristic resonance frequencies at which the medium absorbs the electromagnetic radiation through oscillations of bound electrons. Far from the medium resonances, the refractive index $n(\omega)$ can be approximated by the Sellmeier equation [45]

$$n^2(\omega) = 1 + \sum_{i=1}^{m} \frac{B_i \omega_i^2}{\omega_i^2 - \omega^2} \tag{2.5}$$

where ω_i is the resonance frequency and B_i is the strength of ith resonance. The parameters ω_i and B_i are obtained experimentally for the material of optical fibres by fitting the measured dispersion curves to Eq. (2.5).

The waveguide dispersion is related to the fibre-design parameters such as core radius a and core-cladding index difference Δ [45–47]. Therefore, these parameters can be intentionally adjusted to design a fibre with desired waveguide dispersion so that the overall fibre dispersion curve meets some particular requirements.

An important feature of chromatic dispersion is that pulses at different wavelengths propagate at different speeds inside a fibre because of a difference in their group velocity, which is called as walk-off effect that plays an important role in the description of the nonlinear phenomena involving two or more closely spaced optical pulses. This walk-off effect is governed by the walk-off parameter d_{12} defined as

$$d_{12} = \beta_1(\lambda_1) - \beta_1(\lambda_2) = \nu_g^{-1}(\lambda_1) - \nu_g^{-1}(\lambda_2) \tag{2.6}$$

where λ_1 and λ_2 are the centre wavelengths of two pulses and β_1 at these wavelengths is evaluated using Eq. (2.3a). In the normal-dispersion regime ($\beta_2 > 0$ or $D < 0$), a longer wavelength travels faster, while the opposite occurs in the anomalous-dispersion region ($\beta_2 < 0$ or $D > 0$). The group-velocity difference plays an important role for nonlinear effects involving two or more optical channels, such as cross-phase modulation and stimulated Raman scattering.

2.2 Fibre Nonlinearities

Fibre nonlinearities originate from the nonlinear response of a dielectric medium to intense electromagnetic fields. Basically, this nonlinear response

can be modelled as anharmonic motion of bound electrons under the influence of an applied field. As a result, instead of being linear in the electric field $\mathbf{E}$, the total polarization $\mathbf{P}$ induced by electric dipoles satisfies the more general relation [48–51]:

$$\mathbf{P} = \varepsilon_0 \left(\chi^{(1)} \cdot \mathbf{E} + \chi^{(2)} : \mathbf{EE} + \chi^{(3)} \vdots \mathbf{EEE} + \cdots \right) \tag{2.7}$$

where ε_0 is the vacuum permittivity and $\chi^{(i)}$ $(i = 1, 2, \ldots)$ is ith order susceptibility. Generally, $\chi^{(i)}$ is a tensor of rank $i+1$. The linear susceptibility $\chi^{(1)}$ stands for the dominant contribution to $\mathbf{P}$, which results in the the refractive index n and the fibre attenuation coefficient α as shown in the previous section. $\chi^{(2)}$ vanishes for optical fibre made of silica glasses. Therefore, the lowest-order nonlinear effects in optical fibres originate from the third-order susceptibility $\chi^{(3)}$.

In addition to nonlinear refraction, which is a nonlinear effect governed by the third-order susceptibility $\chi^{(3)}$, there is another category of nonlinearities in optical fibres known as stimulated inelastic scattering. There is another manifestation of fibre nonlinearity governed by the third-order susceptibility $\chi^{(3)}$, which can generate new frequencies, such as third-harmonic generation and four-wave mixing (FWM). However, unless special efforts are made to achieve phase matching, the nonlinear processes that involve generation of new frequencies are not efficient in optical fibres. Because these nonlinearities are quite weak in practice, they may require very strong intensity or very long fibre length to take significant effect. For example, the parametric processes studied in [32–34] take fibre lengths of thousands of kilometers to show their impact. Since the focus of this thesis is on the applications

of subcarrier multiplexing in access network where the fibre length is seldom longer than 100 km, only nonlinear refraction and stimulated inelastic scattering are studied in detail.

2.2.1 Nonlinear Refraction

Nonlinear refraction is due to changes in the refractive index with optical power. As has been mentioned above, the response of any dielectric to light becomes nonlinear for intense electromagnetic fields. Therefore the refractive index will be intensity dependent. In its simplest form, the refractive index after including the nonlinear effect can be written as

$$n_{NL}(\omega, |E|^2) = n(\omega) + n_2|E|^2 \tag{2.8}$$

where $n(\omega)$ is the linear part of refractive index given by Eq. (2.5), $|E|^2$ is the optical intensity inside the fibre and n_2 is the nonlinear-index coefficient related to $\chi^{(3)}$.

The mode-propagation constant β is related to refractive index by Eq. (2.1). Hence β is now intensity dependent since refractive index is intensity dependent. It means that when a lightwave travels along a fibre, nonlinear refraction will induce intensity dependent phase shift to the optical field. Its magnitude can be obtained by

$$\phi = n_{NL}k_0L = (n + n_2|E|^2)k_0L \tag{2.9}$$

where $k_0 = 2\pi/\lambda$ and L is the fibre length. The intensity-dependent nonlinear phase shift $\phi_{NL} = n_2k_0L|E|^2$ is due to self-phase modulation (SPM) since the phase shift is self-induced.

Another optical field having a different wavelength, direction, or state of polarization can also induce nonlinear phase shift to an optical field; this phenomenon is called cross-phase modulation (XPM). Its origin can be understood by noting that the total electric field $\mathbf{E}$ is given by

$$\mathbf{E} = \frac{1}{2}\hat{x}[E_1 \exp(-j\omega_1 t) + E_2 \exp(-j\omega_2 t) + \text{c.c.}] \tag{2.10}$$

when two optical fields at frequencies ω_1 and ω_2, polarized along the x axis, propagate simultaneously inside the fibre. (The abbreviation c.c. stands for complex conjugate). The nonlinear phase shift for the field at ω_1 is then given by

$$\phi_{NL} = n_2 k_0 L(|E_1|^2 + 2|E_2|^2) \tag{2.11}$$

where the terms that generate polarization at frequencies other than ω_1 and ω_2 have been neglected because of their non-phase-matched character. The two terms on the right-hand side of Eq. (2.11) are due to SPM and XPM respectively. Clearly, for equally intense optical fields of different wavelengths, the contribution to the nonlinear phase shift by XPM is twice that of SPM.

Hence nonlinear refraction induces intensity dependent nonlinear phase fluctuation to original optical field, which is time dependent and therefore new frequency components are generated. Because of fibre dispersion, these new frequency components travel at different speeds and then lead to additional intensity change, that is, the nonlinear phase shift is converted to nonlinear intensity distortion by fibre dispersion.

2.2.2 Stimulated Inelastic Scattering

The nonlinear effects governed by the third-order susceptibility $\chi^{(3)}$ are elastic because no energy is exchanged between the electromagnetic field and the dielectric medium. For the nonlinear effects resulted from stimulated inelastic scattering, the optical field transfers part of its energy to the nonlinear medium. In optical fibres, stimulated Raman scattering (SRS) and stimulated Brillouin scattering (SBS) [52–54], are the two important nonlinear effects of this type. Both of them are related to vibrational excitation modes of silica. The main difference between the two is that optical phonons participate in SRS while acoustic phonons participate in SBS.

Both SRS and SBS involve a photon of the incident field (called the pump) annihilated to create a photon at a lower frequency (belonging to the Stokes wave) and a phonon with the right energy and momentum to conserve the energy and the momentum. Besides, a higher-energy photon at the so-called anti-Stokes frequency can also be created if a phonon of right energy and momentum is available. Even though SRS and SBS are very similar in their origin, different dispersion relations for acoustic and optical phonons lead to some basic differences between the two. A fundamental difference is that SBS in optical fibres occurs only in the backward direction whereas SRS can occur in both directions.

The complete description of SRS and SBS in optical fibres is quite involved. However, the initial growth of the Stokes wave can be described by a simple relation. For SRS, this relation is given by

$$\frac{dP_s}{dz} = g_R P_p P_s \tag{2.12}$$

where P_s is the Stokes intensity, P_p is the pump intensity and g_R is the Raman gain coefficient. A similar relation holds for SBS with g_R replaced by the Brillouin-gain coefficient g_B. For silica fibres, the Raman-gain spectrum is found to be very broad, extending up to 30 THz [52] while the Brillouin-gain spectrum is extremely narrow, with a bandwidth less than 100 MHz [53]. For SRS, the peak gain $g_R \approx 7 \times 10^{-14}\,\mathrm{m/W}$ at pump wavelengths near $1.5\,\mu\mathrm{m}$ and occurs for the Stokes shift of about 13 THz. For SBS, the peak gain is about $6 \times 10^{-11}\,\mathrm{m/W}$ for a narrow-bandwidth pump and decreases by a factor of $\Delta\nu_p/\Delta\nu_B$ for a broad-bandwidth pump, where $\Delta\nu_p$ is the pump bandwidth and $\Delta\nu_B$ is the Brillouin-gain bandwidth.

Different from nonlinear refraction, SRS and SBS exhibit a threshold-like behaviour. Significant conversion of pump energy to Stokes energy occurs only when the pump intensity exceeds a certain threshold level. For SRS, in a single-mode fibre with fibre loss α and length L, when $\alpha L \gg 1$, the threshold pump intensity is given by [54]

$$P_p^{th} \approx \frac{16\alpha}{g_R} \tag{2.13}$$

Typically $P_p^{th} \sim 10\,\mathrm{MW/cm^2}$ and SRS can be observed at a pump power $\sim 1\,\mathrm{W}$. The threshold pump intensity for SBS is given by [54]

$$P_p^{th} \approx \frac{21\alpha}{g_B} \tag{2.14}$$

Since the Brillouin-gain coefficient g_B is larger by nearly three orders of magnitude compared with g_R, typical values of SBS threshold are $\sim 1\,\mathrm{mW}$. Such a low threshold may be detrimental for some SCM optical communications systems. Because the Brillouin-gain coefficient g_B decreases with pump

bandwidth, values of SBS threshold can be significantly increased by phase dithering the laser output to intentionally broaden the pump bandwidth. Usually we cannot observe significant SRS in SCM optical communication systems due to the large values of SRS threshold except when Raman amplification is used. However, the nonlinear crosstalk between optical channels due to SRS can still be a limiting factor and should be carefully treated.

2.2.3 Importance of Fibre Nonlinear Effects

As discussed before, the magnitude of the nonlinear effect due to the nonlinear refraction is determined by the nonlinear-index coefficient n_2. Similarly, the Raman- and Brillouin-gain coefficients determine the magnitude of SRS and SBS respectively. However, all the three parameters in silica fibres are smaller by two orders of magnitude or more compared with other common nonlinear media. For example, the typical nonlinear-index coefficient n_2 in silica fibres is in the range $2.2 \sim 3.4 \times 10^{-20}\,\mathrm{m}^2/\mathrm{W}$, depending on both the core composition of fibre and whether the input polarization is preserved inside the fibre or not. Compared to most other nonlinear media, this value is smaller by at least two orders of magnitude.

Although the nonlinear coefficients in fused silica are small, the nonlinear effects in optical fibres can be observed at relatively low power levels. This is due to two important characteristics of single-mode fibres: a small spot size (mode diameter $< 10\,\mu$m) and extremely low loss ($< 1\,$dB/km) in the wavelength range $1.0 - 1.6\,\mu$m. A figure of merit for the efficiency of a nonlinear process is the product PL_{eff} where P is the optical intensity and L_{eff} is the effective length of interaction region [55]. Compared with the efficiency in bulk media, it shows that the efficiency of a nonlinear process

in optical fibres can be improved by a factor [55]

$$\frac{(PL_{eff})_{fibre}}{(PL_{eff})_{bulk}} = \frac{\lambda}{\pi w_0^2 \alpha} \tag{2.15}$$

where w_0 is the spot size of optical intensity. In the wavelength region near $1.55\,\mu$m for optical fibre communication, $\alpha = 0.2\,$dB/km and the enhancement factor can approach 10^9. It is this tremendous enhancement in the efficiency of the nonlinear processes that makes nonlinear effects due to fibre significant at low power levels. Therefore, nonlinear distortion due to fibre should be carefully studied in SCM optical fibre communication systems.

2.3 Nonlinear Propagation Equation

The propagation of optical waves in a single mode fibre is governed by Maxwell's equations which lead to the wave equation [56]

$$\nabla^2 \mathbf{E} - \frac{1}{c^2}\frac{\partial^2 \mathbf{E}}{\partial t^2} = \mu_0 \frac{\partial^2 \mathbf{P}}{\partial t^2} \tag{2.16}$$

where $\mathbf{E}$ is the electric field vector, $\mathbf{P}$ is the induced electric polarization, μ_0 is the vacuum permeability and c is the speed of light in vacuum.

For very weak optical powers, the induced electric polarization is related to $\mathbf{E}$ according to [49, 50]

$$\mathbf{P}_L(\mathbf{r}, t) = \varepsilon_0 \int_{-\infty}^{\infty} \chi^{(1)}(t - t') \cdot \mathbf{E}(\mathbf{r}, t') dt' \tag{2.17}$$

where ε_0 is the the vacuum permittivity. To account for fibre nonlinearities, a nonlinear electric polarization part has to be included. If we include only the third-order nonlinear effects governed by $\chi^{(3)}$, the induced electric

polarization consists of two parts such that

$$\mathbf{P}(\mathbf{r},t) = \mathbf{P}_L(\mathbf{r},t) + \mathbf{P}_{NL}(\mathbf{r},t) \tag{2.18}$$

where the nonlinear part $\mathbf{P}_{NL}$ is related to the electric field by the general relation [49, 50]

$$\begin{aligned}\mathbf{P}_{NL}(\mathbf{r},t) = \varepsilon_0 \int_{-\infty}^{\infty}\int_{-\infty}^{\infty}\int_{-\infty}^{\infty} \chi^{(3)}(t-t_1, t-t_2, t-t_3) \vdots \\ \times \mathbf{E}(\mathbf{r},t_1)\mathbf{E}(\mathbf{r},t_2)\mathbf{E}(\mathbf{r},t_3)dt_1dt_2dt_3\end{aligned} \tag{2.19}$$

Eq. (2.16) now reduces to

$$\nabla^2\mathbf{E} - \frac{1}{c^2}\frac{\partial^2\mathbf{E}}{\partial t^2} = \mu_0\frac{\partial^2\mathbf{P}_L}{\partial t^2} + \mu_0\frac{\partial^2\mathbf{P}_{NL}}{\partial t^2} \tag{2.20}$$

Even though Eqs. (2.16) $\sim$ (2.19) are very general, they are quite complicated and some simplifying approximations are necessary. Because the nonlinear effects are relatively weak in silica fibres, the nonlinear polarization $\mathbf{P}_{NL}$ in Eq. (2.18) can be treated as a small perturbation to the total induced polarization. Besides, the optical field is assumed to maintain its polarization along the fibre length so that a scalar approach is valid. Moreover, the optical field is assumed to be quasi-monochromatic, i.e., the pulse spectrum centred at ω_0 is assumed to have a spectral width $\Delta\omega$ such that $\Delta\omega/\omega_0 \ll 1$. Given that $\omega_0 \sim 10^{15}$ rad/s, the last approximation is valid for pulses as short as 0.1 ps. For such slowly varying envelope approximation, it is useful to separate the rapidly varying part of the electric field by writing it in the form

$$\mathbf{E}(\mathbf{r},t) = \frac{1}{2}\hat{x}[E(\mathbf{r},t)\exp(-j\omega_0 t) + \text{c.c.}] \tag{2.21}$$

where $\hat{x}$ is the polarization unit vector and $E(\mathbf{r},t)$ is a slowly varying function

of time (relative to the optical period) standing for the envelope. Similarly the polarization components $\mathbf{P}_L$ and $\mathbf{P}_{NL}$ can be written as

$$\mathbf{P}_L(\mathbf{r},t) = \frac{1}{2}\hat{x}[P_L(\mathbf{r},t)\exp(-j\omega_0 t) + \text{c.c.}] \tag{2.22a}$$

$$\mathbf{P}_{NL}(\mathbf{r},t) = \frac{1}{2}\hat{x}[P_{NL}(\mathbf{r},t)\exp(-j\omega_0 t) + \text{c.c.}] \tag{2.22b}$$

For pulse widths greater than 1 ps, the nonlinear response can be assumed to be instantaneous and the time dependence of $\chi^{(3)}$ in Eq. (2.19) is given by the product of three delta functions of the form $\delta(t-t_1)$. Eq. (2.19) then reduces to

$$\mathbf{P}_{NL} = \varepsilon_0 \chi^{(3)} \vdots \mathbf{E}(\mathbf{r},t)\mathbf{E}(\mathbf{r},t)\mathbf{E}(\mathbf{r},t) \tag{2.23}$$

Eq. (2.19) results in a term oscillating at ω_0 and another term oscillating at the third-harmonic frequency $3\omega_0$. Only the first term is considered since the latter requires phase matching and is generally negligible in optical fibres. With Eq. (2.22b), $P_{NL}(\mathbf{r},t)$ is given by

$$P_{NL}(\mathbf{r},t) \approx \varepsilon_0 \varepsilon_{NL} E(\mathbf{r},t) \tag{2.24}$$

where the nonlinear contribution to the dielectric constant is defined as

$$\varepsilon_{NL} = \frac{3}{4}\chi^{(3)}_{xxxx}|E(\mathbf{r},t)|^2 \tag{2.25}$$

Note that ε_{NL} is intensity dependent and therefore Eq. (2.20) is nonlinear after substituting Eq. (2.24) into Eq. (2.20). To make solution possible, ε_{NL} is treated as a constant during the derivation of the propagation equation due to the slowly varying envelope approximation and the perturbative nature of P_{NL}. Given Eqs. (2.20) $\sim$ (2.22), the Fourier transform $\tilde{E}(\mathbf{r},\omega-\omega_0)$

defined as

$$\tilde{E}(\mathbf{r}, \omega - \omega_0) = \int_{-\infty}^{\infty} E(\mathbf{r}, t) \exp[j(\omega - \omega_0)t] dt \tag{2.26}$$

is found to satisfy the Helmholtz equation

$$\nabla^2 \tilde{E} + \varepsilon(\omega) k_0^2 \tilde{E} = 0 \tag{2.27}$$

where $\sim$ denotes the Fourier transform, $k_0 = \omega/c$ and

$$\varepsilon(\omega) = 1 + \tilde{\chi}_{xx}^{(1)}(\omega) + \varepsilon_{NL} \tag{2.28}$$

is the dielectric constant whose nonlinear part ε_{NL} is given by Eq. (2.25). The dielectric constant ε is related to the nonlinear refractive index $n(\omega)$ and the nonlinear absorption coefficient $\alpha(\omega)$ by the following equation

$$\varepsilon = (n_{NL} + \frac{j\alpha_{NL}c}{2\omega})^2 \tag{2.29}$$

Because of ε_{NL}, both n_{NL} and α_{NL} are intensity dependent. It is customary to introduce

$$n_{NL} = n + n_2|E|^2 \tag{2.30a}$$

$$\alpha_{NL} = \alpha + \alpha_2|E|^2 \tag{2.30b}$$

where n and α are the intensity independent parts of n_{NL} and α_{NL}, respectively. Neglecting the very small terms proportional to $|E|^4$, Eqs. (2.25), (2.28) and (2.29) result in

$$n_2 = \frac{3}{8n}\mathrm{Re}(\chi_{xxxx}^{(3)}) \tag{2.31a}$$

$$\alpha_2 = \frac{3\omega_0}{4nc}\mathrm{Im}(\chi_{xxxx}^{(3)}) \tag{2.31b}$$

In the derivation of Eqs. (2.31), the terms with α/k_0 are neglected because they are much smaller than the terms with n in optical fibres. As α_2 is relatively small for silica fibres, it is ignored in the following derivations, leaving n_2 as the parameter to measure the fibre nonlinearity.

Eq. (2.27) can be solved by using the method of separation of variables. Assuming a solution of the form

$$\tilde{E}(\mathbf{r}, \omega - \omega_0) = F(x, y)\tilde{A}(z, \omega - \omega_0)\exp(j\beta_0 z) \tag{2.32}$$

where $\tilde{A}(z, \omega - \omega_0)$ is a slowly varying function of z and β_0 is the propagation constant at ω_0. Eq. (2.27) reduces to the following two equations for $F(x, y)$ and $\tilde{A}(z, \omega - \omega_0)$

$$\frac{\partial^2 F}{\partial x^2} + \frac{\partial^2 F}{\partial y^2} + [\varepsilon(\omega)k_0^2 - \beta_{NL}^2]F = 0 \tag{2.33a}$$

$$2j\beta_0 \frac{\partial \tilde{A}}{\partial z} + (\beta_{NL}^2 - \beta_0^2)\tilde{A} = 0 \tag{2.33b}$$

The second derivative $\partial^2\tilde{A}/\partial z^2$ was neglected in Eq. (2.33b) since $\tilde{A}(z, \omega - \omega_0)$ is assumed to be a slowly varying function of z. Moreover, a new term, $\beta_{NL}^2 F\tilde{A}\exp(j\beta_0 z)$, is introduced into Eqs. (2.33a) and (2.33b) with opposite signs to stand for the frequency-dependent propagation constant. The solution of eigenvalue Eq. (2.33a) determines β_{NL} by using the first-order perturbation theory. Besides, the dielectric constant $\varepsilon(\omega)$ in Eq. (2.33a) can be approximated by

$$\varepsilon = (n + \Delta n)^2 \approx n^2 + 2n\Delta n \tag{2.34}$$

where Δn is a small perturbation given by

$$\Delta n = n_2|E|^2 + \frac{j\tilde{\alpha}}{2k_0} \tag{2.35}$$

Eq. (2.33a) is solved by neglecting the fibre nonlinearity at first. Hence, we can find the modal distribution $F(x, y)$ and the corresponding propagation constant $\beta(\omega)$ by replacing ε with n^2. Then we include the effect of Δn in Eq. (2.33a). In the context of first-order perturbation theory, Δn does not affect the modal distribution $F(x, y)$. However, the eigenvalue β_{NL} becomes

$$\beta_{NL}(\omega) = \beta(\omega) + \Delta\beta \tag{2.36}$$

where

$$\Delta\beta = \frac{k_0 \int_{-\infty}^{\infty}\int_{-\infty}^{\infty} \Delta n|F(x,y)|^2 dxdy}{\int_{-\infty}^{\infty}\int_{-\infty}^{\infty} |F(x,y)|^2 dxdy} \tag{2.37}$$

Clearly, $\Delta\beta$ is related to Δn shown by Eq. (2.35) and hence includes the effect of fibre nonlinearity and loss. Taking the approximation $\beta_{NL}^2 - \beta_0^2 \approx 2\beta_0(\beta_{NL} - \beta_0)$, Eq. (2.33b) can be re-written as

$$\frac{\partial \tilde{A}}{\partial z} = j[\beta(\omega) + \Delta\beta - \beta_0]\tilde{A} \tag{2.38}$$

Eq. (2.38) shows that during the propagation along the fibre, each spectral component in the pulse envelope acquires a phase shift whose magnitude is both frequency and intensity dependent.

Eq. (2.38) can be transformed back to time domain after replacing $\beta(\omega)$ by its Taylor series shown by Eq. (2.1). The cubic and higher-order terms in the expansion of Eq. (2.1) are generally negligible if the spectral width $\Delta\omega \ll \omega_0$. During the inverse Fourier transform operation, $\omega - \omega_0$ is replaced

by the differential operator $j(\partial/\partial t)$. Therefore, the resulting equation for $A(z,t)$ becomes

$$\frac{\partial A}{\partial z} = -\beta_1 \frac{\partial A}{\partial t} - \frac{j\beta_2}{2}\frac{\partial^2 A}{\partial t^2} + j\Delta\beta A \tag{2.39}$$

By using Eqs. (2.35) and (2.37), $\Delta\beta$ can be evaluated and substituted in Eq. (2.39); this results in

$$\frac{\partial A}{\partial z} + \beta_1 \frac{\partial A}{\partial t} + \frac{j\beta_2}{2}\frac{\partial^2 A}{\partial t^2} + \frac{\alpha}{2}A = j\gamma|A|^2 A \tag{2.40}$$

where the nonlinear parameter γ is defined as

$$\gamma = \frac{n_2\omega_0}{cA_{eff}} \tag{2.41}$$

The parameter A_{eff} is known as the effective core area and is defined as

$$A_{eff} = \frac{(\int_{-\infty}^{\infty}\int_{-\infty}^{\infty}|F(x,y)|^2 dxdy)^2}{\int_{-\infty}^{\infty}\int_{-\infty}^{\infty}|F(x,y)|^4 dxdy} \tag{2.42}$$

Eq. (2.40) describes propagation of picosecond optical pulse in single-mode fibres. It is often referred to as the nonlinear Schrödinger equation (NLSE) because it can be reduced to that form under certain conditions. It includes the effects of fibre losses through α, of chromatic dispersion through β_1 and β_2 and of fibre nonlinearity through γ. It is customary to simplify Eq. (2.40) further as

$$\frac{\partial A}{\partial z} + \frac{j\beta_2}{2}\frac{\partial^2 A}{\partial T^2} + \frac{\alpha}{2}A = j\gamma|A|^2 A \tag{2.43}$$

by taking the transformation

$$T = t - \frac{z}{\nu_g} \equiv t - \beta_1 z \tag{2.44}$$

which means a frame of reference moving with the pulse at the group velocity ν_g (the so-called retarded frame).

Eq. (2.43) is the simplest nonlinear propagation equation for studying the third-order nonlinear effects resulting from $\chi^{(3)}$ in optical fibres. The term at the right side of Eq. (2.43) leads to nonlinear phase shift, which will be converted to intensity change by chromatic dispersion shown by the second term at the left side of the equation. Because this nonlinear phase shift depends on the optical intensity itself, this effect is known as self-phase modulation (SPM).

The discussion above is for a single optical channel only. If there are two or more optical channels as in the case of WDM system, the nonlinear phase shift can be caused by the optical intensity at other optical channels, which is known as cross-phase modulation (XPM). To describe such cases, a set of coupled equations are necessary, as shown below for two optical channels [57–59]:

$$\frac{\partial A_1}{\partial z} + \frac{1}{\nu_{g1}}\frac{\partial A_1}{\partial t} + \frac{j\beta_{21}}{2}\frac{\partial^2 A_1}{\partial t^2} + \frac{\alpha_1}{2}A_1 = j\gamma_1(|A_1|^2 + 2|A_2|^2)A_1 \tag{2.45a}$$

$$\frac{\partial A_2}{\partial z} + \frac{1}{\nu_{g2}}\frac{\partial A_2}{\partial t} + \frac{j\beta_{22}}{2}\frac{\partial^2 A_2}{\partial t^2} + \frac{\alpha_2}{2}A_2 = j\gamma_2(|A_2|^2 + 2|A_1|^2)A_2 \tag{2.45b}$$

where A_i, ν_{gi}, β_{2i}, α_i and γ_i are the optical field envelope, group velocity, GVD parameter, fibre loss and fibre nonlinearity parameter for the ith channel.

Stimulated Raman scattering (SRS) also leads to interaction between optical channels but it is not included in the model presented above. Introducing the Raman gain coefficient defined by

$$g_p = 2\gamma_p f_R |\tilde{h}_R(\Omega_R)| \tag{2.46a}$$

$$g_s = 2\gamma_s f_R |\tilde{h}_R(\Omega_R)| \tag{2.46b}$$

where f_R represents the fractional contribution of the delayed Raman response to nonlinear polarization P_{NL} and $\tilde{h}_R$ is the Fourier transform of the Raman response function $h(t)$ with gain peak located at Ω_R, the coupled amplitude equations including both nonlinear refraction and Raman effects are [60]:

$$\begin{aligned} &\frac{\partial A_p}{\partial z} + \frac{1}{\nu_{gp}}\frac{\partial A_p}{\partial t} + \frac{j\beta_{2p}}{2}\frac{\partial^2 A_p}{\partial t^2} + \frac{\alpha_p}{2}A_p \\ &\quad = j\gamma_p\left[|A_p|^2 + (2-f_R)|A_s|^2\right]A_p - \frac{g_p}{2}|A_s|^2 A_p \end{aligned} \tag{2.47a}$$

$$\begin{aligned} &\frac{\partial A_s}{\partial z} + \frac{1}{\nu_{gs}}\frac{\partial A_s}{\partial t} + \frac{j\beta_{2s}}{2}\frac{\partial^2 A_s}{\partial t^2} + \frac{\alpha_s}{2}A_s \\ &\quad = j\gamma_s\left[|A_s|^2 + (2-f_R)|A_p|^2\right]A_s + \frac{g_s}{2}|A_p|^2 A_s \end{aligned} \tag{2.47b}$$

where p stands for the pump channel and s stands for the Stokes channel.

If only SRS is considered and continuous wave (CW) propagation is assumed, the interaction through SRS is then governed by much simpler coupled equations

$$\frac{dP_s}{dz} = g_R P_p P_s - \alpha_s P_s \tag{2.48a}$$

$$\frac{dP_p}{dz} = -\frac{\omega_p}{\omega_s} g_R P_p P_s - \alpha_p P_p \tag{2.48b}$$

where I is the channel intensity, ω is the optical angular frequency and g_R

is the Raman-gain coefficient.

2.4 Numerical Method for Solution of NLSE

It is not possible to obtain an exact solution of NLSE (Eq. (2.40 or 2.43)) analytically when both the dispersion and the fibre nonlinearities are present, except in the very special case of soliton transmission. Therefore a number of numerical algorithms have been developed to solve NLSE. The split-step Fourier (SSF) method is one of the most popular methods because of its good accuracy and relatively modest computing cost [61, 62].

2.4.1 Split-Step Fourier Method

Eq. (2.43) can be expressed as

$$\frac{\partial A}{\partial z} = (\hat{D} + \hat{N})A \tag{2.49}$$

where $\hat{D}$ is a differential operator that accounts for dispersion and absorption in a linear medium and $\hat{N}$ is a nonlinear operator that governs the effect of fibre nonlinearities on pulse propagation. The operators are given by

$$\hat{D} = -\frac{j\beta_2}{2}\frac{\partial^2}{\partial T^2} - \frac{\alpha}{2} \tag{2.50a}$$

$$\hat{N} = j\gamma|A|^2 \tag{2.50b}$$

When the electric field envelope $A(z,T)$ has propagated from z to $z+\Delta z$, the analytical solution of Eq. (2.43) will have the form of

$$A(z+\Delta z, T) = \exp\left[\Delta z(\hat{D}+\hat{N})\right]A(z,T) \tag{2.51}$$

SSF method ignores the noncommutating nature of the operators $\hat{D}$ and $\hat{N}$. Therefore

$$A(z+\Delta z,T) \approx \exp(\Delta z\hat{D})\exp(\Delta z\hat{N})A(z,T) \tag{2.52}$$

Eq. (2.52) means that $A(z+\Delta z,T)$ can be estimated by applying the two operators independently. The exponential operator $\exp(\Delta z\hat{D})$ can be evaluated in the Fourier domain using the prescription

$$\exp(\Delta z\hat{D})B(z,T) = F_T^{-1}\exp\left[\Delta z\hat{D}(j\omega)\right]F_T B(z,T) \tag{2.53}$$

where F_T denotes the Fourier-transform operation, $\hat{D}(j\omega)$ is obtained by replacing the differential operator $\partial/\partial T$ by $j\omega$ and ω is the frequency in the Fourier domain. Therefore SSF first Fourier transforms $A(z,T)$ to $A(z,j\omega)$, multiplies the result by $\exp[\Delta z\hat{D}(j\omega)]$ and then inverse-Fourier transforms the multiplication result, and finally multiplies the transformation result by $\exp(\Delta z\hat{N})$ to get $A(z+\Delta z,T)$. Then repeat the procedure above to calculate the next section till the end. It has been reported that when the maximum phase shift ($\Phi_{max} = \gamma|A_p|^2\Delta z$, A_p is the peak value of $A(z,T)$) due to nonlinear operator is below 0.05 rad, SSF gives a good result for simulation of most contemporary optical communication systems.

When simulating the performance of WDM systems, the numerical model can be too complicated to be practical when the channel number is great if the total optical field is split into individual channel fields. A simpler approach solves a single NLSE by using an input field of the form

$$A(0,T) = \sum_{m=1}^{M} A_m(0,T)\exp\left[j(\omega_m-\omega_0)\right] \tag{2.54}$$

where $A_m(0,T)$ is the input signal belonging to the mth channel and M is the number of channels. This technique includes the SPM, XPM and four wave mixing (FWM) effects for all channels automatically.

2.4.2 Accuracy of SSF Numerical Method

In this thesis, the results predicted by the analytical expressions derived in later chapters have been compared with those obtained by SSF numerical method. Therefore the accuracy of SSF method should be addressed first by comparing with a known theoretical prediction. It is known that Eq. (2.43) can lead to soliton solutions by applying the inverse scattering method in a lossless fibre. To support solitons, the dispersion should be in anomalous region ($\beta_2 < 0$ or $D > 0$) and the input pulse should have a hyperbolic secant shape. One of the solutions is the fundamental soliton, which propagates without change of pulse shape for arbitrarily long distance in an ideal case. For fundamental soliton, the following equation should be satisfied [26]

$$N^2 = \frac{L_D}{L_{NL}} = \frac{\gamma P_0 T_0^2}{|\beta_2|} = 1 \tag{2.55}$$

where P_0 is the peak power of the pulse and T_0 is the pulse half-width (at $1/e$-intensity point) and dispersion length $L_D = T_0^2/|\beta_2|$, nonlinear length $L_{NL} = (\gamma P_0)^{-1}$ respectively. We chose $T_0 = 10\,\text{ps}$, $D = 1\,\text{ps/nm}\cdot\text{km}$, $\gamma = 2.43\,\text{W}^{-1}/\text{km}$ and P_0 to satisfy Eq. (2.55). The resulting L_D is about 78 km and we simulated by SSF numerical method till $150L_D$ which is over 10000 km. The results by theoretical calculation as well as by SSF numerical method are shown in Figure 2.1 for comparison. Note that the magnitude scale is logarithmic. In the simulation, a maximum phase shift of 0.01 rad was used. The results show that the error introduced by SSF method is

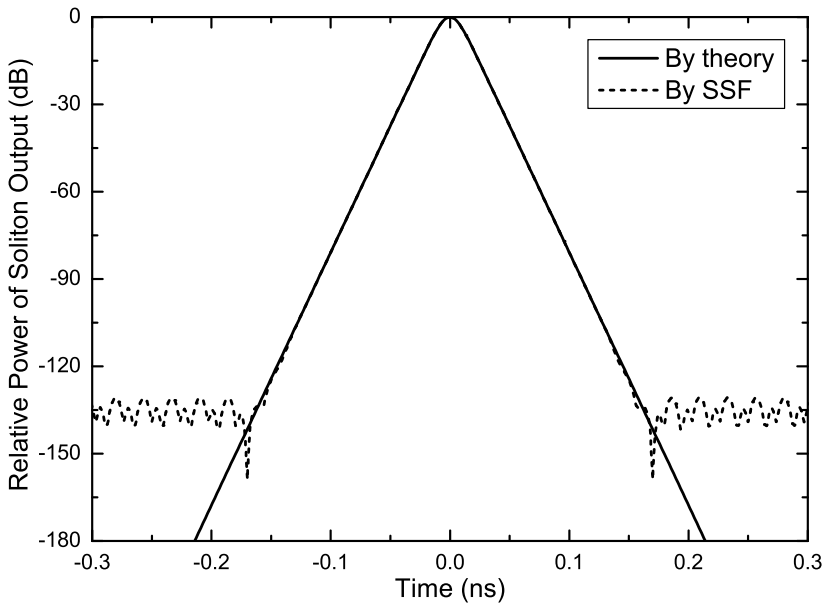

Figure 2.1: Simulation results for soliton output based on theory and SSF numerical method (normalized to peak power).

negligible. Hence the numerical results by SSF method provide a reliable reference.

2.5 Literature Review

To meet the increasing bandwidth demand in access networks, SCM optical fibre communication systems have attracted attention for decades. In the early stage, the studies centred on HFC CATV systems with a single optical channel [4, 63] where the subcarrier frequencies were quite low. However, a typical SCM optical communication system today may also involve WDM techniques [5, 43, 44, 64, 65]. The subcarrier frequencies have also increased from RF to millimetre-wave band; this in turn requires more sophisticated technologies such as external modulation, electrooptical upconversion, microwave remote generation, optical phase lock loop, etc., [16, 19, 36–39, 66–69]. Thus, system using SCM technique have become more complicated with time.

The impairment induced by optical fibre link in SCM systems is always a major concern in system design. This impairment can come from optical transceiver, fibre dispersion and fibre nonlinearities [21–24, 29, 36, 40, 42–44, 65, 66, 70–73]. P. P. Mitra and J. B. Stark have shown that the information capacity of optical fibre communications is limited by nonlinearities [74]. Many works have confirmed the great impact of various nonlinearities in optical fibre links, such as SPM, XPM, SRS and DD-MZM, on the system performance [5, 29–31, 75]. Normally, the impairment due to the optical fibre link is frequency dependent because the fibre dispersion, the fibre nonlinearities and the response of modulators and photodetectors are frequency dependent. Therefore, the systems operating at higher frequencies may encounter more serious impairments than those at lower frequencies. Because the modulating subcarrier frequencies in current SCM systems tend to be in the millimetre wave frequency range, such as those shown in Table 1.1, the study of such impairment becomes very important.

The most serious problem caused by fibre dispersion is RF power fading. Since fibre dispersion creates phase difference between the two side bands of a double sideband modulated optical carrier, RF power detected at the receiver will fade completely when the two side bands are out of phase. Therefore, optical single sideband (OSSB) modulation is typically implemented through dual-drive Mach-Zehnder modulator (DD-MZM) to combat power fading due to fibre dispersion for many SCM systems, especially microwave fibre-optic links [5, 42, 69]. This, plus its wider modulation bandwidth compared with direct modulation of laser diode, makes DD-MZM quite popular in SCM systems [19, 76–79].

However, DD-MZM exhibits a cosine transfer function. The distortion due to MZM external modulator in conventional digital optical fibre communication systems has been studied intensively due to the extensive usage of the MZM in these systems [80, 81]. Then, the nonlinear distortion due to DD-MZM should also be addressed in an SCM system using DD-MZM. Currently, the analysis of this nonlinear distortion due to DD-MZM is limited to some small signal approximation cases [40, 42] or complicated series expansion [36, 65, 66]. Hence the applications of those results are rather limited. This is an important problem addressed in this thesis; considerable effort has been spent in deriving closed form expressions for the cases where large RF signals are applied to DD-MZM.

The nonlinear distortion due to fibre nonlinearity also has attracted attention in SCM systems. Normally in conventional digital optical fibre communication systems, numerical methods such as SSF and Volterra series approach are used to analyse the nonlinear distortion due to fibre nonlinearity [82,83]. For SCM systems, analytical studies with closed-form expressions are preferred. M. R. Phillips calculated the second and third harmonics in the case of lossless fibre due to SPM in [84], and later, in [85], fibre loss was included to get a new expression for CSO and two limits for CTB. In 1996 an experiment [86] was conducted to verify the CSO induced by SPM, which showed that it could cause intolerable amounts of CSO distortion in external modulation systems even when the transmission distance is only a few tens of kilometres. In 1995 the effects of XPM in WDM SCM systems were investigated [87]. Following that, experiment as well as theoretical analysis was performed in [43]. Both analyses were based on two channels

modulated by a single tone with the same frequency. An analysis for two channels with one CW and the other single tone modulated was also introduced in [29, 43, 44, 65, 72, 73].

The methods of the analyses for fibre nonlinearities in SCM lightwave systems available so far are not adequate to fully understand the impairment due to fibre nonlinearities. For instance, the analysis in [43, 44] is adequate when the modulating subcarrier frequency is not very high, as the case is in CATV systems. However, when the frequency goes up to tens of GHz, the models in [43, 44] will result in significant error even for short fibre links since these models essentially predict an infinite increase of nonlinear distortion along with the fibre length, which in practice is impossible. The models presented by other authors, such as those in [28, 29, 65, 88], are still based on pump-probe model and generally cannot be used for the analysis of the intermodulation across optical channels due to XPM. Solution of these problems has been attempted in this thesis.

For SCM systems with WDM, the analyses are normally based on two optical channels to study the effects of SRS and XPM [28,29,43,44,65,72,73,88]. The results based on two optical channels can be easily expanded to a system with more optical channels by regarding the system as a summation of several systems with two optical channels only [29, 75]. The interactions between these two-optical-channel systems are neglected in this approach. This is reasonable since these are generally weaker, especially for systems with short fibre length as faced by most SCM systems used in access networks. Therefore, in this thesis, we also follow this model with two optical channels only to study SCM systems with WDM.

Chapter 3

Nonlinear Distortion due to DD-MZM

Optical modulators are an essential component in lightwave systems. However, generally, these may also be the most important source of nonlinear distortion in the systems, especially in single-wavelength channel systems. Direct modulation of laser diode (LD) is the most straightforward method to modulate the lightwave. Hence the nonlinear distortion due to direct modulation has been studied intensively [21–24, 70]. However, the modulation bandwidth of direct modulation is quite limited. Therefore, external modulators, such as dual-drive Mach-Zehnder external modulators (DD-MZM), are widely used in broadband applications [76].

For many years, DD-MZM and its variants have been used widely in the fibre-optic field for various purposes, such as communications, sensing and measurements [89, 90]. Often, a DD-MZM is driven by one or more radio frequency (RF) or microwave subcarriers. For example, in communication field, there has been an increasing interest in microwave fibre optic

links in recent years, which deliver microwave signals through optical fibre, taking advantage of the extremely low loss of fibre. Such systems cover a spectral range from several gigahertz to tens of gigahertz and are widely proposed for various applications such as high-speed wireless local area network and antenna remoting [19,77–79]. For all these applications, DD-MZM plays an important role due to its wider modulation bandwidth and higher performance compared with direct modulation; besides modulation, such a modulator can also provide functions such as harmonic-generation and electrooptical upconversion.

For different applications, the DD-MZM may operate at different settings. Some systems drive the DD-MZM by large amplitude microwave subcarriers to meet the signal-to-noise ratio (SNR) requirement; some systems use small signal modulation but with a large number of subcarriers such as hybrid fibre coax (HFC) systems; some other systems bias the DD-MZM at some nonlinear operating point to realize functions such as electrooptical upconversion [36]. No matter what the applications of the DD-MZM, we always try to maximize the system performance. This requires a thorough knowledge of the DD-MZM due to its important role in the systems. A general and accurate analytical model will permit study of all systems in a uniform manner and should be very helpful for system design. However, due to the inherent nonlinearity of DD-MZM, typically small signal approximation has been used, e.g., [40, 42]. Results of the more general and rigorous analyses have been in terms of infinite series [36,65,66]. In particular, these works are for single-subcarrier modulation [66], or electrooptical upconversion where only one subcarrier is applied to the DD-MZM [36, 66]. For the subcarrier multiplexing (SCM) system studied in [65], only small signal modulation is

considered. Therefore, an exact analytical model for SCM systems using DD-MZM is lacking; if closed-form expressions are available, these will be a convenient and powerful tool for us to understand the nonlinear distortion in such systems.

In this chapter, we present an exact analytical model to study the dispersive transmission of microwave fibre-optic links using DD-MZM for single-subcarrier modulation at first. The effects of fibre nonlinearity are ignored in this chapter because these will be considered in Chapter 5. The model presented here results in simple closed form expressions for the RF power spectrum at the output of the detector. The model is more general than that used in [66] in that the modulation indices of the two DD-MZM drives can be unbalanced; such a scheme has been proposed to produce some chirped signal [42]. Hence, these results can be applied to almost all types of operation of DD-MZM. Expressions for two special cases, optical double sideband modulation (ODSB) and optical single sideband modulation (OSSB), are also included; based on these, calculated results are presented in a novel manner, providing insight into the evolution and power fading of fundamental subcarrier and 2nd harmonics. Then, based on the study for single-subcarrier modulation, the analysis is extended to subcarrier multiplexing (SCM) cases. We show that in an intensity modulation/direct detection (IM/DD) dispersive fibre-optic system using DD-MZM, the system can be completely studied through a set of closed form expressions. Two special cases are studied in detail: ODSB and OSSB. For these cases, some important system parameters, such as 1-dB compression point, the input 3rd-order intercept point (IIP3) and the system capacity, are derived for the first time. While this study is in a scenario of dispersive microwave fibre-optic links,

the results presented here can be used for all applications using DD-MZM and its variants. We believe that such an exact and generalized analysis of an SCM optical fibre system using DD-MZM, resulting in closed-form expressions, has not been reported earlier.

The rest of the chapter is organized as follows. The architecture of DD-MZM as well as its transfer function are introduced. Then the exact analytical model for single-subcarrier modulation using DD-MZM is present. The harmonic analyses for two special cases, ODSB and OSSB are presented. The next section contains the general theoretical analysis for multi-subcarrier modulation. Once again, we analyze ODSB and OSSB modulation in detail for this multi-subcarrier modulation case. In the following section, we give a thorough analysis of system performance for ODSB and OSSB modulation respectively, presenting some new results for important system parameters; also presented are measured results for intermodulation products (IMPs) of different orders. The final section summarizes and concludes this chapter.

3.1 Transfer Function of DD-MZM

External modulated optical systems using DD-MZM offer a number of advantages arising from the use of continuous-wave (CW) laser sources. Semiconductor lasers exhibit reduced relative intensity noise (RIN) when not modulated and problems such as chirp and distortion in the laser are eliminated. Probably the major attraction of such systems is the ability to use higher power solid-state sources with lower RIN for some applications. On the other hand, the main disadvantage of external modulated SCM systems is the nonlinearity of the light output power versus voltage transfer characteristics of DD-MZM.

A DD-MZM has two waveguides with equal length. The refractive index of the waveguides can be changed a little by applying an electric field. This refractive index change is proportional to the strength of the electric field. An input optical field splits equally into two parts, which enter and propagate through the two waveguides separately. The refractive index change due to the applied electric field leads to the relative optical field phase variation according to the strength of the electric field. Therefore, the combination of the two waveguides' output results in interference and finally leads to intensity variation according to the electric field.

Typically, only one waveguide of a MZM has an electric field applied, which is the so-called single-drive MZM (SD-MZM). A DD-MZM means that both waveguides have an electric field applied. SD-MZM has been widely used in optical communication systems as external intensity modulator for years, providing much better extinction ratio than direct modulation of laser. However, the DD-MZM provides a greater flexibility to control the properties of modulation output and enables one to realize more functions such as OSSB modulation and harmonic generation desired in some applications. Moreover, SD-MZM can be viewed as a special case of DD-MZM. Hence, the analysis of DD-MZM is also useful to analyze SD-MZM.

Assuming that the input optical field is $A_i(t)$ and the phase variations in the two waveguides due to the applied electric fields are $\pi V_1(t)/V_\pi$ and $\pi V_2(t)/V_\pi$ where V_π is the voltage required to vary the phase of optical field

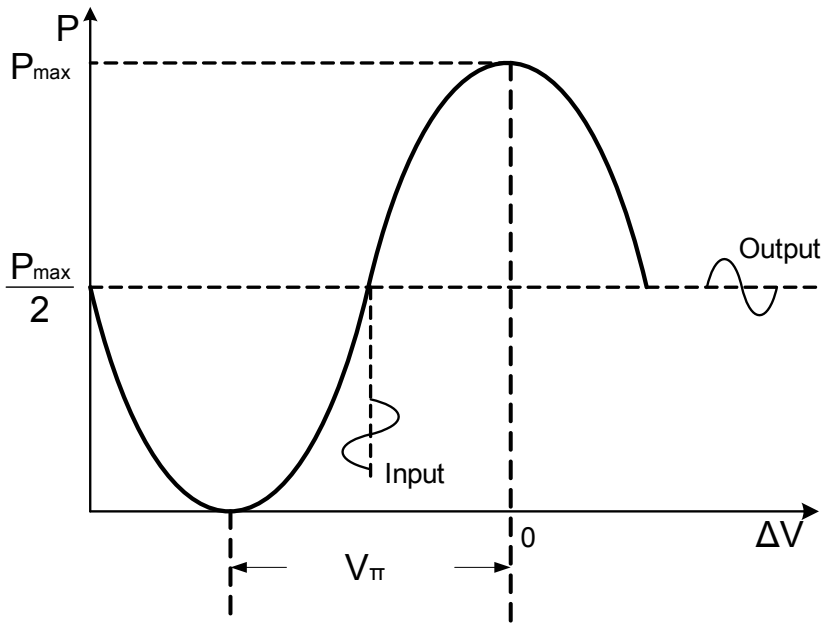

Figure 3.1: Transfer function of DD-MZM (Output optical intensity P vs. the applied electric field difference ΔV). P_{max} is the maximum output optical intensity.

by π, the output optical field of a DD-MZM can be written as

$$A_o(t) = \frac{1}{2}A_i(t) \cdot \exp\left[j\frac{\pi V_1(t)}{V_\pi}\right] + \frac{1}{2}A_i(t) \cdot \exp\left[j\frac{\pi V_2(t)}{V_\pi}\right] \tag{3.1}$$

Eq. (3.1) shows that the input optical field $A_i(t)$ is equally split into two branches to enter the two waveguides. The phase variations in the two waveguides due to the applied electric fields $V_1(t)$ and $V_2(t)$ result in the phase modulation of the signal in the two waveguides as shown by the two terms at the right hand side of Eq. (3.1). The outputs of the two waveguides are then combined together to form the final output optical field $A_o(t)$.

Hence, the conjugate of the output optical field is

$$A_o^*(t) = \frac{1}{2}A_i^*(t) \cdot \exp\left[-j\frac{\pi V_1(t)}{V_\pi}\right] + \frac{1}{2}A_i^*(t) \cdot \exp\left[-j\frac{\pi V_2(t)}{V_\pi}\right] \tag{3.2}$$

The output intensity is then

$$\begin{aligned} P_o(t) &= |A_o(t)|^2 = A_o(t)A_o^*(t) \\ &= \frac{1}{2}P_i(t) + \frac{1}{2}P_i(t)\cos\left[\pi\frac{V_1(t) - V_2(t)}{V_\pi}\right] \\ &= \frac{1}{2}P_i(t) + \frac{1}{2}P_i(t)\cos\left[\pi\frac{\Delta V(t)}{V_\pi}\right] \end{aligned} \tag{3.3}$$

where $P_i(t) = |A_i(t)|^2$ is the input optical intensity and $\Delta V(t) = V_1(t) - V_2(t)$. Eq. (3.3) shows that the output optical intensity of a DD-MZM is determined by the difference between the two electric fields and the output power versus voltage transfer function is a raised-cosine, as shown in Figure 3.1.

The raised-cosine transfer functions of DD-MZM leads to operation at a bias point known as the quadrature point (the half-power point) for most applications. From the DD-MZM transfer functions or P-ΔV characteristics of Eq. (3.3), it can be seen that the slope efficiency and therefore link gain can be improved by using DD-MZM with low V_π. Even for a given modulation depth, overall link gain can be further enhanced simply by increasing the source power level (P_i). At the quadrature point, even-order nonlinearities are minimised but odd-order are problematical. In some SCM systems using equi-spaced subcarriers, a large number of triple beat products will fall at frequencies coincident with the subcarrier frequencies, especially near the centre of the band.

The above analysis of DD-MZM does not include the effect of fibre dispersion. Usually, a practical SCM optical communication system has some dispersion and this dispersion will change the overall impact of DD-MZM

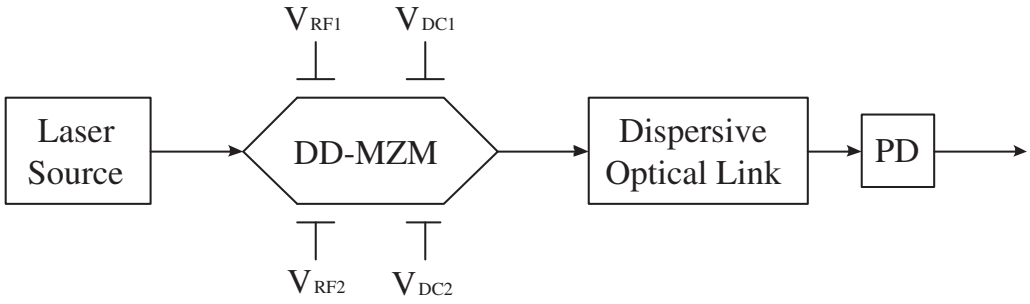

Figure 3.2: Subcarrier multiplexing dispersive microwave fibre-optic link using DD-MZM. PD: Photo-detector.

significantly. Figure 3.2 shows a dispersive microwave fibre-optic link using DD-MZM for subcarrier multiplexing. The electric voltages applied on the two branches of a DD-MZM consist of a dc bias term and an RF component:

$$V_1(t) = V_{DC1} + \sum_{i=1}^{M} V_{RF1i} \sin(\omega_{rfi} + \psi_{RF1i}) \tag{3.4a}$$

$$V_2(t) = V_{DC2} + \sum_{i=1}^{M} V_{RF2i} \sin(\omega_{rfi} + \psi_{RF2i}) \tag{3.4b}$$

where V_{DC1}, V_{DC2} are the dc terms, V_{RF1i}, ψ_{RF1i} and V_{RF2i}, ψ_{RF2i} are the amplitude and phase of the i-th RF component on the two branches respectively and ω_{rfi} is the angular frequency of the i-th RF component. M is the total number of subcarriers. The parameters in Eq. (3.4) are related to the parameters used for derivation later according to the following equations:

$$m_{1i} = \frac{\pi V_{RF1i}}{V_\pi} \tag{3.5a}$$

$$m_{2i} = \frac{\pi V_{RF2i}}{V_\pi} \tag{3.5b}$$

$$\omega_i = \omega_{rfi} \tag{3.5c}$$

$$\theta'_{1i} = \psi_{RF1i} \tag{3.5d}$$

$$\theta_{0i} = \psi_{RF2i} \tag{3.5e}$$

$$\theta_2 = \frac{\pi(V_{DC1} - V_{DC2})}{V_\pi} \tag{3.5f}$$

where V_π is the DD-MZM switching voltage.

3.2 Analysis for Single-Subcarrier Modulation Using DD-MZM

3.2.1 The Exact Analytical Model

We consider a generalized case where the drives in the DD-MZM are unbalanced. Then, the output optical field envelope of Mach-Zehnder Modulator (MZM) can be written as [91]:

$$\begin{aligned} A(t) &= A_0 \cdot \exp[jm_1 \cos(\omega_{rf} t + \theta_1) + j\theta_2] + A_0 \cdot \exp[jm_2 \cos(\omega_{rf} t)] \\ &= A_0 \cdot \sum_{n=-\infty}^{\infty} a_n \cdot \exp(jn\omega_{rf} t) \qquad (3.6a) \\ a_n &= j^n \cdot [J_n(m_1) \exp(jn\theta_1 + j\theta_2) + J_n(m_2)] \qquad (3.6b) \end{aligned}$$

where m_1 and m_2 are modulation indices of the two branches of DD-MZM respectively, ω_{rf} is the angular frequency of the modulating microwave signal, θ_1 is the phase difference between the microwave drives of the two branches and θ_2 is the bias phase shift. $J_n(x)$ is the Bessel function of first kind with order n and argument x. Next, due to fibre dispersion, the output spectrum at fibre length z is written as

$$\begin{aligned} \tilde{A}(z,\omega) &= \tilde{A}(\omega) \cdot \exp\left(\frac{j\beta_2 \omega^2 z}{2}\right) \\ &= 2\pi A_0 \sum_{n=-\infty}^{\infty} a_n \cdot \exp\left[\frac{j\beta_2 (n\omega_{rf})^2 z}{2}\right] \delta(\omega - n\omega_{rf}) \qquad (3.7) \end{aligned}$$

where $\tilde{A}(z,\omega)$ and $\tilde{A}(\omega)$ are the Fourier transform of optical field envelope at fibre length z and 0, respectively, β_2 is the 2nd-order fibre dispersion

parameter. Similarly, we can get the expression for the conjugate of optical field envelope. Then the spectrum of the optical power incident on the photodetector for detection is

$$\begin{aligned}
\tilde{P}(z,\omega) &= \frac{\tilde{A}(z,\omega) \otimes \tilde{A}^*(z,\omega)}{2\pi} \\
&= 2\pi A_0^2 \sum_{N=-\infty}^{\infty} \tilde{P}(z, N\omega_{rf}) \cdot \delta(\omega - N\omega_{rf}) \qquad (3.8a) \\
\tilde{P}(z, N\omega_{rf}) &= \sum_{k=-\infty}^{\infty} a_{k+N} a_k^* \exp\left[\frac{j\beta_2(N^2+2Nk)\omega_{rf}^2 z}{2}\right] \\
&= \exp\left(\frac{jN\phi}{2}\right) \sum_{k=-\infty}^{\infty} a_{k+N} a_k^* \exp(jk\phi) \qquad (3.8b) \\
a_{k+N}a_k^* &= j^N e^{jN\theta-1} J_{N+k}(m_1) J_k(m_1) + j^N J_{N+k}(m_2) J_k(m_2) \\
&\quad + j^N e^{j(N\theta_1+\theta_2)} J_{N+k}(m_1) J_k(m_2) e^{jk\theta_1} \\
&\quad + j^N e^{-j\theta_2} J_{N+k}(m_2) J_k(m_1) e^{-jk\theta_1} \qquad (3.8c)
\end{aligned}$$

where $\otimes$ denotes convolution and $N = n - k$, $\phi = \beta_2 N \omega_{rf}^2 z$. With Eq. (3.8c), Eq. (3.8b) can be re-written as

$$\begin{aligned}
\tilde{P}(z, N\omega_{rf}) &= \exp\left[jN\left(\theta_1 + \frac{\phi+\pi}{2}\right)\right] \cdot \sum_{k=-\infty}^{\infty} J_{N+k}(m_1) J_k(m_1) e^{jk\phi} \\
&\quad + \exp\left[j\frac{N(\phi+\pi)}{2}\right] \cdot \sum_{k=-\infty}^{\infty} J_{N+k}(m_2) J_k(m_2) e^{jk\phi} \\
&\quad + \exp\left[jN\left(\theta_1 + \frac{\phi+\pi}{2}\right) + j\theta_2\right] \cdot \sum_{k=-\infty}^{\infty} J_{N+k}(m_1) J_k(m_2) e^{jk(\phi+\theta_1)} \\
&\quad + \exp\left[j\frac{N(\phi+\pi)}{2} - j\theta_2\right] \cdot \sum_{k=-\infty}^{\infty} J_{N+k}(m_2) J_k(m_1) e^{jk(\phi-\theta_1)} \qquad (3.9)
\end{aligned}$$

Let $\alpha_1 = \alpha_2 = \phi$, $\alpha_3 = \phi + \theta_1$ and $\alpha_4 = \phi - \theta_1$. With Graf's addition theorem [91], Eq. (3.9) reduces to

$$\tilde{P}(z, N\omega_{rf}) = \exp\left[jN\left(\theta_1 + \frac{\phi+\pi}{2} + \chi_1\right)\right] \cdot J_N(w_1)$$

$$
\begin{aligned}
&+\exp\left[jN\left(\frac{\phi+\pi}{2}+\chi_2\right)\right]\cdot J_N(w_2)\\
&+\exp\left[jN\left(\theta_1+\frac{\phi+\pi}{2}+\chi_3\right)+j\theta_2\right]\cdot J_N(w_3)\\
&+\exp\left[jN\left(\frac{\phi+\pi}{2}+\chi_4\right)-j\theta_2\right]\cdot J_N(w_4) \qquad (3.10a)
\end{aligned}
$$

$$w_i=\sqrt{u_i^2+v_i^2-2u_iv_i\cos\alpha_i} \qquad (3.10b)$$

$$u_i-v_i\cos(\alpha_i)=w_i\cos\chi_i \qquad (3.10c)$$

$$v_i\sin\alpha_i=w_i\sin\chi_i \qquad (3.10d)$$

where $u_1=v_1=m_1$ for w_1 , $u_2=v_2=m_2$ for w_2, $u_3=m_1$ and $v_3=m_2$ for w_3, $u_4=m_2$ and $v_4=m_1$ for w_4. u_i, v_i and w_i form a triangle with α_i and χ_i as two of its angles. Specially, if $\alpha_i=0$, then Eq. (3.10) leads to $\chi_i=0$ and $w_i=u_i-v_i$.

The parameter ϕ, representing the accumulated fibre dispersion, plays a critical role in the four terms of Eq. (3.10), showing the importance of fibre dispersion in characterizing the evolution of harmonics along fibre. The four terms in the right hand side of the equation represent the coherent interference results of the outputs of the two waveguides of the DD-MZM at the photodetector after dispersive transmission. They show that the evolution of harmonics follows the Bessel functions of the first kind whose oder is the order of the harmonics. The values of modulation indices, bias point, phase difference between RF carriers and the parameter ϕ characterize the relationship between the four terms. Compared to conventional analyses in terms of small signal approximation or infinite series, e.g., [36,40,42,65,66], Eq. (3.10) gives us a complete and accurate description of each harmonic, in a very neat, closed form, for dispersive transmission in microwave fibre optic links using DD-MZM and hence greatly simplifies our analyses of such

links without any loss of accuracy.

3.2.2 ODSB and OSSB for Single-Subcarrier Modulation

ODSB and OSSB modulation are the two most popular formats in microwave fibre-optic links. For the commonly used case of balanced drives, $m_1 = m_2 = m$ for both formats and $\chi_i = (\pi - \alpha_i)/2$, $w_i = 2m \cdot \sin(\alpha_i/2)$.

For ODSB modulation, $\theta_1 = \pi$, $\chi_1 = \chi_2 = (\pi - \phi)/2$, $\chi_3 = -\phi/2$ and $\chi_4 = \pi - \phi/2$. Using Eq. (3.10), one gets:

$$\tilde{P}(z, N\omega_{rf}) = 2 \cdot J_N\left(2m \sin\frac{\phi}{2}\right) + 2 \cdot j^N \cos(\theta_2) \cdot J_N\left(2m \cos\frac{\phi}{2}\right) \tag{3.11a}$$

$$\tilde{P}(z, N\omega_{rf}) = 2 \cdot j^{N-1} \sin(\theta_2) \cdot J_N\left(2m \cos\frac{\phi}{2}\right) \tag{3.11b}$$

Eq. (3.11a) and Eq. (3.11b) are for even and odd order harmonics, respectively.

For OSSB modulation, $\theta_1 = \pi/2$, $\chi_1 = \chi_2 = (\pi - \phi)/2$, $\chi_3 = \pi/4 - \phi/2$ and $\chi_4 = 3\pi/4 - \phi/2$. Then

$$\begin{aligned}\frac{\tilde{P}(z, N\omega_{rf})}{\exp(j5N\pi/4)} = 2 \cdot \cos\frac{N\pi}{4} \cdot J_N\left(2m \sin\frac{\phi}{2}\right) \\ + \exp(j\theta_2) \cdot J_N\left\{2m \sin\left[\frac{\phi}{2} + \left(\frac{\pi}{4}\right)\right]\right\} \\ + \exp(-j\theta_2) \cdot J_N\left\{2m \sin\left[\frac{\phi}{2} - \left(\frac{\pi}{4}\right)\right]\right\}\end{aligned} \tag{3.12}$$

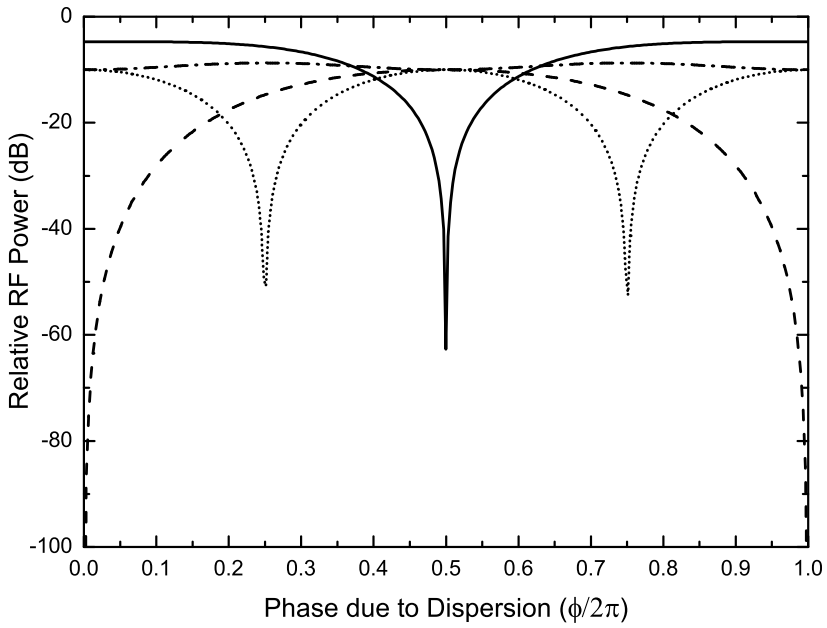

Figure 3.3: Detected microwave signal power for fundamental and second harmonic normalized to the detected dc level vs $\phi/(2\pi)$ for ODSB modulation. (N, θ_2) is (1, $\pm\pi/2$) for solid line, (2, $\pm\pi/2$) for dashed line, (2, 0) for dotted line and (2, $\pm\pi$) for dash-dot line. Modulation index = 0.92.

Eqs. (3.11) and (3.12) show that the harmonic evolution along fibre is completely characterized by two simple parameters, ϕ and θ_2. ϕ is a key parameter, incorporating the effect of fibre dispersion parameter and length, as well as microwave frequency and harmonic order.

As a demonstration of the application of the above expressions, Figures 3.3 and 3.4 show the detected microwave signal magnitudes for fundamental signal and second harmonic as a function of $\phi/(2\pi)$, for ODSB and OSSB modulation, respectively, for a few different bias settings of the modulator. Numerical results (not shown) are exactly the same as the analytical results calculated from Eqs. (3.11) and (3.12). The simple expressions in Eqs. (3.11) and (3.12) also make performance prediction quite easy and enable one to optimize settings (m and θ_2) of DD-MZM for different applications such as upconversion and harmonic generation. For example, $m = 0.92$ is chosen in

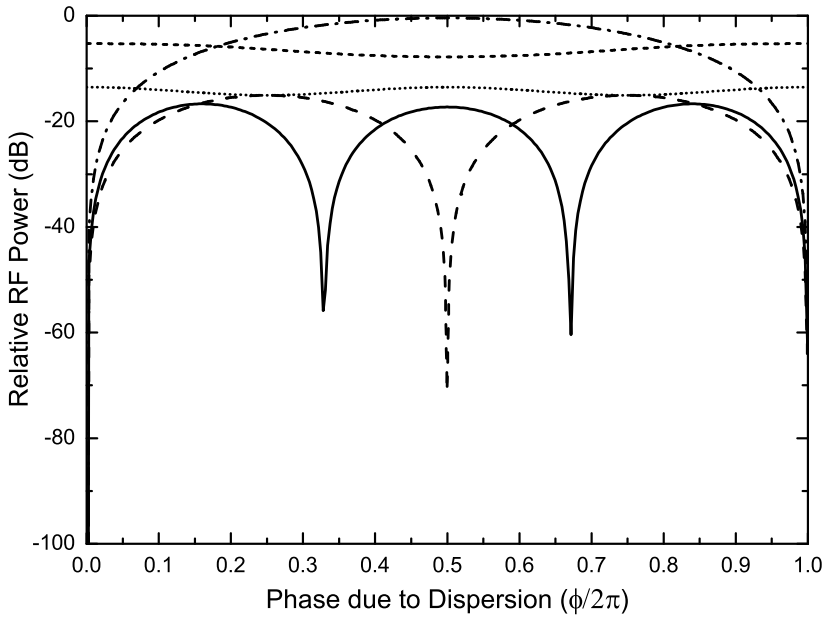

Figure 3.4: Detected microwave signal power for fundamental and second harmonic normalized to the detected dc level vs $\phi/(2\pi)$ for OSSB modulation. (N, θ_2) is (1, $\pm\pi/2$) for short dash line, (1, 0) for dash-dot line, (1, $\pm\pi$) for solid line, (2, $\pm\pi/2$) for dashed line, (2, 0) and (2, $\pm\pi$) for dotted line. Modulation index = 1.

Figure 3.3 for ODSB modulation, which maximizes the detected microwave fundamental signal magnitude for bias $\pm\pi/2$ (the solid line) according to Eq. (3.11). Larger m will not result in link performance improvement; it will cause stronger harmonics and more dips in Figure 3.3, meaning quicker power fading. Similarly, for OSSB modulation, $m = 1$ used in Figure 3.4 also maximizes the detected microwave fundamental signal magnitude for bias 0 (the dash-dot line) and it is the smallest one of the 3 bias settings to realize the same goal.

Figures 3.3 and 3.4 also show some cases without significant power fading: (2, $\pm\pi$) for ODSB, (1, $\pm\pi/2$), (2, 0) and (2, $\pm\pi$) for OSSB. The first two have been studied extensively [5, 42, 66, 92]. However, it can be shown that the expressions for (2, 0) and (2, $\pm\pi$) of OSSB are the same as that for (2, $\pm\pi$) of ODSB except being smaller by half and a $\pi/4$ rotation, which shows

that these cases may also be useful in application of harmonics generation. On the contrary, a noteworthy case is (1, $\pm\pi$) of OSSB, which experiences very serious power fading compared with other cases. Such quick power fading cases may be useful for some microwave photonic filter applications. The results for OSSB, corresponding to (N, θ_2) = (2, 0), (2, $\pm\pi$), and (1, $\pm\pi$), do not appear to have been discussed in the literature so far.

3.3 Analysis for Multi-Subcarrier Modulation Using DD-MZM

In this section, the derivation for single subcarrier modulation in Section 3.2 is generalized to multi-subcarrier modulation. Therefore, vectors, with each entry representing one subcarrier, are used throughout this section. The definitions of some symbols are listed in Table 3.1.

3.3.1 The Exact Analytical Model

For microwave fibre-optic links with subcarrier multiplexing (SCM), the output optical field envelope of Mach-Zehnder Modulator (MZM) can be written as:

$$\begin{aligned} A(t) &= A_0 \exp\left[j\mathbf{m}_1\mathbf{cos}(\boldsymbol{\omega}_{rf}t + \boldsymbol{\theta}'_1) + j\theta_2\right] \\ &\quad + A_0 \exp\left[j\mathbf{m}_2\mathbf{cos}(\boldsymbol{\omega}_{rf}t + \boldsymbol{\theta}_0)\right] \\ &= A_0 \sum_{n_1=-\infty}^{\infty} \cdots \sum_{n_M=-\infty}^{\infty} a_{\mathbf{n}} \cdot \exp(j\mathbf{n}\boldsymbol{\omega}_{rf}t) \end{aligned} \tag{3.13a}$$

$$\begin{aligned} a_n &= j^{\Sigma\mathbf{n}} \cdot \left[\Pi\mathbf{J}_{\mathbf{n}}(\mathbf{m}_1)\right] \exp(j\mathbf{n}\boldsymbol{\theta}'_1 + j\theta_2) \\ &\quad + j^{\Sigma\mathbf{n}} \cdot \left[\Pi\mathbf{J}_{\mathbf{n}}(\mathbf{m}_2)\right] \exp(j\mathbf{n}\boldsymbol{\theta}_0) \end{aligned} \tag{3.13b}$$

Table 3.1: The Definitions of Some Symbols

$\mathbf{N} =$ $(N_1 \ \cdots \ N_M)$	harmonic orders of subcarriers
$\mathbf{m}_1 =$ $(m_{11} \ \cdots \ m_{1M})$	modulation indices of subcarriers in one branch of the DD-MZM
$\mathbf{m}_2 =$ $(m_{21} \ \cdots \ m_{2M})$	modulation indices of subcarriers in the other branch of DD-MZM
$\boldsymbol{\omega}_{rf} =$ $(\omega_{rf1} \ \cdots \ \omega_{rfM})^T$	angular frequency of subcarriers
$\boldsymbol{\theta}_1 =$ $(\theta_{11} \ \cdots \ \theta_{1M})$	phase difference between the subcarriers in the branches of the DD-MZM
θ_2	bias phase shift of the DD-MZM
$\mathbf{J_n}(\mathbf{x}) =$ $(J_{n_1}(x_1) \ \cdots \ J_{n_M}(x_M))$	a vector of the Bessel functions of the first kind
$\mathbf{F}(\mathbf{x}) =$	a vector of function F, $\mathbf{F}(\mathbf{x}) = (\mathrm{F}(x_1) \ \cdots \ \mathrm{F}(x_M))$
β_2	the 2nd-order fiber dispersion parameter
$D = 17\,\mathrm{ps/nm \cdot km}$	the dispersion parameter and the value used in the paper
Σ	an operator, $\Sigma\mathbf{a} = a_1 + \ \cdots \ + a_M$
Π	an operator, $\Pi\mathbf{a} = a_1 a_2 \ \cdots \ a_M$
$\bullet$	an operator, $\mathbf{a} \bullet \mathbf{b} = (a_1 b_1 \ \cdots \ a_M b_M)$
$(x)_M$	a vector, $(x)_M = (x \ \cdots \ x)$

where A_0 is the optical field amplitude in one branch of the DD-MZM; $\mathbf{m}_1 = (m_{11} \cdots m_{1M})$ and $\mathbf{m}_2 = (m_{21} \cdots m_{2M})$ are the modulation indices of the two branches of DD-MZM respectively with each element for one microwave subcarrier; $\boldsymbol{\omega}_{rf} = (\omega_{rf1} \cdots \omega_{rfM})^T$ is the angular frequency of each modulating microwave subcarrier; $\boldsymbol{\theta}'_1 = (\theta'_{11} \cdots \theta'_{1M})^T$, $\boldsymbol{\theta}_0 = (\theta_{01} \cdots \theta_{0M})^T$ are the initial phases of microwave subcarriers for the two branches of DD-MZM respectively with each element for one microwave subcarrier and θ_2 is the bias phase shift; $\mathbf{n} = (n_1 \cdots n_M)$ is the harmonic order of each microwave subcarrier; $\mathbf{J_n}(\mathbf{x})$ is a function vector with its each element equal to $J_{n_i}(x_i)$, the Bessel function of first kind with order n_i and argument x_i; M is the total subcarrier number. Next, due to fibre dispersion, the output spectrum at fibre length z is written as:

$$\begin{aligned}\tilde{A}(z,\omega) &= \tilde{A}(\omega)\cdot\exp\left(\frac{j\beta_2\omega^2 z}{2}\right)\\ &= 2\pi A_0\cdot\sum_{n_1=-\infty}^{\infty}\cdots\sum_{n_M=-\infty}^{\infty}\\ &\quad a_{\mathbf{n}}\cdot\exp\left[\frac{j\beta_2(\mathbf{n}\boldsymbol{\omega}_{rf})^2 z}{2}\right]\delta(\omega-\mathbf{n}\boldsymbol{\omega}_{rf})\end{aligned} \tag{3.14}$$

where $\tilde{A}(z,\omega)$ and $\tilde{A}(\omega)$ are the Fourier transform of optical field envelope at fibre length z and 0 respectively, β_2 is the 2nd-order fibre dispersion parameter. Similarly, we can get the expression for the conjugate of optical field envelope. Then the spectrum of the optical power incident on the photodetector for detection is:

$$\begin{aligned}\tilde{P}(z,\omega) &= \frac{\tilde{A}(z,\omega)\otimes\tilde{A}^*(z,\omega)}{2\pi}\\ &= 2\pi A_0^2\sum_{N_1=-\infty}^{\infty}\cdots\sum_{N_M=-\infty}^{\infty}\\ &\quad \tilde{P}(z,\mathbf{N}\boldsymbol{\omega}_{rf})\delta(\omega-\mathbf{N}\boldsymbol{\omega}_{rf})\end{aligned} \tag{3.15a}$$

$$\tilde{P}(z,\mathbf{N}\boldsymbol{\omega}_{rf}) = \exp\left(\frac{j\mathbf{N}\boldsymbol{\Phi}}{2}\right)\sum_{k_1=-\infty}^{\infty}\cdots\sum_{k_M=-\infty}^{\infty} a_{\mathbf{k}+\mathbf{N}}a_{\mathbf{k}}^{*}\exp(j\mathbf{k}\boldsymbol{\Phi}) \tag{3.15b}$$

$$\begin{aligned}\frac{a_{\mathbf{k}+\mathbf{N}}a_{\mathbf{k}}^{*}}{j^{\Sigma\mathbf{N}}} = {} & e^{j\mathbf{N}\boldsymbol{\theta}_1'}\left[\Pi\mathbf{J}_{\mathbf{N}+\mathbf{k}}(m_1)\right]\left[\Pi\mathbf{J}_{\mathbf{k}}(m_1)\right] \\ & + e^{j\mathbf{N}\boldsymbol{\theta}_0}\left[\Pi\mathbf{J}_{\mathbf{N}+\mathbf{k}}(m_2)\right]\left[\Pi\mathbf{J}_{\mathbf{k}}(m_2)\right] \\ & + e^{j(\mathbf{N}\boldsymbol{\theta}_1'+\theta_2)}\left[\Pi\mathbf{J}_{\mathbf{N}+\mathbf{k}}(m_1)\right]\left[\Pi\mathbf{J}_{\mathbf{k}}(m_2)\right]e^{j\mathbf{k}\boldsymbol{\theta}_1} \\ & + e^{j(\mathbf{N}\boldsymbol{\theta}_0-\theta_2)}\left[\Pi\mathbf{J}_{\mathbf{N}+\mathbf{k}}(m_2)\right]\left[\Pi\mathbf{J}_{\mathbf{k}}(m_1)\right]e^{-j\mathbf{k}\boldsymbol{\theta}_1}\end{aligned} \tag{3.15c}$$

where $\otimes$ denotes convolution, $\mathbf{k} = (k_1 \cdots k_M)$, $\boldsymbol{\Phi} = \beta_2 z(\boldsymbol{\omega}_{rf}\mathbf{N}\boldsymbol{\omega}_{rf})$ and $\mathbf{N} = \mathbf{n}-\mathbf{k} = (N_1 \cdots N_M)$. Each element in $\mathbf{N}$ stands for the harmonic order of one subcarrier in the spectrum after intensity detection. For example, N_1 is the harmonic order of the first subcarrier. Therefore, $\mathbf{N}$ denotes the intermodulation distortion (IMP) pattern and $\mathbf{N}\boldsymbol{\omega}_{rf}$ is the angular frequency of intermodulation products (IMPs). $\boldsymbol{\theta}_1 = \boldsymbol{\theta}_1' - \boldsymbol{\theta}_0$ stands for the phase difference between the two branches for each microwave subcarrier. Let $\boldsymbol{\alpha}_1 = \boldsymbol{\alpha}_2 = \boldsymbol{\Phi}$, $\boldsymbol{\alpha}_3 = \boldsymbol{\Phi} + \boldsymbol{\theta}_1$ and $\boldsymbol{\alpha}_4 = \boldsymbol{\Phi} - \boldsymbol{\theta}_1$. For simplicity, we take one product in the third term of Eq. (3.15c) for demonstration of the derivation.

$$\begin{aligned}&\frac{a_{k_i+N_i}a_{k_i}^{*}\exp(jk_i\Phi_i)}{j^{N_i}\exp(N_i\theta_{1i}'+\theta_2)} \\ &\quad = \sum_{k_i=-\infty}^{\infty} J_{N_i+k_i}(m_{1i})J_{k_i}(m_{2i})\exp(jk_i\alpha_{3i}) \\ &\quad = e^{jN_i\chi_{3i}}J_{N_i}(w_{3i})\end{aligned} \tag{3.16a}$$

$$w_{3i} = \sqrt{m_{1i}^2 + m_{2i}^2 - 2m_{1i}m_{2i}\cos(\alpha_{3i})} \tag{3.16b}$$

$$w_i\cos(\chi_{3i}) = m_{1i} - m_{2i}\cos(\alpha_{3i}) \tag{3.16c}$$

$$m_{2i}\sin(\alpha_{3i}) = w_{3i}\sin(\chi_{3i}) \tag{3.16d}$$

The Graf's addition theorem is used for the derivation of Eq. (3.16) [91]. Therefore, we can re-write Eq. (3.15b) as:

$$\begin{aligned}\frac{\tilde{P}(z,\mathbf{N}\boldsymbol{\omega}_{rf})}{j^{\Sigma\mathbf{N}}\exp(j\mathbf{N}\boldsymbol{\theta}_0)} &= e^{j\mathbf{N}\left(\boldsymbol{\theta}_1+\frac{\boldsymbol{\Phi}}{2}+\boldsymbol{\chi}_1\right)}\cdot\left[\Pi\mathbf{J}_{\mathbf{N}}(\mathbf{w}_1)\right]\\ &\quad+e^{j\mathbf{N}\left(\frac{\boldsymbol{\Phi}}{2}+\boldsymbol{\chi}_2\right)}\cdot\left[\Pi\mathbf{J}_{\mathbf{N}}(\mathbf{w}_2)\right]\\ &\quad+e^{j\mathbf{N}\left(\boldsymbol{\theta}_1+\frac{\boldsymbol{\Phi}}{2}+\boldsymbol{\chi}_3\right)+j\theta_2}\cdot\left[\Pi\mathbf{J}_{\mathbf{N}}(\mathbf{w}_3)\right]\\ &\quad+e^{j\mathbf{N}\left(\frac{\boldsymbol{\Phi}}{2}+\boldsymbol{\chi}_4\right)-j\theta_2}\cdot\left[\Pi\mathbf{J}_{\mathbf{N}}(\mathbf{w}_4)\right] \qquad (3.17a)\end{aligned}$$

$$\mathbf{w}_i = \left[\mathbf{u}_i{}^2+\mathbf{v}_i{}^2-2\mathbf{u}_i\bullet\mathbf{v}_i\bullet\mathbf{cos}(\boldsymbol{\alpha}_i^T)\right]^{\frac{1}{2}} \qquad (3.17b)$$

$$\mathbf{w}_i\bullet\mathbf{cos}(\boldsymbol{\chi}_i^T) = \mathbf{u}_i-\mathbf{v}_i\bullet\mathbf{cos}(\boldsymbol{\alpha}_i^T) \qquad (3.17c)$$

$$\mathbf{v}_i\bullet\mathbf{sin}(\boldsymbol{\alpha}_i^T) = \mathbf{w}_i\bullet\mathbf{sin}(\boldsymbol{\chi}_i^T) \qquad (3.17d)$$

$\bullet$ in Eq. (3.17) denotes array multiplication, that is, the entry-by-entry product of two vectors with the same dimensions and $\mathbf{u}_1=\mathbf{v}_1=\mathbf{m}_1$ for $\mathbf{w}_1$, $\mathbf{u}_2=\mathbf{v}_2=\mathbf{m}_2$ for $\mathbf{w}_2$, $\mathbf{u}_3=\mathbf{m}_1$ and $\mathbf{v}_3=\mathbf{m}_2$ for $\mathbf{w}_3$, $\mathbf{u}_4=\mathbf{m}_2$ and $\mathbf{v}_4=\mathbf{m}_1$ for $\mathbf{w}_4$. $\mathbf{u}_i$, $\mathbf{v}_i$ and $\mathbf{w}_i$ form a triangle with $\boldsymbol{\alpha}_i$ and $\boldsymbol{\chi}_i$ as two of its angles. Eq. (3.17a) shows that the initial phase relationship between various microwave subcarriers does not have an effect on the final detected microwave signal magnitude except for a fixed phase shift according to $\mathbf{N}\boldsymbol{\theta}_0$.

3.3.2 ODSB and OSSB for Multi-Subcarrier Modulation

ODSB and OSSB modulation are the two most popular formats in microwave fibre-optic links. For both cases, the two branches of DD-MZM are driven at the same RF power, that is, $\mathbf{m}_1=\mathbf{m}_2=\mathbf{m}$. Hence, we can find that $\boldsymbol{\chi}_i=\left[(\pi)_M-\boldsymbol{\alpha}_i\right]/2$, $\mathbf{w}_i=2\mathbf{m}\bullet\mathbf{sin}\left(\boldsymbol{\alpha}_i^T\right)$, and $(\pi)_M=(\pi\cdots\pi)$ with M entries.

3.3.2.1 ODSB Modulation

For ODSB modulation, DD-MZM is typically biased at the quadrature point and the phase difference between the two RF drives is π. Here we keep the bias point arbitrary for generality. Therefore, $\boldsymbol{\theta}_1 = (\pi)_M$, $\boldsymbol{\chi}_1 = \boldsymbol{\chi}_2 = \big[(\pi)_M - \boldsymbol{\Phi}\big]/2$, $\boldsymbol{\chi}_3 = -\boldsymbol{\Phi}/2$ and $\boldsymbol{\chi}_4 = (\pi)_M - \boldsymbol{\Phi}/2$. Using Eq. (3.17), one can get:

$$\begin{aligned}\frac{\tilde{P}(z,\mathbf{N}\boldsymbol{\omega}_{rf})}{\exp(j\mathbf{N}\boldsymbol{\theta}_0)} &= 2\cdot\Pi\mathbf{J}_{\mathbf{N}}\left(2\mathbf{m}\bullet\mathbf{sin}\frac{\boldsymbol{\Phi}^T}{2}\right)\\ &\quad +2\cdot j^{\Sigma\mathbf{N}}\cos(\theta_2)\cdot\Pi\mathbf{J}_{\mathbf{N}}\left(2\mathbf{m}\bullet\mathbf{cos}\frac{\boldsymbol{\Phi}^T}{2}\right)\end{aligned} \tag{3.18a}$$

$$\frac{\tilde{P}(z,\mathbf{N}\boldsymbol{\omega}_{rf})}{\exp(j\mathbf{N}\boldsymbol{\theta}_0)} = 2\cdot j^{\Sigma\mathbf{N}-1}\sin(\theta_2)\cdot\Pi\mathbf{J}_{\mathbf{N}}\left(2\mathbf{m}\bullet\mathbf{cos}\frac{\boldsymbol{\Phi}^T}{2}\right) \tag{3.18b}$$

Eq. (3.18a) and Eq. (3.18b) are for subcarriers or intermodulation products (IMPs) with even $\Sigma\mathbf{N}$ and odd $\Sigma\mathbf{N}$ respectively.

Specially, for single-subcarrier modulation, Eq. (3.18a) and Eq. (3.18b) simplify into the following equations:

$$\begin{aligned}\frac{\tilde{P}(z,N\omega_{rf})}{\exp(jN\theta_0)} &= 2\cdot J_N\left(2m\sin\frac{\phi}{2}\right)\\ &\quad +2\cdot j^N\cos(\theta_2)\cdot J_N\left(2m\cos\frac{\phi}{2}\right)\end{aligned} \tag{3.19a}$$

$$\frac{\tilde{P}(z,N\omega_{rf})}{\exp(jN\theta_0)} = 2\cdot j^{N-1}\sin(\theta_2)\cdot J_N\left(2m\cos\frac{\phi}{2}\right) \tag{3.19b}$$

Eq. (3.19a) and Eq. (3.19b) are for even and odd order harmonics, respectively, and are identical to Eq. (3.11a) and Eq. (3.11b), respectively.

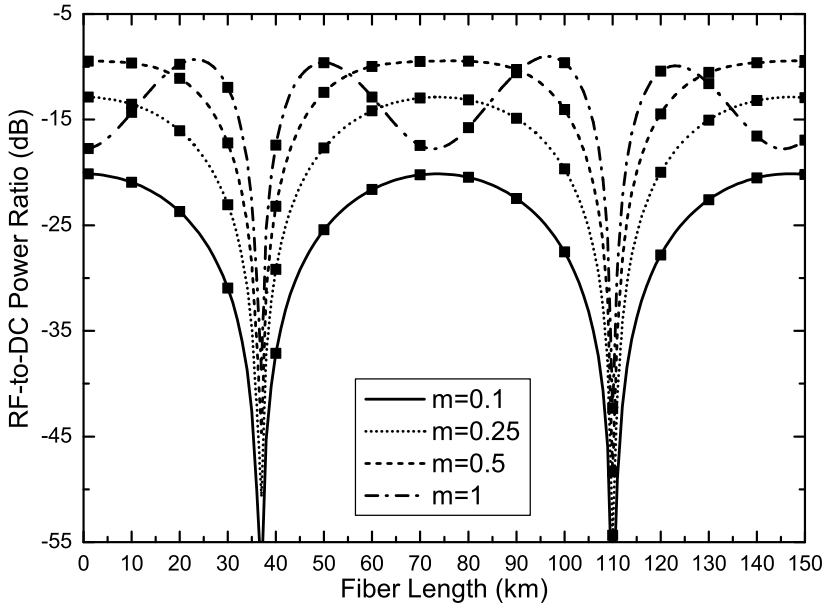

Figure 3.5: The detected RF power of the fundamental subcarrier normalized to detected dc power versus fiber length for several modulation indices for ODSB modulation. The markers represent the results of numerical simulation.

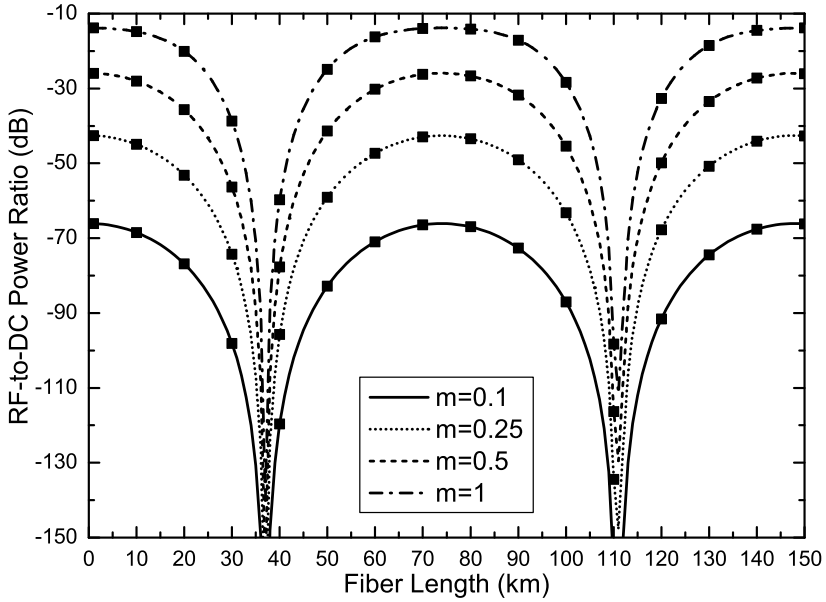

Figure 3.6: The detected RF power of the 3rd-order IMP normalized to detected dc power versus fiber length for several modulation indices for ODSB modulation. The markers represent the results of numerical simulation.

For the case of two DSB subcarriers propagating in a dispersive optical fiber link, Figures. 3.5 and 3.6 show calculated results, obtained from Eq. (3.18b), for the evolution of the fundamental subcarrier and the 3rd-order IMP (IMP3) along the fiber length. The angular frequencies of the modulating subcarriers are $\boldsymbol{\omega}_{rf}/(2\pi) = (10 \quad 10.1)$ GHz. The fundamental subcarrier $\mathbf{N} = (1 \quad 0)$ and the IMP3 $\mathbf{N} = (2 \quad -1)$ are shown in Figures. 3.5 and 3.6, respectively, for several values of modulation index. The well-known power fading behaviour for ODSB modulation due to dispersion is clearly visible. Numerical simulations based on split step Fourier (SSF) method [26] are also performed with fiber nonlinearity parameter set to 0 and the calculation step set to the whole fiber length. The simulation results shown as square markers are exactly the same as those by our analysis.

3.3.2.2 OSSB Modulation

For OSSB modulation, DD-MZM is typically biased at the quadrature point and the phase difference between the two RF drives is $\pi/2$. Similar to the ODSB case, we keep the bias point arbitrary for generality. Therefore, $\boldsymbol{\theta}_1 = (\pi/2)_M$, $\boldsymbol{\chi}_1 = \boldsymbol{\chi}_2 = \big[(\pi)_M - \boldsymbol{\Phi}\big]/2$, $\boldsymbol{\chi}_3 = (\pi/4)_M - \boldsymbol{\Phi}/2$ and $\boldsymbol{\chi}_4 = (3\pi/4)_M - \boldsymbol{\Phi}/2$. Then Eq. (3.17) leads to:

$$\begin{aligned}
&\frac{\tilde{P}(z, \mathbf{N}\boldsymbol{\omega}_{rf})}{\exp\big[j5(\Sigma\mathbf{N})\pi/4 + j\mathbf{N}\boldsymbol{\theta}_0\big]} \\
&= 2 \cdot \cos\frac{\pi\Sigma\mathbf{N}}{4} \cdot \Pi\mathbf{J}_{\mathbf{N}}\left(2\mathbf{m} \bullet \mathbf{sin}\frac{\boldsymbol{\Phi}^T}{2}\right) \\
&\quad + \exp(j\theta_2) \cdot \Pi\mathbf{J}_{\mathbf{N}}\left\{2\mathbf{m} \bullet \mathbf{sin}\left[\frac{\boldsymbol{\Phi}^T}{2} + \left(\frac{\pi}{4}\right)_M\right]\right\} \\
&\quad + \exp(-j\theta_2) \cdot \Pi\mathbf{J}_{\mathbf{N}}\left\{2\mathbf{m} \bullet \mathbf{sin}\left[\frac{\boldsymbol{\Phi}^T}{2} - \left(\frac{\pi}{4}\right)_M\right]\right\}
\end{aligned} \tag{3.20}$$

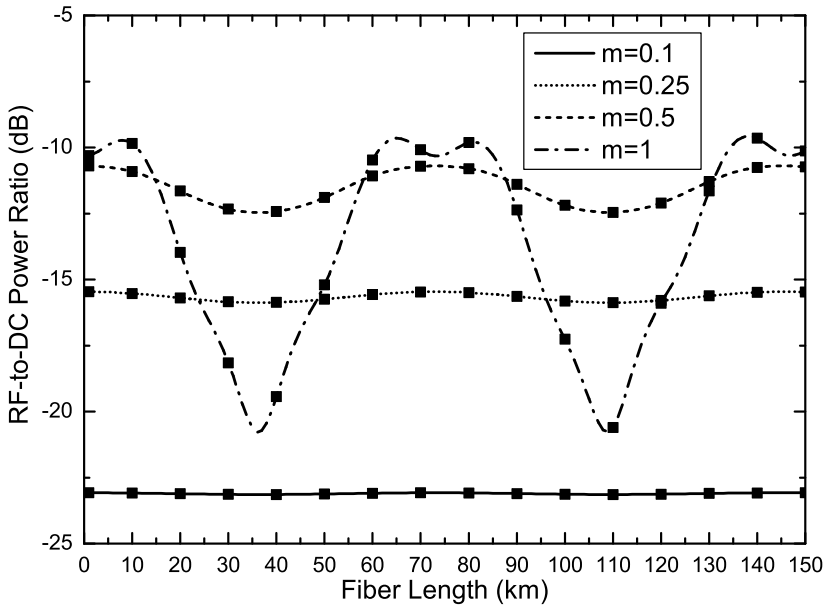

Figure 3.7: The detected RF power of the fundamental subcarrier normalized to detected dc power versus fiber length for several modulation indices for OSSB modulation. The markers represent the results of numerical simulation.

Specially, for single-subcarrier modulation, Eq. (3.20) simplifies into the following equation:

$$\begin{aligned}
&\frac{\tilde{P}(z, N\omega_{rf})}{\exp(j5N\pi/4 + jN\theta_0)} \\
&= 2 \cdot \cos\frac{N\pi}{4} \cdot J_N\left(2m \sin\frac{\phi}{2}\right) \\
&\quad + \exp(j\theta_2) \cdot J_N\left\{2m \sin\left[\frac{\phi}{2} + \left(\frac{\pi}{4}\right)\right]\right\} \\
&\quad + \exp(-j\theta_2) \cdot J_N\left\{2m \sin\left[\frac{\phi}{2} - \left(\frac{\pi}{4}\right)\right]\right\}
\end{aligned} \tag{3.21}$$

which is identical to Eq. (3.12).

For the case of two SSB subcarriers propagating in a dispersive optical fiber link, Figures. 3.7 and 3.8 show calculated results, obtained from Eq. (3.20), for the evolution of the fundamental subcarrier and the IMP3 along the fiber length. The angular frequencies of the modulating subcarriers are

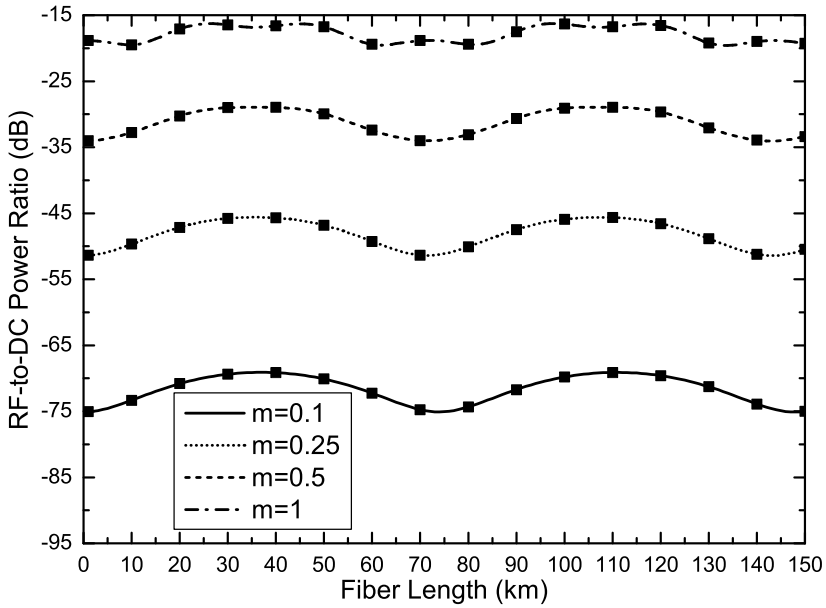

Figure 3.8: The detected RF power of the 3rd-order IMP normalized to detected dc power versus fiber length for several modulation indices for OSSB modulation. The markers represent the results of numerical simulation.

$\boldsymbol{\omega}_{rf}/(2\pi) = (10 \quad 10.1)$ GHz. The fundamental subcarrier $\mathbf{N} = (1 \quad 0)$ and the IMP3 $\mathbf{N} = (2 \quad -1)$ are shown in Figures. 3.7 and 3.8, respectively, for several values of modulation index. The numerical simulation results shown by the square markers are exactly the same as those based on our analysis. Unlike DSB, neither the fundamental subcarrier nor the IMP3 experience deep power fading. However IMP3 experiences power level fluctuation while the power of the fundamental subcarrier shows clear fluctuation only at large modulation indices. This fluctuation will be discussed in detail in the following section.

3.4 Intermodulation and Dynamic Range Analysis for Microwave Fibre-Optic Links

Without loss of generality, henceforth the discussion and derivation are for ODSB and OSSB modulation only. Also we assume that the subcarrier frequencies are very closely spaced around a centre frequency, ω_{rf}. Therefore, $\boldsymbol{\omega}_{rf} \approx (\omega_{rf0})_M$. Basically, we then use a two-subcarrier modulation model for our discussion. Hence, $\mathbf{N} = (1 \quad 0)$ and $\mathbf{N} = (0 \quad 1)$ for modulating subcarriers themselves and $\mathbf{N} = (2 \quad -1)$ and $\mathbf{N} = (-1 \quad 2)$ for the 3rd-order IMPs.

3.4.1 ODSB Modulation

For ODSB modulation, Eq. (3.18b) leads to:

$$\begin{aligned} |\tilde{P}(z,\omega_{rf1})| &= 2|\sin(\theta_2)| \cdot |J_1[2m_1 \cdot \cos(\omega_{rf1}\varphi_1)]| \\ &\quad \cdot |J_0[2m_2 \cdot \cos(\omega_{rf2}\varphi_1)]| \qquad (3.22a) \\ |\tilde{P}(z,2\omega_{rf2}-\omega_{rf1})| &= 2|\sin(\theta_2)| \cdot |J_1[2m_1 \cdot \cos(\omega_{rf1}\varphi_2)]| \\ &\quad \cdot |J_2[2m_2 \cdot \cos(\omega_{rf2}\varphi_2)]| \qquad (3.22b) \end{aligned}$$

where $\varphi_1 = \beta_2 z\omega_{rf1}/2$ and $\varphi_2 = \beta_2 z(\omega_{rf2} - \omega_{rf1})/2$. Given that $\omega_{rf1} \approx \omega_{rf2} \approx \omega_{rf}$ and hence $\varphi_1 \approx \varphi_2 \approx \varphi$, when m_1, m_2 are small (< 1), Eq. (3.22) can be approximated to:

$$\begin{aligned} |\tilde{P}(z,\omega_{rf1})| &\approx 2m_1 \cdot |\sin(\theta_2)| \\ &\quad \cdot |\cos(\omega_{rf}\varphi)| \qquad (3.23a) \\ |\tilde{P}(z,2\omega_{rf2}-\omega_{rf1})| &\approx m_1 m_2^2 \\ &\quad \cdot |\sin(\theta_2)| \cdot |\cos(\omega_{rf}\varphi)|^3 \qquad (3.23b) \end{aligned}$$

Assuming $m_1 = m_2 = m$, with Eq. (3.19b) and Eq. (3.23a), we can find the 1-dB compression point by solving the following equation for ODSB single-subcarrier modulation:

$$20 \cdot \log\left|\frac{x}{J_1(2x)}\right| = 1 \tag{3.24}$$

where $x = m \cdot \cos(\omega_{rf}\varphi)$. Hence, the 1-dB compression point for ODSB single-subcarrier modulation is $x = 0.475$. Note that this value will gradually drop when the number of modulating subcarriers increases. The general equation for multi-subcarrier cases is:

$$20 \cdot \log\left|\frac{x}{J_1(2x) \cdot J_0^{M-1}(2x)}\right| = 1 \tag{3.25}$$

Therefore, $x = 0.275$ for two-subcarrier modulation and $x = 0.214$ for triple-subcarrier modulation. It then shows that for the same input RF power for each subcarrier into DD-MZM, the output RF power level for each subcarrier decreases as the number of modulating subcarriers increases. This is expected since more energy is transferred to IMPs as the number of subcarriers increases. The estimate of the relationship between output RF power level and the number of subcarriers may be desired for system design. According to the following relation [91]:

$$1 = J_0(x) + 2\sum_{k=1}^{\infty} J_{2k}(x) \tag{3.26}$$

we can take the approximation $J_0(2m) \approx 1 - 2J_2(2m)$ when $m < 1$. According to Eq. (3.18b), we find the output RF power loss due to subcarrier multiplexing:

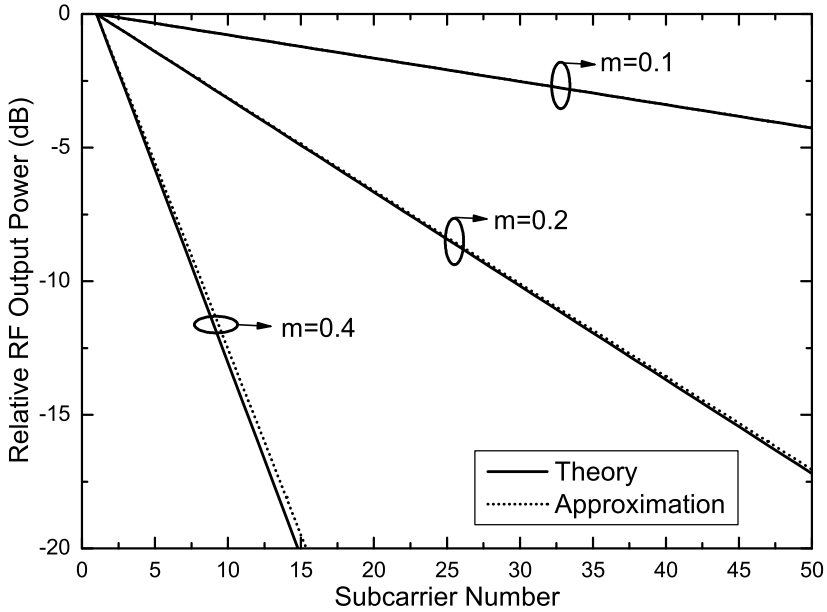

Figure 3.9: The relative output RF power loss due to subcarrier multiplexing for several modulation indices. The solid lines are calculated using Eq. (3.18) and the short dot lines are calculated using Eq. (3.27).

$$\begin{aligned} ML &= 20\log\frac{J_1(2m)J_0^{M-1}(2m)}{J_1(2m)} \\ &\approx -8.7(M-1)m^2 \end{aligned} \tag{3.27}$$

Fig. 3.9 shows the output RF power loss of each subcarrier for multi-subcarrier modulation relative to the output power of single-subcarrier modulation for several modulation indices. The curves calculated by using the approximation in (3.27) match very well those by exact theory even for moderately high modulation index. The figure shows that for a given reduction in output power the number of subcarriers drops quickly as the modulation index increases, limiting the system capacity greatly. If we set the maximum number of subcarriers at which 1 dB input RF power leads to 1 dB output RF power loss due to subcarrier multiplexing, we can find the following relationship:

$$-8.7(M-1)(10^{0.1}m^2 - m^2) = -1$$

$$\Rightarrow (M-1)m^2 \approx 0.44 \tag{3.28}$$

Hence a modulation index 0.1 can support 45 subcarriers. Moreover, since m^2 is directly related to the SNR of the link, Eq. (3.28) is actually an equation for the system capacity using DD-MZM.

For multi-subcarrier modulation, spur-free dynamic range (SFDR) is also an important parameter, which can be characterized by the input 3rd-order intercept point (IIP3). This parameter can be obtained by equating Eq. (3.23a) and Eq. (3.23b). Then:

$$2x \cdot |\sin(\theta_2)| = x^3 \cdot |\sin(\theta_2)| \tag{3.29}$$

Clearly, $x = \sqrt{2}$ for IIP3.

Note that the 1-dB compression point and IIP3 defined by x include effects of fibre dispersion and driving RF power and hence they can compensate each other. For ODSB modulation, fibre dispersion degrades the system sensitivity due to power fading but does not change its dynamic range (DR) because each 1 dB power fading leads to 3 dB decrease of the 3rd-order IMP and 1 dB increase of 1-dB compression point (increasing driving RF power to compensate power fading). This means that, essentially, the power fading due to fibre dispersion for ODSB modulation undermines the modulation depth and can be compensated by increasing the driving RF power without any loss of linearity of the link.

Also note that Eq. (3.25) and Eq. (3.29) are independent of the dc

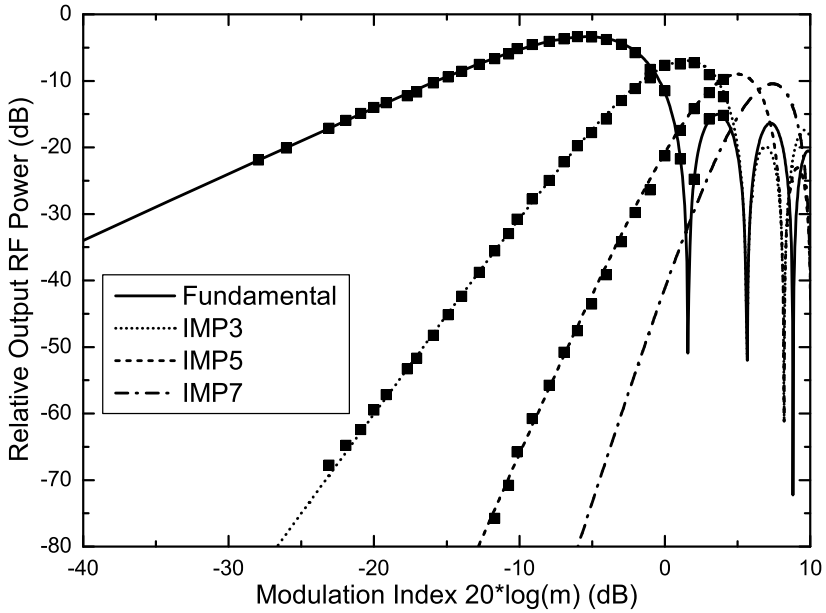

Figure 3.10: Relative detected RF power (fundamental, IMP3, IMP5 and IMP7) versus the square of modulation index for ODSB modulation. The markers are experiment results. The fibre length is 40 km and the two modulating subcarrier frequencies are 1 GHz and 1.1 GHz.

bias, θ_2. Therefore the dc bias does not have an effect on the link linearity. Besides, for fundamental subcarriers, with Eq. (3.18b) and (3.19b), we can easily conclude that the dc bias does not have any effect on all odd order IIPs. In practice, the bias point may not be at ideal quadrature point. Therefore, for ODSB modulation, the unideal bias point does not add to the odd order nonlinearity of the dispersive link except for some output RF power loss. This point is even intentionally employed for some special purposes [44]. However, because the noise level due to shot and thermal noise remains unchanged, this output RF power loss will eventually cause degradation of SNR and SFDR.

For the two-subcarrier DSB modulation case, Figure 3.10 shows the relative detected RF power versus the square of modulation index for fundamental ($\mathbf{N} = (1 \quad 0)$), IMP3 ($\mathbf{N} = (2 \quad -1)$), IMP5 ($\mathbf{N} = (3 \quad -2)$) and IMP7

($\mathbf{N} = (4 \quad -3)$). These results have been calculated using Eq. (3.18) for a 40 km standard single mode fiber (SSMF). Because other factors, such as link gain and photodetector response, are not included, the power in Figure 3.10 only means a relative value. This figure also includes measured values, up to a modulation index of about 5 dB, for the fundamental, IMP3 and IMP5. During the experiment, the relationship between the input RF power and m is decided by the relative power between the fundamental and IMP3 for $m = 0.2$. The measured RF power for $m = 0.2$ is compared with the calculated RF power based on the data sheet of the DD-MZM (JDSU, Model 21013114) taking into account the measured RF loss. The difference between these two power levels is less than 1.5 dB, which is reasonable since not all RF loss can be measured accurately. The other values of m in the experiment data are then decided according to their input RF power difference with the case of $m = 0.2$. The results obtained from our analysis closely match the experiment results. It can be seen that the fundamental subcarrier and the IMPs experience multiple power dips at large values of modulation index, clearly showing the energy transfer between them; the dips in the power of the fundamental correspond to the peaks in the power of the IMPs.

3.4.2 OSSB Modulation

For OSSB modulation, Eq. (3.20) leads to:

$$\begin{aligned} |\tilde{P}(z,\omega_{rf1})| = \big|&\sqrt{2}J_1[2m_1\sin(\omega_{rf1}\varphi_1)]J_0[2m_2\sin(\omega_{rf2}\varphi_1)] \\ &+e^{j\theta_2}J_1[2m_1\sin(\omega_{rf1}\varphi_1+\pi/4)] \\ &\cdot J_0[2m_2\sin(\omega_{rf2}\varphi_1+\pi/4)] \\ &+e^{-j\theta_2}J_1[2m_1\sin(\omega_{rf1}\varphi_1-\pi/4)] \end{aligned}$$

$$\cdot J_0[2m_2\sin(\omega_{rf2}\varphi_1-\pi/4)]\big| \tag{3.30a}$$

$$\begin{aligned}|\tilde{P}(z,2\omega_{rf2}-\omega_{rf1})| &\\ =\big|&\sqrt{2}J_1[2m_1\sin(\omega_{rf1}\varphi_2)]J_2[2m_2\sin(\omega_{rf2}\varphi_2)]\\ &+e^{j\theta_2}J_1[2m_1\sin(\omega_{rf1}\varphi_2+\pi/4)]\\ &\cdot J_2[2m_2\sin(\omega_{rf2}\varphi_2+\pi/4)]\\ &+e^{-j\theta_2}J_1[2m_1\sin(\omega_{rf1}\varphi_2-\pi/4)]\\ &\cdot J_2[2m_2\sin(\omega_{rf2}\varphi_2-\pi/4)]\big|\end{aligned} \tag{3.30b}$$

For small signal modulation, Eq. (3.30) can be approximated as:

$$\begin{aligned}|\tilde{P}(z,\omega_{rf1})| \approx m_1\big|&\sqrt{2}\cdot\sin(\omega_{rf}\varphi)\\ &+e^{j\theta_2}\cdot\sin(\omega_{rf}\varphi+\pi/4)\\ &+e^{-j\theta_2}\cdot\sin(\omega_{rf}\varphi-\pi/4)\big|\end{aligned} \tag{3.31a}$$

$$\begin{aligned}|\tilde{P}(z,2\omega_{rf2}-\omega_{rf1})| \approx \frac{m_1m_2^2}{2}\big|&\sqrt{2}\cdot\sin^3(\omega_{rf}\varphi)\\ &+e^{j\theta_2}\cdot\sin^3(\omega_{rf}\varphi+\pi/4)\\ &+e^{-j\theta_2}\cdot\sin^3(\omega_{rf}\varphi-\pi/4)\big|\end{aligned} \tag{3.31b}$$

For commonly used OSSB modulation, $\theta_2=\pm\pi/2$, then Eq. (3.31) reduces to:

$$|\tilde{P}(z,\omega_{rf1})|\approx\sqrt{2}m_1 \tag{3.32a}$$

$$|\tilde{P}(z,2\omega_{rf2}-\omega_{rf1})|\approx\frac{m_1m_2^2}{4}\sqrt{5-3\cos(2\omega_{rf}\varphi)} \tag{3.32b}$$

Eq. (3.32) shows that the fundamental subcarrier does not experience power fading while the 3rd-order IMP experience 6 dB power fluctuation. Therefore, unlike ODSB modulation, both 1-dB compression point and the IIP3

for OSSB modulation change with accumulated fibre dispersion.

Assuming $m_1 = m_2 = m$, equating Eq. (3.32a) and Eq. (3.32b) lets us find the IIP3:

$$m^2 = 4\sqrt{\frac{2}{5 - 3\cos(2\omega_{rf}\varphi)}} \tag{3.33}$$

Hence $m = 2$ for the largest IIP3 and $m = \sqrt{2}$ for the smallest IIP3.

Similarly, the 1-dB compression point is also dispersion dependent but in a rather complicated form. Generally, Eq. (3.30a) has its maximum value at $\omega_{rf}\varphi = 0$ and minimum value at $\omega_{rf}\varphi = \pm\pi/2$. Then the maximum and minimum 1-dB compression point can be found by solving the following equations:

$$20 \cdot \log\left|\frac{\sqrt{2}m_{max}}{2J_1(\sqrt{2}m_{max})J_0^{M-1}(\sqrt{2}m_{max})}\right| = 1 \tag{3.34a}$$

$$20 \cdot \log\left|\frac{m_{min}}{J_1(2m_{min})J_0^{M-1}(2m_{min})}\right| = 1 \tag{3.34b}$$

Eq. (3.30a) is expanded to multi-carrier case to get Eq. (3.34). It is easy to find from Eq. (3.34) that $m_{max} = \sqrt{2}m_{min}$. Therefore, for single-tone modulation, $m_{max} = 0.672$ and $m_{min} = 0.475$; for two-tone modulation, $m_{max} = 0.388$ and $m_{max} = 0.275$; for triple-tone modulation, $m_{max} = 0.302$ and $m_{max} = 0.214$. For the system capacity, it is easy to find that Eq. (3.27) and Eq. (3.28) derived for ODSB can also be used for OSSB to estimate the worst results.

We should note that, even though the maximum 1-dB compression point and IIP3 in OSSB increase 3 dB with respect to ODSB, the output RF power of OSSB is 3 dB less than ODSB at the same driving RF power. Therefore

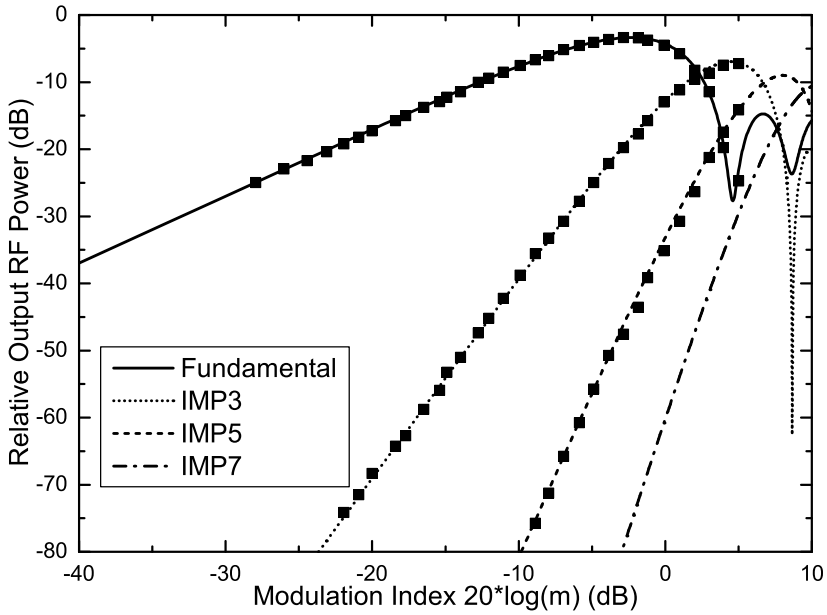

Figure 3.11: Relative detected RF power (fundamental, IMP3, IMP5 and IMP7) versus the square of modulation index for OSSB modulation. The markers are experiment results. The fibre length is 40 km and the two modulating subcarrier frequencies are 1 GHz and 1.1 GHz.

OSSB does not show better linearity than ODSB. When the link is dispersive, the linearity of OSSB links may even be 3 dB worse than ODSB links. The greatest advantage of using OSSB is to avoid sensitivity degradation due to power fading.

For the two-subcarrier SSB modulation case, Figure 3.11 shows the relative detected RF power versus the square of modulation index for fundamental ($\mathbf{N} = (1 \quad 0)$), IMP3 ($\mathbf{N} = (2 \quad -1)$), IMP5 ($\mathbf{N} = (3 \quad -2)$) and IMP7 ($\mathbf{N} = (4 \quad -3)$). These results have been calculated using Eq. (3.20) for a 40 km SSMF. Because other factors, such as link gain and photodetector response, are not included, the power in Figure 3.11 only means a relative value. This figure also includes measured values, up to a modulation index of about 5 dB, for the fundamental, IMP3 and IMP5. During the experiment, the relationship between the input RF power and m is decided following the

same method as in the case of DSB. The results obtained from our analysis closely match the experiment results. Very similar to the DSB case, the SSB case also shows power dips for the fundamental subcarriers and the IMPs.

3.5 Summary and Conclusion

We have presented an exact analytical model to study the dispersive transmission of SCM fibre-optic links using DD-MZM. The model results in simple, new, closed form expressions for output power spectrum, permitting an accurate and fast analysis of such links. In general, for SCM links, the RF output of one subcarrier is not decided by its input solely. Instead, other RF inputs have significant impact on the output of a particular subcarrier. Moreover, the evolution of one subcarrier and the IMPs in a dispersive fibre link depends not only on the frequency of the subcarrier itself but also on the frequency of the other subcarriers. Therefore, the behaviour of subcarriers is inter-dependent on each other. This complicated behaviour can be analyzed quickly through our closed form expressions as demonstrated in this chapter.

Based on our model, we have studied two commonly used modulation methods, ODSB and OSSB, in detail. Simple expressions for some important system parameters, such as 1-dB compression point, the IIP3 and the system capacity, have been derived for the first time. ODSB shows serious power fading under dispersive transmission while OSSB does not experience such power fading except some power level fluctuation along fibre. However, OSSB does not show better linearity than ODSB. Instead, the linearity of OSSB may be even 3 dB worse than that of ODSB under dispersive transmission. For both modulation methods, at the same input RF power level, the output RF power level drops as the number of multiplexing subcarriers

increases. Because the output SNR is directly proportional to the output RF power, the SNR of the system degrades as the output RF power level drops. Hence, the capacity of a system using DD-MZM is actually limited by a bound arising from the nonlinear distortion due to the DD-MZM, which has been given by our analysis. For the case of two subcarriers, for both ODSB and OSSB, a very good match is observed between the analytical results derived here and the measured results for the power level of the fundamental subcarrier and IMPs.

Finally, given that the model presented here is general and exact, its application can be extended to other fields using DD-MZM and its variants, enabling us to perform quick and accurate analysis of such systems.

Chapter 4

Nonlinear Distortion due to Stimulated Inelastic Scattering

In Chapter 3, the nonlinear distortion due to dual-drive Mach-Zehnder external modulators (DD-MZM) for dispersive transmission has been analyzed in detail. Besides nonlinear distortion caused by DD-MZM, fibres also introduce nonlinear distortions. In this chapter, the nonlinear distortions due to stimulated inelastic scattering in fibre, including stimulated Brillouin scattering (SBS) and stimulated Raman scattering (SRS), are discussed. SBS is notorious for its very low threshold, which limits the launched optical power seriously. Therefore, for SBS, we study the noise due to fibre dispersion in radio-over-fibre (RoF) links where phase dithering is used to suppress SBS. Our analysis and experiment show that, besides the random noise due to phase modulation, there are discrete spectral lines spaced at dither rate in the detected signal, which may act as interference. Our analysis reveals that the sharp rising/falling edges of the phase dithering signal can cause these discrete spectral lines. We demonstrate that the low pass filtering of the

phase dithering signal can suppress such noise and interference. With regard to SRS, the nonlinear distortion due to SRS between optical channels is studied through analytical and numerical analysis, which shows the low pass character of SRS induced nonlinear distortion. Therefore the nonlinear distortion due to SRS is significant for systems that have low subcarrier frequencies and large spacing between optical channels.

4.1 Stimulated Brillouin Scattering

Radio-over-fibre (RoF) technique can provide broadband access in a cost efficient way if the cost of the access network can be shared among many users. To achieve this, many techniques such as subcarrier multiplexing (SCM) [5], wavelength division multiplexing (WDM) [64] and higher order modulation formats [93] have been proposed. In addition to these techniques, increasing the launched optical power is the easiest way to support more users. However this optical power is limited by SBS due to the presence of a strong optical carrier in RoF system. Besides, SBS threshold decreases as fibre length gets longer. Therefore SBS greatly limits the number of users in an RoF system. Typically, one can suppress SBS by phase dithering technique [44], which has been used for years in hybrid fibre coax (HFC) CATV systems. But the RF frequency in RoF links is much higher than that in HFC CATV systems and the RoF links are longer. Due to fibre dispersion in RoF links, the phase dithering can convert to undesired intensity noise and degrade a system's performance. Therefore RoF links are more vulnerable to problems caused by phase dithering and need careful examination.

Generally phase dithering involves large signal modulation, which means that the phase shift can approach π. However, to the best of knowledge of

the authors, only small signal modulation models [94] have been reported so far; these small signal models cannot satisfactorily account for the effects of phase dithering in practice.

In this section, after a brief introduction to Brillouin-gain spectrum, we examine the effects of using phase dithering to suppress SBS in an RoF system. We present a large signal modulation model, which explains our experiment results satisfactorily. For the first time, we theoretically show the origin of discrete spectral lines observed in the spectrum of detected phase dithered signal, which can be a strong interference source for some multicarrier systems. Our theory shows that these spectral lines can be removed either by low pass filtering the phase dithering signal or by fibre dispersion compensation; this is confirmed experimentally by implementing low pass filtering which is the simpler of the two remedies.

4.1.1 Brillouin-Gain Spectrum

Basically, the process of SBS can be modelled as a nonlinear interaction between the pump and Stokes fields through an acoustic wave which is generated by the pump field through the process of electrostriction [51]. This acoustic wave in turn modulates the refractive index of the medium to form an index grating. The pump-induced index grating scatters the pump light through Bragg diffraction, resulting in a scattered light downshifted in frequency because of the Doppler shift associated with the index grating moving at the acoustic velocity v_A. This scattering process can also be viewed quantum-mechanically as the annihilation of a pump photon to create a Stokes photon and an acoustic phonon simultaneously. Since both the energy and the momentum must be conserved during each scattering event,

the frequencies and the wave vectors of the three waves are related by [26]

$$\Omega_B = \omega_p - \omega_s \tag{4.1a}$$

$$\mathbf{k}_B = \mathbf{k}_p - \mathbf{k}_s \tag{4.1b}$$

where Ω_B, ω_p and ω_s are the angular frequencies, and $\mathbf{k}_B$, $\mathbf{k}_p$ and $\mathbf{k}_s$ are the wave vectors of the acoustic, pump and Stokes waves, respectively.

The frequency Ω_B and the wave vector $\mathbf{k}_B$ of the acoustic wave satisfy the standard dispersion relation [26]

$$\Omega_B = v_A|\mathbf{k}_B| \approx 2v_A|\mathbf{k}_p| \sin\left(\frac{\theta}{2}\right) \tag{4.2}$$

where θ is the angle between the pump and Stokes fields and $|\mathbf{k}_p| \approx |\mathbf{k}_s|$ is used in Eq. (4.1). Eq. (4.2) shows that the frequency shift of the Stokes wave depends on the scattering angle. In particular, Ω_B is maximum in the backward direction ($\theta = \pi$) and vanishes in the forward direction ($\theta = 0$). In a single-mode optical fibre, the only relevant directions are the forward and backward directions. Therefore, SBS occurs only in the backward direction with the Brillouin frequency shift given by [26]

$$\nu_B = \frac{\Omega_B}{2\pi} = \frac{2\bar{n}v_A}{\lambda_p} \tag{4.3}$$

where Eq. (4.2) was used with $|\mathbf{k}_p| = 2\pi\bar{n}/\lambda_p$ and $\bar{n}$ is the modal index at the pump wavelength λ_p. If we use $v_A = 5.96\,\text{km/s}$ and $\bar{n} = 1.45$, the values appropriate for silica fibres are $\nu_B \approx 11.1$ GHz at $\lambda_p = 1.55\,\mu\text{m}$.

The Brillouin-gain spectrum $g_B(\Omega)$ characterizes the growth of the Stokes

wave of SBS with a peak at $\Omega = \Omega_B$. A noteworthy character of SBS is that the spectral width of the gain spectrum is very small ($\sim$ MHz) because it is related to the damping time of acoustic waves or the phonon lifetime. In fact, if acoustic waves are assumed to decay as $\exp(-\Gamma_B t)$, the Brillouin gain has a Lorentzian spectrum of the form [51]

$$g_B(\Omega) = g_p \frac{(\Gamma_B/2)^2}{(\Omega - \Omega_B)^2 + (\Gamma_B/2)^2} \tag{4.4}$$

where the peak value of the Brillouin-gain coefficient occurring at $\Omega = \Omega_B$ is given by [95]

$$g_p \equiv g_B(\Omega_B) = \frac{2\pi^2 \bar{n}^7 p_{12}^2}{c\lambda_p^2 \rho_0 v_A \Gamma_B} \tag{4.5}$$

where p_{12} is the longitudinal elasto-optic coefficient and ρ_0 is the material density. The full width at half maximum (FWHM) of the gain spectrum is related to Γ_B as $\Delta\nu_B = \Gamma_B/(2\pi)$ while the phonon lifetime itself is related to Γ_B as $T_B = \Gamma_B^{-1} \sim 10\,\text{ns}$.

Noting from Eq. (4.3) that ν_B varies inversely with λ_p, $\Delta\nu_B$ is expected to obey a λ_p^{-2} dependence on the pump wavelength. Therefore the dependence on λ_p is cancelled out in Eq. (4.5). As a result, the peak value g_p is nearly independent of the pump wavelength. Taking the typical parameter values of fused silica into Eq. (4.5), $g_p \approx 5 \times 10^{-11}$ m/W, which is larger by nearly three orders of magnitude compared with that of the Raman-gain coefficient shown later. As a result, the threshold of SBS is much lower than that of SRS. However, this value is only for a narrow-bandwidth pump. As mentioned in Chapter 2, for a broadband pump with bandwidth $\Delta\nu_p$, the peak value of Brillouin gain is reduced by a factor of $\Delta\nu_p/\Delta\nu_B$ [96] and then the SBS threshold can be increased.

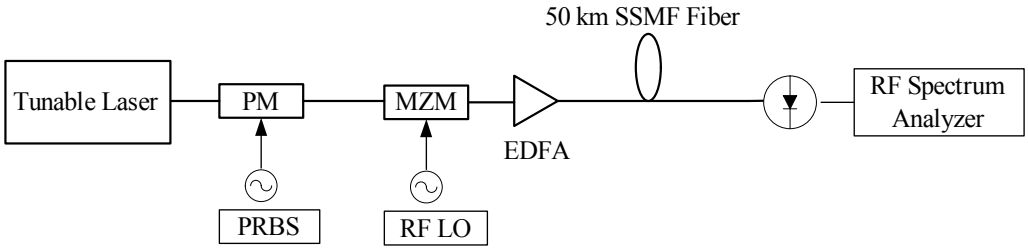

Figure 4.1: Experiment setup of an RoF link using phase dithering to suppress SBS. PM: Phase modulator; MZM: Mach-Zehnder modulator; EDFA: Erbium-doped fibre amplifier; SSMF: Standard single mode fibre.

4.1.2 Analytical Model

A typical RoF link using phase dithering is shown in Figure 4.1. Because dithering the phase of optical carrier can widen the laser linewidth, SBS is then suppressed significantly. This method has been used in HFC CATV systems for years and potentially, it can also be used in RoF systems. However, this random phase dithering can be converted to intensity noise by fibre dispersion. In this section, we set up an original analytical model to analyze this conversion from phase dithering to intensity noise.

It is well known that the propagation of optical envelope in a single mode fibre is governed by nonlinear Schrödinger equation (NLSE). Neglecting the terms related to fibre nonlinearity, NLSE can be rewritten as [26]

$$\frac{\partial A}{\partial z} + \frac{j\beta_2}{2}\frac{\partial^2 A}{\partial T^2} + \frac{\alpha}{2}A = 0 \tag{4.6}$$

where $A = A(z,T)$ is the optical field envelope, β_2 is the second-order fibre dispersion parameter and α is the fibre loss parameter. Fourier transform of Eq. (4.6) results in

$$\frac{\partial \tilde{A}}{\partial z} - \frac{j\beta_2\omega^2}{2}\tilde{A} + \frac{\alpha}{2}\tilde{A} = 0 \tag{4.7}$$

where $\sim$ denotes Fourier transform. Eq. (4.7) results in an analytical solution in frequency domain

$$\tilde{A}(z,\omega) = \tilde{A}(0,\omega) \cdot \exp\left(\frac{j\beta_2\omega^2 z}{2}\right) \cdot \exp\left(-\frac{\alpha z}{2}\right) \tag{4.8}$$

Besides fibre loss, Eq. (4.8) shows that each spectral component of the input signal acquires a frequency dependent phase shift, which leads to the distortion of pulse shape. The phase modulation will be converted to intensity modulation under dispersive transmission. For phase dithering, the phase modulation signal is a random data stream. Therefore, the resultant intensity modulation is an undesired noise source in subcarrier multiplexing systems.

The conjugate equation of Eq. (4.6) results in the solution for A^*, the conjugate of A

$$\tilde{A}^*(z,\omega) = \tilde{A}^*(0,\omega) \cdot \exp\left(-\frac{j\beta_2\omega^2 z}{2}\right) \cdot \exp\left(-\frac{\alpha z}{2}\right) \tag{4.9}$$

Therefore, the detected signal spectrum, which is proportional to the optical power spectrum, can be written as

$$\begin{aligned}\tilde{P}(z,\omega) &= \tilde{A} \otimes \tilde{A}^* \\ &= e^{-\alpha z}\left[\tilde{A}_0 \cdot \exp\left(\frac{j\beta_2\omega^2 z}{2}\right)\right] \otimes \left[\tilde{A}_0^* \cdot \exp\left(-\frac{j\beta_2\omega^2 z}{2}\right)\right]\end{aligned} \tag{4.10}$$

where $\otimes$ denotes convolution, $A_0 = A(0,T)$ and $A_0^* = A^*(0,T)$. After Taylor expansion of $\exp(j\beta_2\omega^2 z/2)$ and $\exp(-j\beta_2\omega^2 z/2)$, Eq. (4.10) reduces to

$$\frac{\tilde{P}(z,\omega)}{\exp(-\alpha z)} = \sum_{n=0}^{\infty} \frac{(-j\beta_2 z)^n}{2^n n!}\left(-\omega^2\right)^n \tilde{A}_0 \otimes \sum_{k=0}^{\infty} \frac{(j\beta_2 z)^k}{2^k k!}\left(-\omega^2\right)^k \tilde{A}_0^* \tag{4.11}$$

In time domain, Eq. (4.11) reduces to

$$\frac{P(z,T)}{\exp(-\alpha z)} = \sum_{n=0}^{\infty}\sum_{k=0}^{\infty} \frac{(-j\beta_2 z)^n}{2^n n!}\frac{(j\beta_2 z)^k}{2^k k!}\frac{\partial^{(2n)}A_0}{\partial T^{(2n)}}\frac{\partial^{(2k)}A_0^*}{\partial T^{(2k)}} \tag{4.12}$$

The various order derivatives in Eq. (4.12) show that the rising and falling edge of the input signal plays an important role in the shape and the spectrum of the final detected signal.

Even though Eq. (4.12) is an exact solution, it does not show clearly the relationship between the phase modulation and the detected signal. Several transformation have to be made to reveal this relationship.

$$A(z,T) = U(z,T)\cdot\exp(-\alpha z) \tag{4.13a}$$

$$U(z,T) = \sqrt{P(z,T)}\cdot\exp[j\phi(z,T)] \tag{4.13b}$$

$$B(z,T) = \ln U(z,T) = \frac{1}{2}\ln P(z,T) + j\phi(z,T) \tag{4.13c}$$

where $P(z,T)$ and $\phi(z,T)$ are the intensity and phase of the optical field envelope $A(z,T)$ respectively. Eq. (4.13) defines a logarithm signal of the original signal, which helps us to find the relationship between phase modulation and the detected signal. With these definitions, NLSE reduces to

$$\frac{\partial B}{\partial z} + \frac{j\beta_2}{2}\frac{\partial^2 B}{\partial T^2} + \frac{j\beta_2}{2}\left(\frac{\partial B}{\partial T}\right)^2 = 0 \tag{4.14}$$

To be able to handle this nonlinear equation, one usually has to make some simplifying approximations. Here we assume that the generated noise due to fibre dispersion is small and hence assume that the nonlinear term in Eq.(4.14) does not change over fibre length. Then $(\partial B/\partial T)^2 = (\partial B_0/\partial T)^2$, where $B_0 = B(0,T)$. With this approximation and Fourier transformation

of Eq.(4.14)

$$\frac{\partial \tilde{B}}{\partial z} - \frac{j\beta_2\omega^2}{2}\tilde{B} - \frac{j\beta_2}{2}(\omega\tilde{B}_0) \otimes (\omega\tilde{B}_0) = 0 \tag{4.15}$$

where $\otimes$ denotes convolution. We can find a solution:

$$\begin{aligned} F[B] = F[B_0] \cdot \exp\left(\frac{j\beta_2\omega^2 z}{2}\right) \\ + \left[1 - \exp\left(\frac{j\beta_2\omega^2 z}{2}\right)\right] \cdot \frac{1}{\omega^2} \cdot F\left[\left(\frac{\partial B_0}{\partial T}\right)^2\right] \end{aligned} \tag{4.16}$$

where $F[\bullet]$ denotes Fourier transform. In a similar manner, through the conjugate form of Eq. (4.14), we can find the solution for conjugate logarithm signal, $F[B^*]$. Further, assume that $P(z,T) = P(0) \cdot P'(z,T)$ where $P(0)$ is the average optical intensity and $P'(z,T)$ stands for the modulated microwave signals or subcarriers normalized to the average optical intensity. Therefore, using Eq. (4.13c) and the relationship $F[\ln P] = F[B + B^*] = F[B] + F[B^*]$, we get

$$\begin{aligned} F[\ln P'] = F[\ln P_0'] \cdot \cos\theta - 2 \cdot F[\phi_0] \cdot \sin\theta \\ + \beta_2 z \left\{\frac{1}{4} F\left[\left(\frac{\partial \ln P_0'}{\partial T}\right)^2\right] - F\left[\left(\frac{\partial \phi_0}{\partial T}\right)^2\right]\right\} \cdot \sin\left(\frac{\theta}{2}\right) \cdot \mathrm{Sa}\left(\frac{\theta}{2}\right) \\ + \beta_2 z \cdot F\left[\frac{\partial P_0'}{\partial T} \cdot \frac{\partial \phi_0}{\partial T}\right] \cdot \mathrm{Sa}(\theta) \end{aligned} \tag{4.17}$$

where $P_0' = P'(0,T)$, $\phi_0 = \phi(0,T)$, $\mathrm{Sa}(x) = \sin(x)/x$ and $\theta = \beta_2\omega^2 z/2$. At the right hand side of Eq. (4.17), the first term and the second term show the intensity-to-intensity and the phase-to-intensity conversion after dispersive transmission, respectively. The other two terms involve the time derivatives of the intensity and the phase, and hence show the impact of the rising and falling edges of the modulation signal.

Instead of giving the detected signal spectrum directly, Eq. (4.17) gives

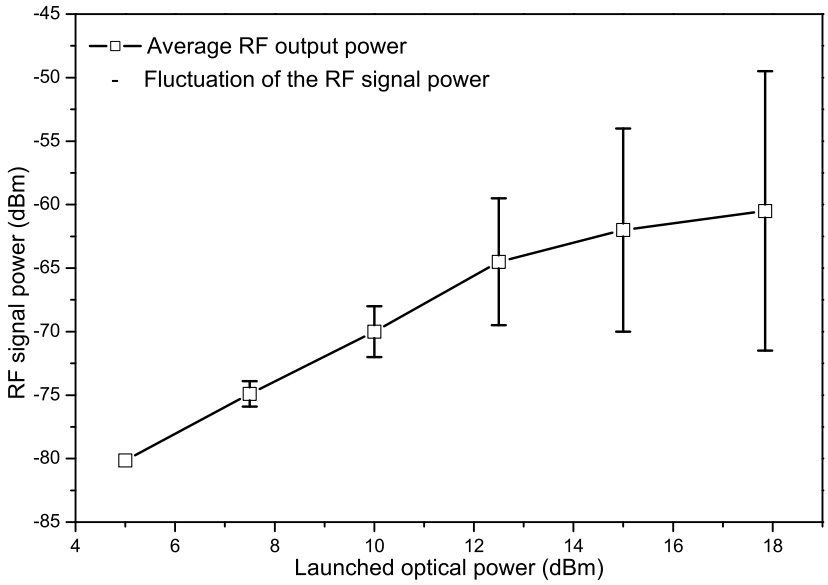

Figure 4.2: Measured RF average power as well as fluctuation range with SBS present.

the logarithm of the detected signal spectrum. However, through Taylor expansion, we can get

$$\begin{aligned} F[P] &= F[P_0 \cdot P'] = P_0 \cdot F[\exp(F^{-1}[F[\ln P']])] \\ &= 2\pi P_0 \delta(\omega) + P_0 \sum_{n=1}^{\infty} \frac{1}{n!} F\left[(F^{-1}[F[\ln P']])^n\right] \\ &\approx 2\pi P_0 \delta(\omega) + P_0 \cdot F[\ln P'] \end{aligned} \tag{4.18}$$

where $F^{-1}[\bullet]$ denotes inverse Fourier transformation. Therefore the logarithm spectrum actually reveals the character of detected spectrum.

4.1.3 Noise due to Phase Dithering

The experiment setup shown in Figure 4.1 is used to study the noise due to phase dithering to suppress SBS. A phase modulator dithers the optical phase of a laser with a 1 Gbps pseudorandom bit stream (PRBS). The output of the phase modulator is modulated by an RF subcarrier at 5 GHz applied through the Mach-Zehnder modulator (MZM) with a modulation

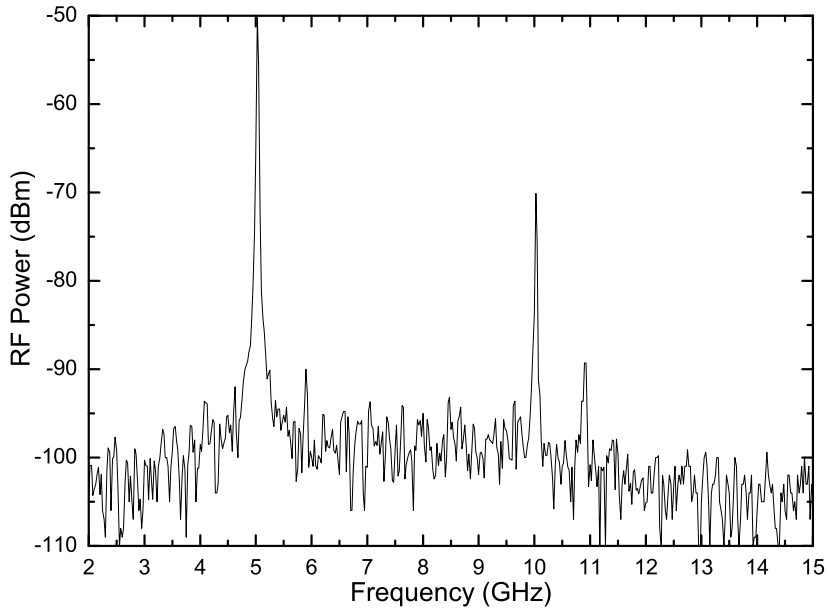

Figure 4.3: Detected spectrum without phase dithering (measured).

index of 0.1. The optical power launched into the fiber is 10 dBm except in Figure 4.2 where the optical power launched into the fiber is variable. The 50 km standard single mode fibre (SSMF) has a dispersion parameter of $D = 17\,\mathrm{ps/km \cdot nm}$.

The spectrum of the photodetected signal, analyzed by RF spectrum analyzer, is shown in Figures 4.3 and 4.4, without and with phase dithering, respectively. To clearly see the noise level change due to phase dithering and fibre dispersion, 1 kHz resolution bandwidth (RBW) of RF spectrum analyzer was chosen so that the inherent spectrum analyzer noise does not interfere with our observation. Shown by Figure 4.2, without phase dithering, when the launched optical power is greater than about 6 dBm, significant SBS is observed and the detected signal level becomes very unstable because the optical power is fluctuating due to the loss induced by backward scattering of SBS [71,97]. Moreover, the power fluctuation range increases with the launched optical power, showing that SBS gets stronger at larger launched

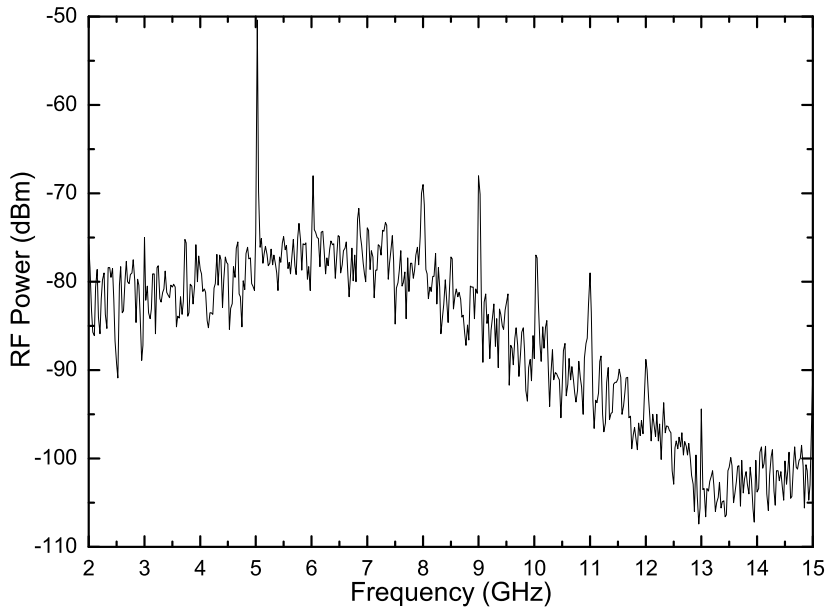

Figure 4.4: Detected spectrum with phase dithering (measured).

optical power. Basically, the average output optical power at the fibre end tends to saturate at a certain level, putting an upper limit on the system capacity.In Figure 4.3 one can observe an RF signal at 10.9 GHz, which is generated by SBS because it can be eliminated by suppressing SBS in later measurements. Even though SBS should generate a backward Stokes wave with a Stokes shift of about 10.9 GHz for 1550 nm system as calculated by Eq. (4.3), this backward Stokes wave can be scattered back by Rayleigh scattering of fibre and observed after detection. Because the Brillouin-gain spectrum occupies a spectrum of tens of MHz, this phenomenon makes SBS extremely troublesome for RoF systems at the band of 10 - 11 GHz because a strong interference around 11 GHz generated by SBS is introduced. Indeed, during our experiment, we observed that 10 GHz RF subcarriers experience much more serious power fluctuation than subcarriers at other frequencies due to the interference between the subcarrier and the Stokes wave of SBS. Detailed observations and analyses have been given in [27].

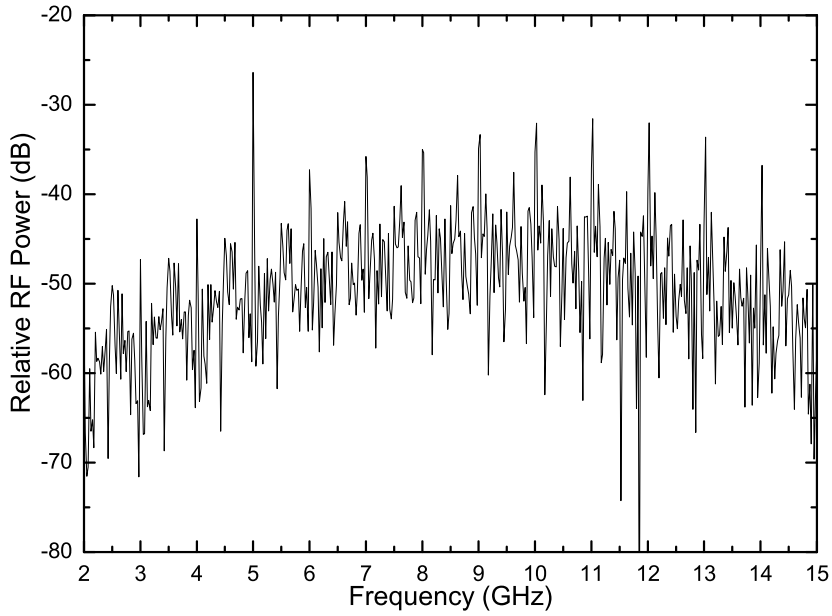

Figure 4.5: Detected spectrum (results calculated from analytical expressions).

To suppress SBS, we phase modulate the tuneable laser (1540 nm) by 1 Gbps binary phase shift keying (BPSK) NRZ pseudorandom signal. The detected signal level becomes quite stable, showing that SBS is suppressed. However, the noise level is greatly increased due to phase modulation to intensity modulation conversion by fibre dispersion. Comparing Figure 4.3 and 4.4, the noise level increases by more than 20 dB when phase dithering is applied, showing the conversion of phase modulation to intensity modulation of the 1 Gbps pseudorandom signal by fibre dispersion.

Also, there are many discrete spectral lines spaced at 1 GHz in the detected spectrum. In Figure 4.4, we can easily identify these spectral lines at 2, 6, 8, 9, 10, 11 GHz even though they are quite small due to the 1 kHz RBW. With small signal analysis only (the first two terms on the right side of Eq. (4.17)), we cannot predict these discrete spectral lines although the noise floor can be predicted because the first two terms on the right hand

side of Eq. (4.17) are directly related to the power spectral density of PRBS but NRZ code used by PRBS does not show these spectral lines. When the other terms in Eq. (4.17) are included, we can predict these spectral lines, as shown in Figure 4.5. Figure 4.5 is calculated by using the same values of physical parameters (PRBS bit rate, RF frequency, optical power, fibre length and dispersion parameter) as those in Figure 4.4 but assuming flat response of the Mach-Zehnder modulator and the photodetector. Figure 4.5 then shows that the spectral lines of the experimental measurement in Figure 4.4 arise from the time derivative of the PRBS used for phase dithering, which physically means that the sharper edges lead to stronger spectral lines. These discrete spectral lines may introduce undesired interference in some multicarrier systems. Besides, as shown by the figure, the interference is much stronger than the noise level. This also makes phase dithering technique to suppress SBS, less attractive in some microwave fibre optic links due to the high noise level and interference, since in the latter systems, the microwave subcarrier frequency is typically larger than phase dithering rate.

4.1.4 Suppression the Noise due to Phase Dithering

According to Eq. (4.17), we can suppress the noise and interference due to phase dithering through either fibre dispersion compensation or windowing the phase dithering signal. Windowing smoothes the phase dithering signal and hence can suppress the discrete spectral lines. It also limits the spectral range of phase dithering signal, lowering the noise level at RF subcarrier. This is confirmed by further experiments, as shown in Figures 4.6 - 4.9, by using the same experiment setup and parameters as those in Figure 4.1.

This time, the RBW is set to 100 kHz so that the interfering spectral

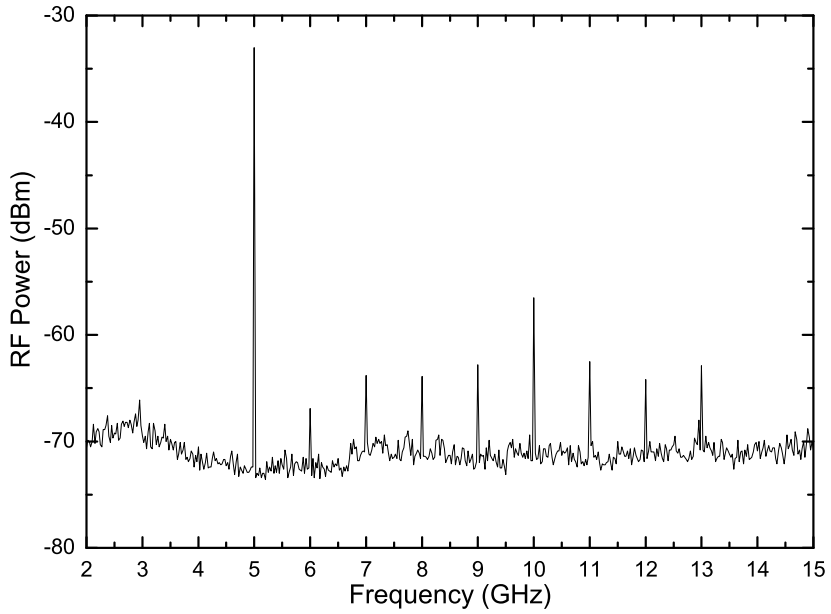

Figure 4.6: Detected spectrum with phase dithering but without filtering the phase dithering signal.

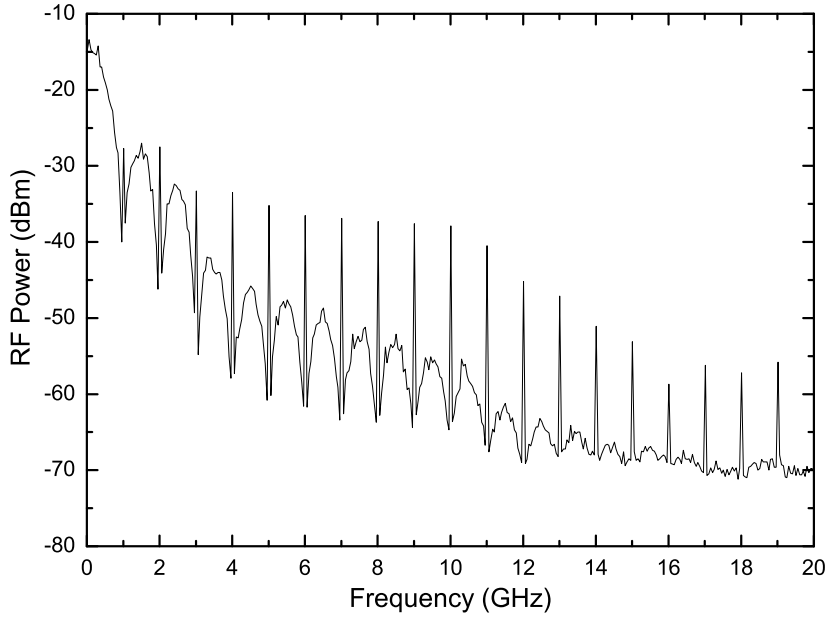

Figure 4.7: The output spectrum of PPG for 1 Gbps PRBS.

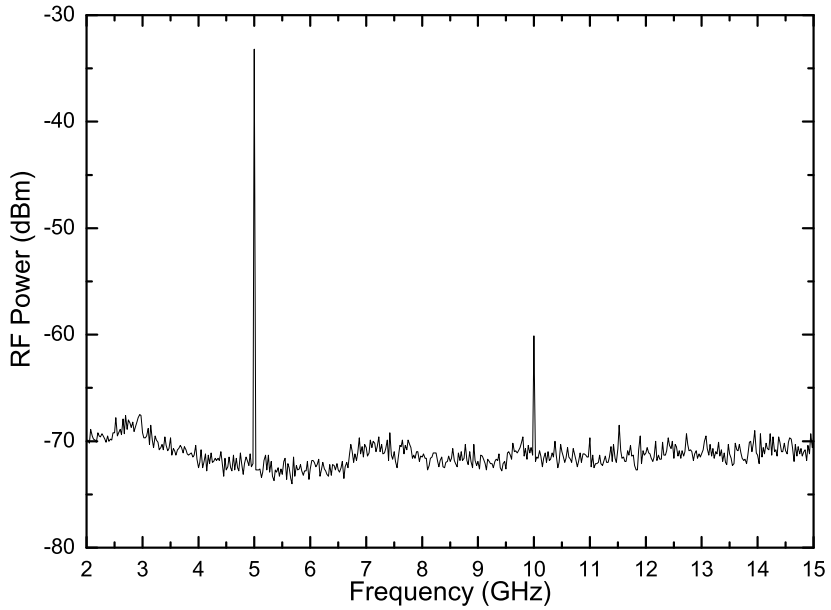

Figure 4.8: Detected spectrum with phase dithering and with filtering the phase dithering signal by a low pass filter with 3 dB cut-off frequency 933 MHz.

lines due to phase dithering are clearly seen (Figure 4.6). Note that, in practice, the output of pulse pattern generator (PPG) is not pure NRZ and consists of many harmonics. In our experiment, the output of the PPG is measured and shown in Figure 4.7. However, the levels of these harmonics are stable while the observed spectral lines in Figure 4.6 are actually unstable, showing that there is some randomness. Therefore, even though the harmonics in the PPG output can cause those spectral lines, a part of those spectral lines is caused by the rising and falling edges of the PRBS data which introduce the randomness. Clearly, both types of spectral lines can be filtered out by low pass filtering of the PPG output. We then filter the PRBS stream before it drives the phase modulator by a low pass filter with a 3-dB cut-off frequency 933 MHz. The results in Figure 4.8 clearly show that low pass filtering successfully remove the spectral lines due to phase dithering.

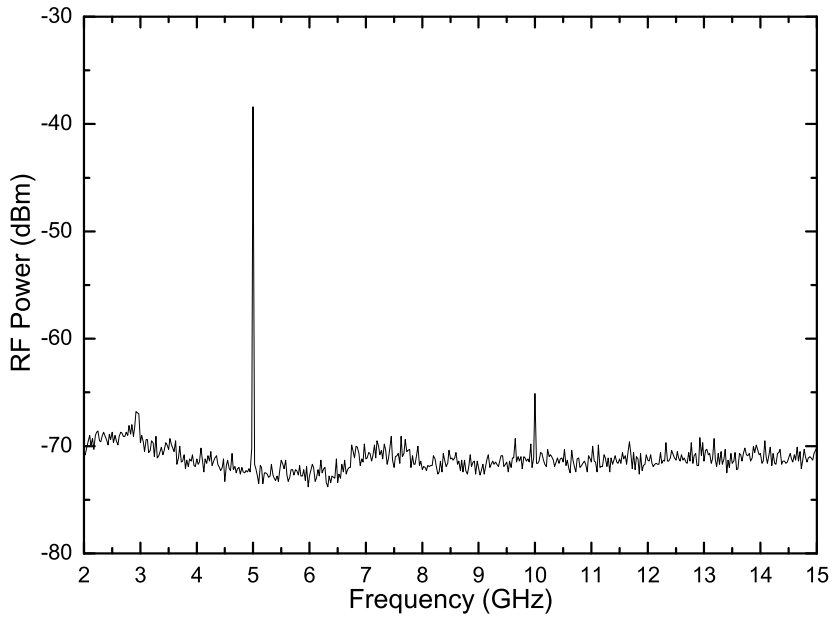

Figure 4.9: Detected spectrum after dispersion compensation

Of course, without fibre dispersion compensation, there is always some residual noise even after filtering. Fibre dispersion compensation can remove almost all of the noise and interference due to phase dithering. The detected spectrum after dispersion compensation is also shown in Figure 4.9. However, low pass filtering is still an attractive technique to suppress noise and interference due to phase dithering in RoF links because it is much simpler than fibre dispersion compensation.

4.2 Stimulated Raman Scattering

Stimulated Raman scattering (SRS) is an important nonlinear process that can turn optical fibres into broadband Raman amplifiers and tuneable Raman lasers. However, on the other hand, it can also severely limit the performance of multichannel lightwave systems by transferring energy from one channel to the neighbouring channels, causing nonlinear crosstalk between channels. In this section, the Raman-gain spectrum is derived first and then

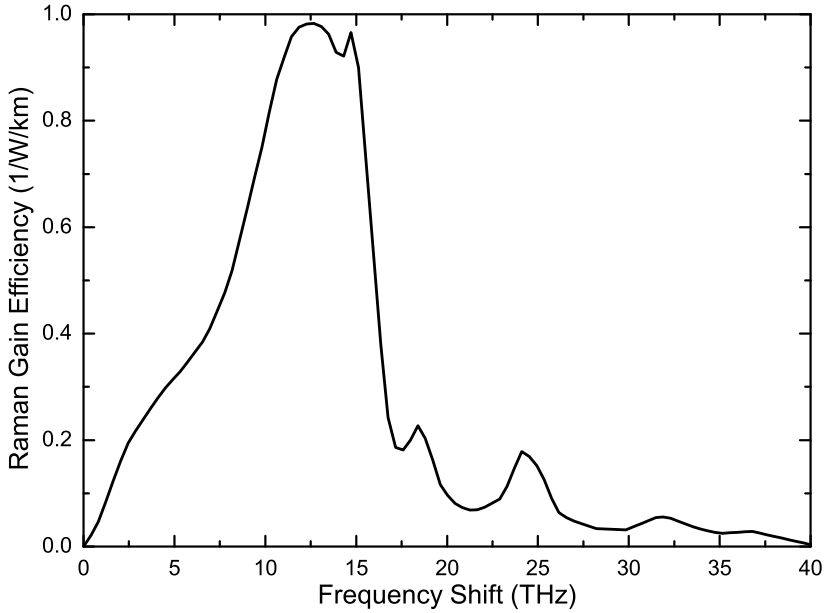

Figure 4.10: Raman-gain spectrum for optical fibre.

we present the analysis of the nonlinear crosstalk due to SRS in wavelength division multiplexing (WDM) SCM systems.

4.2.1 Raman-Gain Spectrum

As shown in Chapter 2, in a simple approach valid under the continuous-wave (CW) and quasi-CW conditions, the initial growth of the Stokes wave is described by [51]

$$\frac{dP_s}{dz} = g_R P_p P_s \tag{4.19}$$

where P_s is the Stokes intensity, P_p is the pump intensity and the Raman-gain coefficient g_R is related to the cross section of spontaneous Raman scattering [49]. The Raman-gain spectrum is given by $g_R(\Omega)$, where Ω stands for the frequency difference between the pump and Stokes waves.

The Raman-gain spectrum for silica fibres was experimentally measured.

Basically, g_R depends on the composition of the fibre core and can vary significantly with the use of different dopants. The most significant feature of the Raman gain in silica fibres is that $g_R(\Omega)$ extends over a large frequency range (up to 40 THz) with a broad peak located near 13 THz as shown in Figure 4.10 [98].

To show how the process of SRS develops, we consider a CW pump beam inside a fibre at optical frequency ω_p propagating in the same direction as a probe beam at frequency ω_s. The probe beam will be amplified due to the Raman gain as long as the frequency difference $\Omega = \omega_p - \omega_s$ lies within the bandwidth of the Raman-gain spectrum. Without the probe beam, spontaneous Raman scattering acts as a probe and is amplified along with propagation. Because spontaneous Raman scattering generates photons in the entire bandwidth of the Raman-gain spectrum, all frequency components are amplified. However, the frequency component for which g_R is maximum is amplified most rapidly. For pure silica, g_R is maximum for the frequency component downshifted from the pump frequency by about 13.2 THz. It has been shown that when the pump power exceeds a threshold value, this component builds up almost exponentially [54]. Consequently, SRS results in the Stokes wave whose frequency is determined by the peak of the Raman gain. The corresponding frequency shift is called the Raman shift (or the Stokes shift). These feature are intentionally exploited for making Raman fibre amplifiers and lasers.

4.2.2 Raman-Induced Nonlinear Crosstalk

Even though fibre amplifier and lasers benefit from the Raman gain, SRS can cause problems in WDM systems. Because a short-wavelength channel can act as a pump for longer-wavelength channels and transfer part of the pulse energy to neighbouring channels, SRS leads to nonlinear crosstalk among channels that may affect the system performance considerably.

To analyze this nonlinear crosstalk in SCM systems, we consider an optical communication link with two optical channels. Due to SRS, the two channels satisfy the following coupled equations [26]

$$\frac{\partial P_1}{\partial z} + \frac{1}{\nu_{g1}}\frac{\partial P_1}{\partial t} = (gP_2 - \alpha)P_1 \tag{4.20a}$$

$$\frac{\partial P_2}{\partial z} + \frac{1}{\nu_{g2}}\frac{\partial P_2}{\partial t} = (-gP_1 - \alpha)P_2 \tag{4.20b}$$

where ν_{gk} is the group velocity for the transmitted signal at wavelength λ_k and g is the standard Raman gain coefficient divided by the fibre effective area. Assuming that the optical intensity at channel k is $P_k = P_{k0}(z,t) \cdot \exp(-\alpha z)$ and considering the walk-off effect between the two channels due to fibre dispersion, Eqs. (4.20) reduce to:

$$\frac{\partial P_{10}(z,T_1)}{\partial z} = gP_{20}(z, T_1 + u_{12})\exp(-\alpha z)P_{10}(z,T_1) \tag{4.21a}$$

$$\frac{\partial P_{20}(z,T_2)}{\partial z} = -gP_{10}(z, T_2 - u_{12})\exp(-\alpha z)P_{20}(z,T_2) \tag{4.21b}$$

where $T_1 = t - z/\nu_{g1}$, $T_2 = t - z/\nu_{g2}$ and $u_{12} = 1/\nu_{g1} - 1/\nu_{g2}$. Fourier transform of Eqs. (4.21) gives

$$\frac{\partial \tilde{P}_{10}(z,\omega)}{\partial z} = g\tilde{P}_{20}(z,\omega)\exp[-(\alpha - j\omega u_{12})z] \otimes \tilde{P}_{10}(z,\omega) \tag{4.22a}$$

$$\frac{\partial \tilde{P}_{20}(z,\omega)}{\partial z} = -g\tilde{P}_{10}(z,\omega)\exp[-(\alpha + j\omega u_{12})z] \otimes \tilde{P}_{20}(z,\omega) \quad (4.22b)$$

where $\sim$ denotes Fourier transform and $\otimes$ denotes convolution. Eq. (4.22) describes the interaction between the subcarriers of the two optical channels through SRS.

For SCM system, the optical intensity is generally written as

$$P(0,T) = P_{avg} \cdot \left[1 + \sum_i m_i \cos(\omega_i T)\right] \quad (4.23)$$

where P_{avg} is the average intensity, i denotes various subcarriers with modulation index m_i. Therefore, the optical intensity spectrum is

$$\tilde{P}(0,\omega) = \pi P_{avg} \cdot \left[2\delta(\omega) + \sum_i m_i \delta(\omega - \omega_i) + \sum_{-i} m_i \delta(\omega - \omega_{-i})\right] \quad (4.24)$$

where δ denotes Dirac Delta function. Hence, the convolution in Eqs. (4.22) reduces to summations and multiplications and can be evaluated easily for SCM systems. Basically, $\tilde{P}(z,\omega)$ cannot be replaced by $\tilde{P}(0,\omega)$ because of the distortion induced by fibre dispersion such as RF power fading. However, as we will see later that for SRS, this replacement is reasonable because SRS exhibits a low pass character.

The interaction between the subcarriers of the two optical channels through SRS shown by Eq. (4.22) generates many new intermodulation products (IMPs) across the two channels. Because higher order IMPs are very small compared with the second order and SRS exhibits low-pass property, we only consider the second-order IMPs, that is, the products generated by the interaction between the subcarriers across the two channels directly. Then

$\tilde{P}_{10}(z,\omega)$ and $\tilde{P}_{20}(z,\omega)$ at the right hand side of Eqs. (4.22) can be replaced by $\tilde{P}_{10}(0,\omega)$ and $\tilde{P}_{20}(0,\omega)$. Integration of Eqs. (4.22) lets us calculate the IMP analytically. For example, we can get the expression for a intermodulation product at $\omega_i+\omega_j$ generated at channel 1 by a subcarrier at ω_i on channel 1 and a subcarrier at ω_j on channel 2, which is

$$IMP2_{SRS12} = gm_1m_2P_{avg1}P_{avg2}z_{e2j}\delta(\omega-\omega_i-\omega_j) \tag{4.25a}$$

$$z_{e2j} = \frac{1-\exp(-\alpha_{2j})}{\alpha_{2j}} \tag{4.25b}$$

$$\alpha_{2j} = \alpha - j\omega_j u_{12} \tag{4.25c}$$

Similarly, the IMPs generated at channel 2 have a similar form

$$IMP2_{SRS21} = -gm_1m_2P_{avg1}P_{avg2}z_{e1j}\delta(\omega-\omega_i-\omega_j) \tag{4.26a}$$

$$z_{e1j} = \frac{1-\exp(-\alpha_{1j})}{\alpha_{1j}} \tag{4.26b}$$

$$\alpha_{1j} = \alpha + j\omega_j u_{12} \tag{4.26c}$$

When one of the two subcarriers is the optical carrier itself, which has a nominal frequency 0, the expressions for IMPs shown by Eqs. (4.25) and (4.26) reduce to those for nonlinear crosstalk due to SRS derived in [43, 44].

Eqs. (4.25) and (4.26) show that the magnitude and phase of the nonlinear crosstalk or IMPs on channel 1 through SRS are determined by the frequency of the interaction subcarrier on channel 2 rather than by the final crosstalk or IMP frequency if the frequencies of the two subcarriers are different. Also, because the Raman-gain, g, is generally larger at larger optical channel spacing, the magnitude of the nonlinear crosstalk or IMPs is then

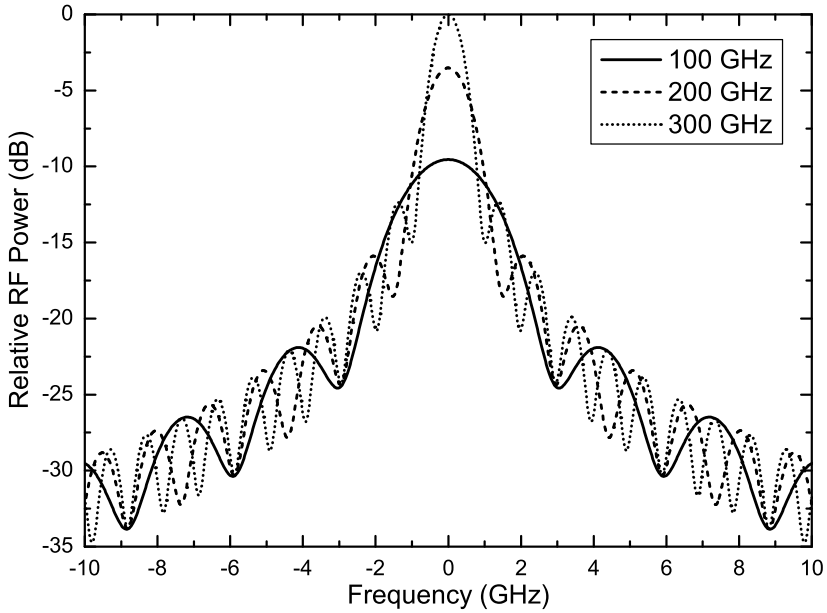

Figure 4.11: The relative RF power of IMPs normalized to the maximum vs. subcarrier frequency for several optical channel spacings. The fibre length is 25 km.

more significant at larger optical channel spacing. Some SCM systems employ WDM technology and occupy a very wide wavelength range. For such systems, the nonlinear crosstalk and IMPs due to SRS should be carefully considered.

Figure 4.11 shows the relative RF power of IMPs normalized to the maximum as a function of subcarrier frequency for several optical channel spacings and a fibre length 25 km. SRS exhibits a low pass character. Besides, the wider the optical channel spacing, the narrower the pass band. Therefore, the crosstalk and IMPs due to SRS are more significant for systems using lower frequency subcarriers such as hybrid fibre-coax (HFC) systems which typically employ subcarriers below 1 GHz. Figure 4.12 shows the phase of IMPs as a function of subcarrier frequency for two optical channels with 100 GHz channel spacing and a fibre length is 25 km. The two channels have opposite phase relationship because one experiences Raman gain

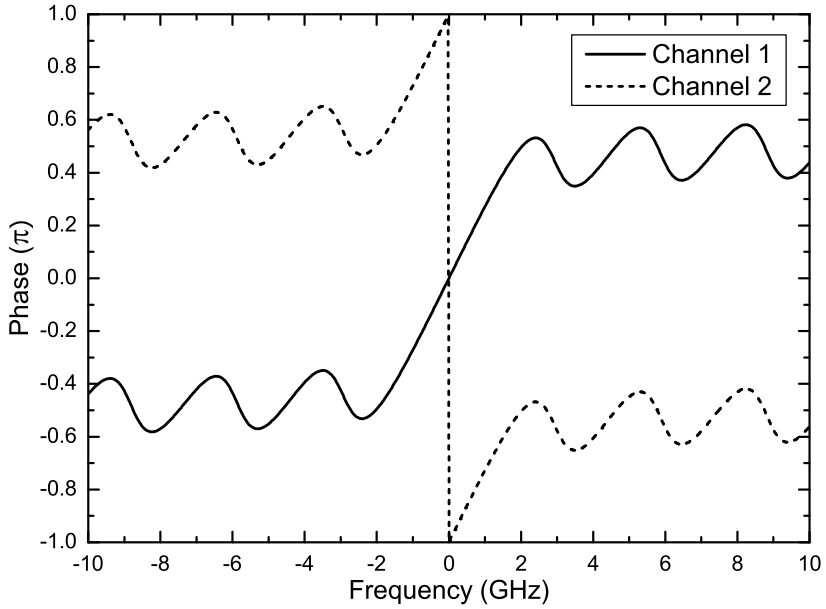

Figure 4.12: The phase of IMPs vs. subcarrier frequency for two optical channels with 100 GHz channel spacing. The fibre length is 25 km.

enhancement while the other experiences Raman gain depletion. The phase increases generally linearly with the subcarrier frequency at low frequency range and eventually fluctuates around $\pi/2$. It has been shown [43, 44] that the crosstalk and IMPs due to SRS and XPM can cancel each other because these can have opposite phase relationship.

4.3 Summary

In this chapter, the impact of stimulated inelastic scattering in optical fibres on SCM systems has been analysed. It is shown that both types of stimulated inelastic scattering, SBS and SRS, may degrade the system performance considerably.

With regard to SBS, the SBS-gain spectrum is very narrow and peaks around 11 GHz in optical fibres. The backward scattered Stokes wave with downshift frequency 10.9 GHz in our experiment leads to significant power

loss. Therefore, SBS puts stringent upper limit on the launched optical power. Besides, the Stokes wave can be reflected back to the forward direction by Rayleigh scattering, presenting itself as a strong interference source at around 11 GHz. Moreover, SBS also causes serious power fluctuation of the detected RF signal. Therefore, SBS should be carefully avoided or suppressed. In our experiment, significant SBS is observed when launched optical power is greater than 6 dBm.

To suppress SBS, one modulates the phase of the laser output by a PRBS stream to widen the output laser spectrum. The SBS threshold is then greatly enhanced. However, due to the fibre dispersion, the phase dithering signal is converted to intensity noise. Moreover, one experiment shows that there are many spectral lines spaced at the PRBS data rate. These spectral lines can be strong interference sources in RoF or microwave fibre-optic links. Our analysis shows that these spectral lines come from two aspects: one is the harmonics in the PPG output; the other is the sharp rising and falling edge of PRBS data stream. Both types of interference can be removed by low pass filtering of the PPG output, which is confirmed by our experiment.

With regard to SRS, the SRS-gain spectrum is very wide. Such broadband gain spectrum can cause significant nonlinear crosstalk and IMPs across optical channels. Moreover, typically, the wider the channel spacing, the stronger the crosstalk level due to SRS. Our analysis shows that SRS exhibits low pass character. Hence, the lower the subcarrier frequency, the stronger the crosstalk level due to SRS. This means that SRS should be carefully treated in HFC systems where the subcarrier frequencies are typically below 1 GHz. We also study the phase relationship of the crosstalk

and IMPs.

Chapter 5

Nonlinear Distortion due to Nonlinear Refraction

In recent years, there has been an increasing interest in exploitation of the microwave region of the electromagnetic spectrum with the help of fibre-optic techniques [19, 77, 78]. The extremely low loss and wide bandwidth of the fibre enable us to distribute microwave signals from a central control station to a number of base stations, resulting in simple base station architectures with low cost and good system flexibility. Microwave fibre-optic links have been widely proposed for many applications such as broadband wireless communications and antenna remoting. Moreover, it is desired to incorporate wavelength division multiplexing (WDM) into microwave fibre-optic links to improve the bandwidth efficiency [38, 64].

Generally, microwave fibre-optic links impose stringent limits on nonlinear distortion. Therefore nonlinear distortion needs to be studied carefully. Both modulator, such as widely used dual-drive Mach-Zehnder Modulator (DD-MZM), and fibre can introduce significant nonlinear distortion in the

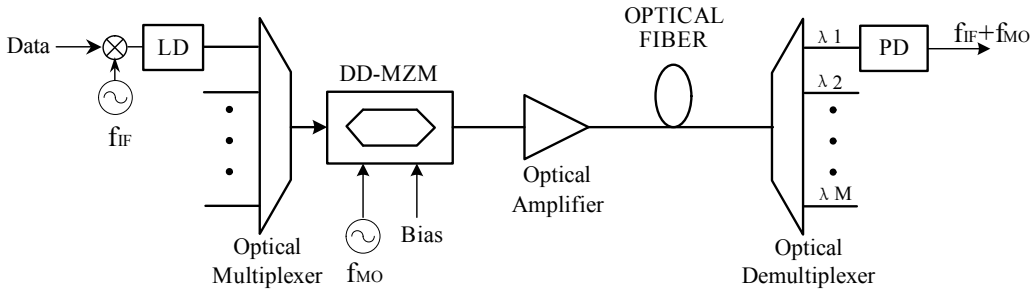

Figure 5.1: A typical electrooptical upconversion system configuration with WDM. LD: laser diode; DD-MZM: dual-drive Mach-Zehnder modulator; PD: photodetector; f_{IF}: the frequency of intermediate frequency oscillator; f_{MO}: the frequency of master oscillator.

links. For single wavelength microwave fibre-optic links, DD-MZM is the dominant source of nonlinear distortion. As shown in Chapter 3, the nonlinear distortion due to the combined effect of DD-MZM and fibre dispersion has been analyzed in the past through exact general analytical models [36,66,99]. For the nonlinear distortion due to fibre, stimulated Brillouin scattering (SBS) must be considered in the system design [71], which has been presented in Chapter 4. Due to the very low SBS threshold of fibres, the launched optical power of a microwave fibre-optic link has to be very low, typically less than 6 dBm, when no special measures are taken to suppress SBS. Such a low launched optical power makes other fibre nonlinearities, such as the third order intermodulation (IMD) due to self-phase modulation (SPM), rather insignificant in a single wavelength link.

The scenario is different in a WDM microwave fibre-optic link where the nonlinear distortion due to cross-phase modulation (XPM) between adjacent optical channels can be significant. Consider an electrooptical upconversion system [36,66] with two optical channels shown in Figure 5.1. Let us assume that each channel is modulated by a 5 GHz subcarrier (f_{IF}) and a 22 GHz subcarrier (f_{MO}) and the upconverted 27 GHz subcarrier ($f_{IF} + f_{MO}$) is the

desired signal. The nonlinear distortion at 27 GHz due to XPM has three components: the first one, called as *nonlinear crosstalk*, is due to the interaction between the intensity change of the 27 GHz subcarrier in one optical channel and the optical carrier in the other optical channel; the second one is due to the interaction between the 5 GHz intensity change in one optical channel and the 22 GHz subcarrier in the other optical channel; the third one is due to the interaction between the 22 GHz intensity change in one optical channel and the 5 GHz subcarrier in the other optical channel. The two latter ones involve the interaction with subcarriers and are called *intermodulation products through fibre nonlinearity* (NIMPs). Therefore, typically, the nonlinear distortion in a WDM microwave fibre-optic link consists of two parts: the nonlinear crosstalk and the NIMPs. The nonlinear crosstalk due to XPM in WDM systems has been studied by many researchers [29,43,44,65,72,73]. Their studies show that the nonlinear crosstalk level due to XPM increases rapidly as the modulation frequency increases, which suggests that the nonlinear crosstalk level for WDM microwave fibre-optic links may be significant even when the launched optical power is well below SBS threshold. However, because these models are essentially based on the pump-probe approach where only one channel is modulated by subcarriers, only nonlinear crosstalk due to XPM can be analyzed. Moreover, even though these models work well to analyze the nonlinear crosstalk due to XPM, the expressions are complicated and hence the impact of various parameters, such as the fibre dispersion, the modulating subcarrier frequencies and the channel spacing, is not very clear.

In this chapter, we present a new analytical model, not based on pump-probe approach, to study the nonlinear distortion due to XPM in dispersive

WDM microwave fibre-optic links. The model predicts quite well the nonlinear distortion due to XPM, including both nonlinear crosstalk and NIMPs, even when the modulating microwave frequencies are in the range of tens of gigahertz and the fibre length is tens of kilometre. Also, we show that after reasonable approximation the nonlinear distortion can be expressed in a very simple form, showing clearly the influence of various parameters. Detailed analyses of the nonlinear distortion for two commonly used modulation methods, optical double sideband (ODSB) and optical single sideband (OSSB), are also presented. Numerical simulations as well as experiments confirm the accuracy of our analytical model. Moreover, the study shows that in an electrooptical upconversion system, the NIMPs can be more detrimental than nonlinear crosstalk.

The rest of this chapter is organized as follows. First we explain the physical mechanism of nonlinear distortion due to nonlinear refraction. Then, we present analytical models for the nonlinear distortion due to nonlinear refraction, followed by the analyses of the nonlinear distortion due to XPM through simulations and experiments. Finally, we summarize and conclude this chapter.

5.1 Distortion due to Nonlinear Refraction

It has been shown in Chapter 2 that the pulse propagation in optical fibres is governed by NLSE when nonlinear refraction is included

$$\frac{\partial A}{\partial z} + \frac{i\beta_2}{2}\frac{\partial^2 A}{\partial T^2} + \frac{\alpha}{2}A = j\gamma|A|^2 A \tag{5.1}$$

where A is the optical field envelope and T stands for a frame of reference moving with the pulse at the group velocity ν_g (the so-called retarded frame). The meaning of various symbols has been explained in Section 2.3. If there is no fibre dispersion, Eq. (5.1) reduces to

$$\frac{\partial A}{\partial z} + \frac{\alpha}{2}A = j\gamma|A|^2 A \tag{5.2}$$

Therefore, we can get

$$\frac{\partial A}{\partial z}A^* + \frac{\alpha}{2}AA^* = j\gamma|A|^2 AA^* \tag{5.3a}$$

$$\frac{\partial A^*}{\partial z}A + \frac{\alpha}{2}A^*A = -j\gamma|A|^2 A^*A \tag{5.3b}$$

Because the optical power $P = |A|^2 = AA^*$, combination of the two equations, Eq. (5.3a) and Eq. (5.3b), results in

$$\frac{\partial P}{\partial z} + \alpha P = 0 \tag{5.4}$$

which give us a solution of the optical power

$$P = |A|^2 = P_0 \exp(-\alpha z) \tag{5.5}$$

where P_0 is the launched optical power. Eq. (5.5) shows that the optical power does not experience distortion except power loss due to fibre loss even though nonlinear refraction is present when there is no fibre dispersion. Replacing $|A|^2$ in Eq. (5.2) by Eq. (5.5), the solution of A is

$$A = A_0 \exp\left(-\frac{\alpha z}{2}\right)\exp(j\gamma P_0 L_e) \tag{5.6a}$$

$$L_e = \frac{1-\exp(-\alpha z)}{\alpha} \tag{5.6b}$$

where A_0 is the initial optical field envelope at the fibre input. Eq. (5.6) shows that without fibre dispersion, nonlinear refraction only introduces a nonlinear phase modulation to the optical field envelope, which will not result in optical power distortion by itself. However, if there is fibre dispersion, this phase modulation gets converted to intensity modulation by dispersive transmission, resulting in optical power distortion. Because most current optical fibre communication systems are intensity modulation and direct detection, this optical power distortion will then leads to the distortion of the final detected signal. For subcarrier multiplexing systems (SCM), this distortion shows up as nonlinear intermodulation and nonlinear crosstalk.

However, when both nonlinear refraction and fibre dispersion are considered, Eq. (5.1) cannot be solved analytically. Therefore, many analytical approximation models have been proposed in the past to find solutions with reasonable approximations for particular applications. Basically, these approximations can be categorized into the following types:

- Assume no fibre dispersion at first and find the phase modulation due to nonlinear refraction. Then calculate the additional intensity distortion due to this phase modulation under dispersive transmission [43, 44];

- Find the intensity evolution for dispersive transmission only. Based on the results, find the intensity distortion due to nonlinear refraction for a tiny fibre section and carry out integration to get the final distortion for the whole fibre span [73, 100, 101];

- Write the optical field envelope in the form of magnitude and phase. Find the coupled equations from NLSE for magnitude

and phase. Neglect the nonlinear terms in the equations and then try to solve the equations analytically [28, 29, 88, 94];

- Treat nonlinear refraction as a small perturbation and use perturbation theory to find the first order nonlinear distortion due to nonlinear refraction [102].

Essentially, all of the above methods are based on the perturbation theory with different levels of approximation for different applications. A comprehensive study based on perturbation theory has been given in [103]. However, the result in [103] is for conventional digital optical fibre communication systems and needs numerical integration for calculation. In this chapter, we follow the idea to use the perturbation theory. However, different from the work in [103], this chapter studies SCM optical fibre communication systems and results in closed-form expressions, providing more physical insights and enabling quicker calculation. Moreover, while systems with only one optical channel are the focus in [103], this chapter focuses on WDM systems. Compared with previous works in SCM optical fibre communication systems, this chapter provides more general and rigorous analyses.

5.2 Nonlinear Crosstalk

When multiple optical wavelengths propagate in a single fibre, XPM can lead to interactions and crosstalk between optical wavelengths. Without fibre dispersion, XPM leads to only the phase modulation of the signals in one optical channel according to the power at other optical channels and hence does not affect intensity modulation and direct detection (IM-DD) systems. However, fibre dispersion can convert this phase modulation into intensity modulation, leading to undesired nonlinear crosstalk. On the other hand,

it is well known that fibre dispersion can lead to subcarrier power fading. Hence, fibre dispersion not only generates but also fades nonlinear crosstalk. The overall effect of XPM and fibre dispersion will result in a nonlinear crosstalk with a finite level.

In this section, we first present an original general analytical model to study the nonlinear crosstalk due to XPM. Then we study two commonly used modulation methods by DD-MZM, ODSB and OSSB, resulting in closed form expressions for nonlinear crosstalk level.

5.2.1 The General Analytical Model

Following the exact analytical model for a dispersive transmission system using a DD-MZM in [99], we assume that the nonlinear distortion due to XPM is a small perturbation of the model in [99]. Instead of relating this perturbation with the model in [99] by a summation, as is done typically, we assume a multiplicative relationship; this assumption will show its advantage later. Therefore we assume that the optical field envelope of an optical channel in a nonlinear dispersive fibre is [103]:

$$A(z,T) = \left[1 + \sum_{n=1}^{\infty} \gamma^n A_n(z,t)\right] \cdot A_0(z,T) \tag{5.7}$$

where γ is the fibre nonlinearity parameter. As will be shown later mathematically, $A_0(z,T)$ is the optical field envelope when there is no XPM and $A_n(z,T)$ is the n-th order nonlinear distortion due to XPM with coefficient γ^n. It is well known that the nonlinear propagation of optical field envelope in single mode fibres is governed by nonlinear Schrödinger equation

(NLSE) [26]

$$\frac{\partial A}{\partial z} + \frac{j\beta_2}{2}\frac{\partial^2 A}{\partial T^2} + \frac{\alpha}{2}A = j\gamma|A|^2 A \tag{5.8}$$

where β_2 is the second order dispersion parameter and α is the fibre loss parameter. For simplicity, we consider the first order perturbation only and now $A(z,T) = \left[1 + \gamma A_1(z,T)\right] \cdot A_0(z,T)$. Substituting Eq. (5.7) into Eq. (5.8) and using perturbation theory, we get the following equations:

$$\frac{\partial A_0}{\partial z} + \frac{j\beta_2}{2}\frac{\partial^2 A_0}{\partial T^2} + \frac{\alpha}{2}A = 0 \tag{5.9a}$$

$$\frac{\partial A_1}{\partial z} + \frac{j\beta_2}{2}\frac{\partial^2 A_1}{\partial T^2} + j\beta_2\frac{\partial A_0}{\partial T}\frac{\partial A_1}{\partial T} = j|A_0|^2 \tag{5.9b}$$

Eq. (5.9b) is obtained by equating the terms with coefficient γ. When we consider small signal modulation (the modulation index $m < 1$), the nonlinear term in Eq. (5.9b), $j\beta_2(\partial_T A_0)(\partial_T A_1)$, is proportional to m^2 while the other terms are proportional to m. Therefore we can safely neglect this nonlinear term and simplify Eq. (5.9b) as:

$$\frac{\partial A_1}{\partial z} + \frac{j\beta_2}{2}\frac{\partial^2 A_1}{\partial T^2} = j|A_0|^2 \tag{5.10}$$

Eq. (5.9a) shows that $A_0(z,T)$ is the optical field envelope evolution with fibre dispersion only. Generally, the expression for the corresponding intensity evolution of $A_0(z,T)$ is known. For example, when using DD-MZM, the intensity evolution, $|A_0|^2$, has been expressed in exact analytical expressions in [99]. This makes Eq. (5.10) easy for solution. The relationship assumed in Eq. (5.7) results in $|A_0|^2$, not $|A_0|^2 A_0$ on the right side of Eq. (5.10), avoiding the complicated convolution operation in the Fourier transform coming

next. Assuming $|A_0|^2 = P_0$, the Fourier transform of Eq. (5.10) is:

$$\frac{\partial \tilde{A}_1}{\partial z} - \frac{j\beta_2\omega^2}{2}\tilde{A}_1 = j\tilde{P}_0 \tag{5.11}$$

where $\tilde{}$ stands for the Fourier transform. The solution of Eq. (5.11) is:

$$\tilde{A}_1(z,\omega) = j\exp(j\kappa z)\int_0^z \tilde{P}_0(z',\omega)\exp(-j\kappa z')\,dz' \tag{5.12}$$

where $\kappa = \beta_2\omega^2/2$. From the conjugate equation of Eq. (5.10), we can also get the solution of $\tilde{A}_1^*$:

$$\tilde{A}_1^*(z,\omega) = -j\exp(-j\kappa z)\int_0^z \tilde{P}_0(z',\omega)\exp(j\kappa z')\,dz' \tag{5.13}$$

where * stands for the complex conjugate. Since the system is IM/DD, the intensity is our concern. Given that now $A(z,T) = \big[1+\gamma A_1(z,T)\big]\cdot A_0(z,T)$, we find that the intensity is:

$$I = |A|^2 = \big[1 + \gamma(A_1 + A_1^*) + \gamma^2|A_1|^2\big]\cdot|A_0|^2 \tag{5.14}$$

By neglecting the term with coefficient γ^2 in Eq. (5.14), Eq. (5.7) enables us to calculate a simple $A_1 + A_1^*$ instead of a complicated multiplication. Therefore, it can then be shown that

$$\begin{aligned}\tilde{A}_1 + \tilde{A}_1^* = {} & 2\cos(\kappa z)\int_0^z \tilde{P}_0(z',\omega)\sin(\kappa z')\,dz' \\ & -2\sin(\kappa z)\int_0^z \tilde{P}_0(z',\omega)\cos(\kappa z')\,dz'\end{aligned} \tag{5.15}$$

The expressions for $\tilde{P}_0(z,\omega)$ are given in Chapter 3 and [99] in terms of Bessel functions. For small signal modulation, the Bessel functions can be

approximated by trigonometric functions and it becomes possible to integrate Eq. (5.15) analytically. With Eq. (5.14), we can easily identify the nonlinear distortion level as:

$$NLD = \gamma(\tilde{A}_1 + \tilde{A}_1^*) \otimes \tilde{P}_0 \tag{5.16}$$

where $\otimes$ denotes convolution. For microwave fibre-optic links, both $(\tilde{A}_1 + \tilde{A}_1^*)$ and $\tilde{P}_0$ consist of Dirac delta functions and the convolution can be performed easily through frequency shift and multiplication. Therefore Eq. (5.16) enables us to find the corresponding nonlinear distortion level at different frequencies.

The above derivation is for a single optical channel and the nonlinear distortion due to SPM. However, the model can be extended to WDM and XPM easily by modifying Eq. (5.10) suitably:

$$\frac{\partial A_1}{\partial z} + \frac{j\beta_2}{2}\frac{\partial^2 A_1}{\partial T^2} = j2P_0'(z, T - \beta_2\Delta\omega z) \tag{5.17}$$

where $P_0'(z, T - \beta_2\Delta\omega z) = |A_0'(z, T - \beta_2\Delta\omega z)|^2$ is the optical intensity of another optical channel at ω_0' inducing XPM to the channel at ω_0, $\Delta\omega = \omega_0 - \omega_0'$ is the angular frequency difference between the two optical channels and $\beta_2\Delta\omega z$ stands for the optical field envelope time delay between the two channels due to the walk-off effect. When one does not consider the walk-off effect, the Fourier transform of P_0' is generally in the form of:

$$\tilde{P}_0' = \tilde{P}_z'(z, \omega)\exp(-\alpha z) \tag{5.18}$$

where $\tilde{P}'_z(z,\omega)$ is the intensity evolution without fibre loss. When the walk-off effect is included, we find that:

$$\begin{aligned}\tilde{P}'_0 &= \tilde{P}'_z(z,\omega)\exp(-\alpha z)\exp(-j\omega\beta_2\Delta\omega z)\\ &= \tilde{P}'_z(z,\omega)\exp(-\mu z)\end{aligned} \tag{5.19}$$

where $\mu = \alpha + j\omega\beta_2\Delta\omega$. The introduction of the new complex fibre loss parameter μ results in the same form of P'_0 with the walk-off effect as that without the walk-off effect. Therefore the expression shown by Eq. (5.15) can also be used for XPM after replacing P_0 by P'_0, α by μ and multiplying by 2 since XPM is two times greater than SPM.

5.2.2 Two Special Cases: ODSB and OSSB

ODSB and OSSB are the two most commonly used modulation methods in microwave fibre-optic links. We discuss the nonlinear crosstalk due to XPM for the standard ODSB and OSSB modulations separately. Some other modulation methods, which can be viewed as the derivatives of ODSB and OSSB, will also be discussed briefly. As shown before, the nonlinear crosstalk comes from the interaction between $(\tilde{A}_1 + \tilde{A}_1^*)$ and $\tilde{P}'_0$. For a certain modulation frequency, typically both $(\tilde{A}_1 + \tilde{A}_1^*)$ and $\tilde{P}'_0$ have infinite harmonic terms and their interaction according to Eq. (5.16) generates infinite new nonlinear crosstalk terms at various frequencies. Here, we just calculate the strongest nonlinear crosstalk term which is generated by the interaction between the subcarrier at frequency 0 in $\tilde{P}_0$ and a subcarrier at frequency ω_2 in $\tilde{P}'_0$. Hence the resulting nonlinear crosstalk is located at ω_2.

5.2.2.1 The ODSB modulation

The standard ODSB modulation can be generated by using a DD-MZM biased at the quadrature point and shifting the phase of one radio frequency (RF) drive to the other by π. Such an ODSB signal does not have chirp, that is, no accompanying phase modulation. Then the small signal approximation of the results for ODSB in Chapter 3 is:

$$\tilde{P}_0'\big|_{\omega_2} = 2m\bar{P}_0' \cos(\kappa_2 z)\exp(-\mu z) \tag{5.20}$$

where $\kappa_2 = \beta_2\omega_2^2/2$ and $\bar{P}_0'$ is the strength of P_0' at the frequency 0 and the beginning of the fibre. Typically, for small signal modulation, $\bar{P}_0'$ equals the average optical power of the channel at ω_0' at the beginning of the fibre. Hence, according to Eq. (5.15) and Eq. (5.16), the strength of the generated nonlinear crosstalk due to XPM at ω_2 is:

$$\begin{aligned} Cr|_{ODSB} = {} & 4m\gamma\bar{P}_0\bar{P}_0' e^{-\mu_2 z}e^{-\alpha z} \\ & \times\left\{\frac{2(e^{\mu_2 z}-1)\mu_2\kappa_2\cos(\kappa_2 z)}{\mu_2^3+4\mu_2\kappa_2^2}\right. \\ & \left.-\frac{\left[e^{\mu_2 z}(2\mu_2^2+4\kappa_2^2)-4\kappa_2^2\right]\sin(\kappa_2 z)}{\mu_2^3+4\mu_2\kappa_2^2}\right\} \end{aligned} \tag{5.21}$$

where $\mu_2 = \alpha + j\omega_2\beta_2\Delta\omega$ and $\bar{P}_0$ is the strength of P_0 at the frequency 0 and the beginning of the fibre.

Besides this standard ODSB modulation without chirp, other modulation methods, such as direct modulation of laser, modulation by using electroabsorption modulator (EAM) or single-electrode MZM, can also produce ODSB formats. Generally, these modulation methods produce intensity modulation with some level of phase modulation, that is, some level of chirp

which can be characterized by a chirp parameter α_c. It can be shown [40] that the intensity evolution for such cases are:

$$\tilde{P}_0'\big|_{\omega_2} = 2m\bar{P}_0'\sqrt{1+\alpha_c^2}\cos\big[\kappa_2 z + \arctan(\alpha_c)\big]\exp(-\mu z) \tag{5.22}$$

Then we can express the nonlinear crosstalk due to XPM for such links as:

$$\begin{aligned} Cr|_{ODSB} = \frac{4m\gamma\bar{P}_0\bar{P}_0' e^{-\mu_2 z}e^{-\alpha z}}{\mu_2^3 + 4\mu_2\kappa_2^2} \\ \times\Big\{2(e^{\mu_2 z}-1)(\mu_2 - 2\kappa_2\alpha_c)\kappa_2\cos(\kappa_2 z) \\ -\big[e^{\mu_2 z}(2\mu_2^2+4\kappa_2^2) - 4\kappa_2^2\big]\sin(\kappa_2 z) \\ +2(1+e^{\kappa_2 z})\mu_2\kappa_2\alpha_c\sin(\kappa_2 z)\Big\} \end{aligned} \tag{5.23}$$

5.2.2.2 The OSSB Modulation

Unlike ODSB, OSSB is immune to RF power fading problem and hence is widely used in microwave fibre-optic links. Typically, OSSB modulation can be generated by using a DD-MZM biased at the quadrature point and shifting the phase of one RF drive to the other by $\pi/2$. The small signal approximation of the results for OSSB in Chapter 3 is:

$$\tilde{P}_0'\big|_{\omega_2} = j\sqrt{2}m\bar{P}_0'\exp(-j\kappa_2 z)\exp(-\mu_2 z) \tag{5.24}$$

Similar to the procedure for the ODSB case, according to Eq. (5.15) and Eq. (5.16), the strength of the generated nonlinear crosstalk due to XPM at ω_2 is:

$$\begin{aligned} Cr|_{OSSB} = j2\sqrt{2}m\gamma\bar{P}_0\bar{P}_0' e^{-(\mu_2+j\kappa_2)z}e^{-\alpha z} \\ \times\frac{e^{\mu_2 z}\big[j(e^{j2\kappa_2 z}-1)\mu_2 + 2\kappa_2\big] - 2\kappa_2}{\mu_2(\mu_2+j2\kappa_2)} \end{aligned} \tag{5.25}$$

Besides generation OSSB by using DD-MZM, some microwave fibre-optic links use remote heterodyning method to generate microwave signal optically by beating the output of two correlated laser sources operating at desired frequency spacing. Such a method can be also viewed as OSSB and it is easy to find that $\tilde{P}_0'$ for such links can also be expressed as Eq. (5.24). Therefore Eq. (5.25) can also be used for the nonlinear crosstalk due to XPM in such links.

5.3 Nonlinear Intermodulation

Nonlinear intermodulation is different from nonlinear crosstalk in that the former involves two subcarriers and results in a new subcarrier called as nonlinear intermodulation product (NIMP) generated by the two subcarriers. This NIMP may appear at such a frequency as to interfere with another original subcarrier. The model for nonlinear crosstalk in the previous section is actually based on pump-probe approach, which means that we assume two channels, one modulated by subcarriers and the other operating as continuous-wave so that the nonlinear time differential terms in the equations can be neglected. When we study the nonlinear intermodulation, this terms cannot be neglected and hence the pump-probe approach is not appropriate any more. Even though NIMP is typically much smaller than nonlinear crosstalk, it is still very important for some systems. For example, the desired subcarriers in electrooptical upconversion systems are also generated by mixing two subcarriers optically. For such systems, the subcarrier-to-crosstalk ratio and upconverted-subcarrier-to-NIMP ratio should be at the same level and hence NIMP may have significant impact on the performance of such systems.

5.3.1 The General Analytical Model

Perturbation theory is still the basis of our analysis. However, the pump-probe approach used in Section 5.2 cannot be used here to derive the expressions for NIMPs. Hence, we assume that

$$A(z,T) = B_0(z,T) + \sum_{n=1}^{\infty} \gamma^n B_n(z,t) \tag{5.26}$$

Therefore, we get the following two equations from NLSE

$$\frac{\partial B_0}{\partial z} + \frac{j\beta_2}{2}\frac{\partial^2 B_0}{\partial T^2} + \frac{\alpha}{2}B_0 = 0 \tag{5.27a}$$

$$\frac{\partial B_1}{\partial z} + \frac{j\beta_2}{2}\frac{\partial^2 B_1}{\partial T^2} + \frac{\alpha}{2}B_1 = j|B_0|^2 B_0 \tag{5.27b}$$

where B_0 is the solution with fibre dispersion only. The Fourier transform of Eq. (5.27) is

$$\frac{\partial \tilde{B}_0}{\partial z} - \frac{j\beta_2\omega^2}{2}\tilde{B}_0 + \frac{\alpha}{2}\tilde{B}_0 = 0 \tag{5.28a}$$

$$\frac{\partial \tilde{B}_1}{\partial z} - \frac{j\beta_2\omega^2}{2}\tilde{B}_1 + \frac{\alpha}{2}\tilde{B}_1 = j\tilde{P}_0 \otimes \tilde{B}_0 \tag{5.28b}$$

where $P_0 = |B_0|^2$. Therefore,

$$\tilde{B}_0 = \tilde{B}(0,\omega)\cdot\exp\left(\frac{j\beta_2\omega^2 z}{2}\right)\cdot\exp\left(-\frac{\alpha z}{2}\right) \tag{5.29a}$$

$$\tilde{B}_1 = j\exp\left(\frac{j\beta_2\omega^2 z}{2}\right)\cdot\exp\left(-\frac{\alpha z}{2}\right)\cdot \int_0^z (\tilde{P}_0 \otimes \tilde{B}_0)\cdot\exp\left(-\frac{j\beta_2\omega^2 z'}{2}\right)\cdot\exp\left(\frac{\alpha z'}{2}\right)dz' \tag{5.29b}$$

From the conjugate form of NLSE, we can get another set of equations, which give us the solution of B_0^* and B_1^*.

$$\tilde{B_0^*} = \tilde{B^*}(0,\omega) \cdot \exp\left(-\frac{j\beta_2\omega^2 z}{2}\right) \cdot \exp\left(-\frac{\alpha z}{2}\right) \tag{5.30a}$$

$$\tilde{B_1^*} = -j \exp\left(-\frac{j\beta_2\omega^2 z}{2}\right) \cdot \exp\left(-\frac{\alpha z}{2}\right) \cdot \int_0^z (\tilde{P_0} \otimes \tilde{B_0^*}) \cdot \exp\left(\frac{j\beta_2\omega^2 z'}{2}\right) \cdot \exp\left(\frac{\alpha z'}{2}\right) dz' \tag{5.30b}$$

For direct detection, we get

$$P = |A|^2 = |B_0 + \gamma B_1|^2 \approx P_0 + \gamma(B_0 B_1^* + B_0^* B_1) \tag{5.31}$$

and hence

$$\tilde{P} \approx \tilde{P_0} + \gamma(\tilde{B_0} \otimes \tilde{B_1^*} + \tilde{B_0^*} \otimes \tilde{B_1}) \tag{5.32}$$

Therefore, the final expression for NIMP is

$$\begin{aligned} NIMP = {} & j\tilde{B_0^*} \otimes \left[\exp\left(\frac{j\beta_2\omega^2 z}{2}\right) \cdot \exp\left(-\frac{\alpha z}{2}\right) \cdot \int_0^z (\tilde{P_0} \otimes \tilde{B_0}) \cdot \exp\left(-\frac{j\beta_2\omega^2 z'}{2}\right) \cdot \exp\left(\frac{\alpha z'}{2}\right) dz'\right] \\ & -j\tilde{B_0} \otimes \left[\exp\left(-\frac{j\beta_2\omega^2 z}{2}\right) \cdot \exp\left(-\frac{\alpha z}{2}\right) \cdot \int_0^z (\tilde{P_0} \otimes \tilde{B_0^*}) \cdot \exp\left(\frac{j\beta_2\omega^2 z'}{2}\right) \cdot \exp\left(\frac{\alpha z'}{2}\right) dz'\right] \end{aligned} \tag{5.33}$$

For microwave fibre-optic links, $\tilde{B_0}$, $\tilde{B_0^*}$ and $\tilde{P_0}$ consist of Dirac delta functions and the convolutions in Eq. (5.33) can be performed easily through frequency shift and multiplication. Therefore Eq. (5.33) enables us to find the corresponding nonlinear distortion due to fibre at different frequencies.

The above derivation is for a single optical channel and the nonlinear

distortion due to SPM. However, the model can be extended to WDM and XPM easily by modifying Eq. (5.27b) as follows:

$$\frac{\partial B_1}{\partial z} + \frac{j\beta_2}{2}\frac{\partial^2 B_1}{\partial T^2} + \frac{\alpha}{2}B_1 = j2P_0'(z, T - \beta_2\Delta\omega z)B_0 \tag{5.34}$$

where $P_0'(z, T - \beta_2\Delta\omega z) = |B_0'(z, T - \beta_2\Delta\omega z)|^2$ is the intensity of another optical channel at ω_0' inducing XPM to the channel at ω_0, $\Delta\omega = \omega_0 - \omega_0'$ is the angular frequency difference between the two channels and $\beta_2\Delta\omega z$ stands for the optical field envelope time delay between the two optical channels due to the walk-off effect. When we do not consider the walk-off effect, the Fourier transform of P_0' is generally of the form:

$$\tilde{P}_0' = \tilde{P}_z'(z, \omega)\exp(-\alpha z) \tag{5.35}$$

where $\tilde{P}_z'(z, \omega)$ is the intensity evolution without fibre loss. When the walk-off effect is included, we find that:

$$\begin{aligned}\tilde{P}_0' &= \tilde{P}_z'(z, \omega)\exp(-\alpha z)\exp(-j\omega\beta_2\Delta\omega z) \\ &= \tilde{P}_z'(z, \omega)\exp(-\mu z)\end{aligned} \tag{5.36}$$

where $\mu = \alpha + j\omega\beta_2\Delta\omega$. The introduction of the new complex fibre loss parameter μ results in the same form of P_0' with the walk-off effect as that without the walk-off effect. Therefore the expression Eq. (5.33) can also be used for XPM after replacing P_0 by P_0', α by μ, and multiplying by 2 since XPM is two times greater than SPM.

	Expressions for ODSB
$\tilde{P}_0'$	$\delta(\omega) + m_2 \cos(\beta_2\omega_2^2 z/2)\delta(\omega-\omega_2) + m_2 \cos(\beta_2\omega_2^2 z/2)\delta(\omega+\omega_2)$
$\tilde{B}_0$	$\delta(\omega) + m_1 \exp(j\beta_2\omega_1^2 z/2)\delta(\omega-\omega_1) + m_1 \exp(j\beta_2\omega_1^2 z/2)\delta(\omega+\omega_1)$
$\tilde{B}_0^*$	$\delta(\omega) + m_1 \exp(-j\beta_2\omega_1^2 z/2)\delta(\omega-\omega_1) + m_1 \exp(-j\beta_2\omega_1^2 z/2)\delta(\omega+\omega_1)$

Table 5.1: The general expressions used in Eq. (5.33) for ODSB modulation.

5.3.2 Two Special Cases: ODSB and OSSB

For SCM systems, Eq. (5.33) is generally integratable. For demonstration, we assume that the frequency of a subcarrier in B_0 is ω_1 and the frequency of a subcarrier in B_0' is ω_2. The general expressions for $\tilde{P}_0'$, $\tilde{B}_0$ and $\tilde{B}_0^*$ are listed in Table 5.1 and 5.2 for ODSB modulation and OSSB modulation respectively. Eq. (5.33) results in many new subcarriers such as those at $\omega_1+\omega_2$ and $\omega_1-\omega_2$, different from those subcarriers which are generated by nonlinear crosstalk and located at either ω_1 or ω_2. These new subcarriers are results of the interaction between at least two subcarriers and their magnitude is generally at the level of $m_1 m_2$. Hence, they can be viewed as a kind of intermodulation through fibre nonlinearity. For XMP, these IMPs will be generated and cause interference across optical channels. Because two subcarriers are involved in the process to generate these NIMPs, one of $\tilde{P}_0'$, $\tilde{B}_0$ and $\tilde{B}_0^*$ must choose $\delta(\omega)$ for the interaction. It is easy to find that $\tilde{P}_0'$ cannot choose $\delta(\omega)$, otherwise the result will be zero. Hence, $\delta(\omega)$ can only be chosen from $\tilde{B}_0$ or $\tilde{B}_0^*$. This greatly simplifies our analytical calculation later. Here we just derive the analytical expressions for the NIMP at $\omega_1+\omega_2$, for different types of modulation on the two optical channels.

Let $\mu_2 = \alpha + j\omega_2\beta_2\Delta\omega$. When both B_0' and B_0 are OSSB modulated, we

	Expressions for OSSB
$\tilde{P}_0'$	$\delta(\omega) + m_2 \exp(j\beta_2\omega_2^2 z/2)\delta(\omega-\omega_2) + m_2 \exp(-j\beta_2\omega_2^2 z/2)\delta(\omega+\omega_2)$
$\tilde{B}_0$	$\delta(\omega) + m_1 \exp(j\beta_2\omega_1^2 z/2)\delta(\omega-\omega_1)$
$\tilde{B}_0^*$	$\delta(\omega) + m_1 \exp(-j\beta_2\omega_1^2 z/2)\delta(\omega-\omega_1)$

Table 5.2: The general expressions used in Eq. (5.33) for OSSB modulation.

find that

$$NIMP|_{\omega_1+\omega_2} = j2m_1m_2\gamma\bar{P}_0\bar{P}_0' \exp(-\alpha z)\cdot \\ [D_1 \cdot L_e(\mu_2 + j\beta_2\omega_1\omega_2) - D_2 \cdot L_e(\mu_2 - j\beta_2\omega_2^2)] \quad (5.37)$$

When B_0' is ODSB modulated and B_0 is OSSB modulated, then

$$NIMP|_{\omega_1+\omega_2} = jm_1m_2\gamma\bar{P}_0\bar{P}_0' \exp(-\alpha z)\cdot \\ \{D_1 \cdot [L_e(\mu_2 + j\beta_2\omega_1\omega_2) + L_e(\mu_2 + j\beta_2\omega_2(\omega_1+\omega_2))] \\ -D_2 \cdot [L_e(\mu_2 - j\beta_2\omega_2^2) + L_e(\mu_2)]\} \quad (5.38)$$

When B_0' is OSSB modulated and B_0 is ODSB modulated, then

$$NIMP|_{\omega_1+\omega_2} = j2m_1m_2\gamma\bar{P}_0\bar{P}_0' \exp(-\alpha z)\cdot \\ [D_1 \cdot L_e(\mu_2 + j\beta_2\omega_1\omega_2) - D_2 \cdot L_e(\mu_2 - j\beta_2\omega_2^2) \\ -D_1^* \cdot L_e(\mu_2 - j\beta_2(\omega_1+\omega_2)\omega_2) + D_2^* \cdot L_e(\mu_2)] \quad (5.39)$$

When both B_0' and B_0 are ODSB modulated, then

$$NIMP|_{\omega_1+\omega_2} = jm_1m_2\gamma\bar{P}_0\bar{P}_0' \exp(-\alpha z)\cdot \\ \{D_1 \cdot [L_e(\mu_2 + j\beta_2\omega_1\omega_2) + L_e(\mu_2 + j\beta_2\omega_2(\omega_1+\omega_2))]$$

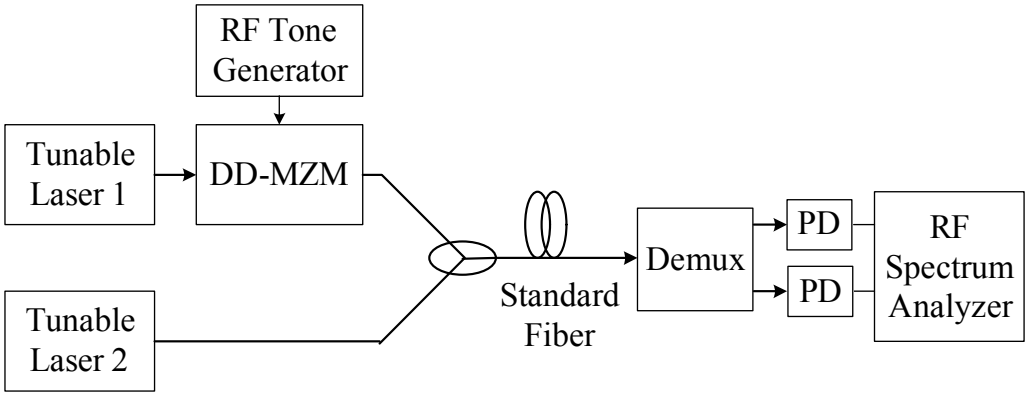

Figure 5.2: The setup for simulations and experiments. Demux: Wavelength demultiplexer; PD: Photodetector.

$$\begin{aligned}
&-D_2 \cdot [L_e(\mu_2 - j\beta_2\omega_2^2) + L_e(\mu_2)] \\
&-D_1^* \cdot [L_e(\mu_2 - j\beta_2\omega_1\omega_2) + L_e(\mu_2 - j\beta_2(\omega_1+\omega_2)\omega_2)] \\
&+D_2^* \cdot [L_e(\mu_2 + j\beta_2\omega_2^2) + L_e(\mu_2)]\} \qquad (5.40)
\end{aligned}$$

In Eq. (5.37) $\sim$ Eq. (5.40),

$$L_e(x) = \frac{1-\exp(-x)}{x} \qquad (5.41a)$$

$$D_1 = \exp\left[j\frac{\beta_2(\omega_1+\omega_2)^2 z}{2}\right] \qquad (5.41b)$$

$$D_2 = \exp\left[j\frac{\beta_2(\omega_1^2-\omega_2^2) z}{2}\right] \qquad (5.41c)$$

$$D_1^* = \exp\left[-j\frac{\beta_2(\omega_1+\omega_2)^2 z}{2}\right] \qquad (5.41d)$$

$$D_2^* = \exp\left[-j\frac{\beta_2(\omega_1^2-\omega_2^2) z}{2}\right] \qquad (5.41e)$$

Note that when $\omega_1 = 0$, Eqs. (5.37) - (5.40) reduce to the expressions for nonlinear crosstalk (Eqs. (5.21) and (5.25)).

5.4 Analysis and Discussion

We study the nonlinear distortion due to XPM in dispersive WDM microwave fibre-optic links by using the setup shown in Fig. 5.2 which matches our analytical model and is also used for experiments. The output of two tuneable laser sources is combined and transmitted in the same fibre. A section of standard single mode fibre is used in the set-up. One of the laser outputs is modulated by an RF tone using a DD-MZM and the other laser output is continuous wave (CW). For simulation purposes, this CW channel can also be modulated so that we can study NIMPs across the two channels. To avoid SBS, the power launched into the fibre for both lasers is kept below 6 dBm. At the output of the fibre, the two channels are demultiplexed and are measured by an RF spectrum analyzer after photodetection. Due to XPM, there will be an RF tone present at the CW channel. The magnitude of the RF tone at this CW channel is a measure of the nonlinear crosstalk level between the two channels.

5.4.1 Calculated Results

The nonlinear crosstalk evolution along a 100 km fibre for ODSB and OSSB are calculated based on Eqs. (5.23) and (5.25), and shown in Figure 5.3 and Figure 5.4 respectively. Both 10 GHz and 20 GHz subcarrier cases are investigated. The optical channel spacing is 100 GHz and the launched optical power is 0 dBm for both channels. The modulation index for both cases is 0.1; the fibre loss parameter $\alpha = 0.2\,\mathrm{dB/km}$; the fibre dispersion parameter $D = 17\,\mathrm{ps/nm{\cdot}km}$ ($D = -2\pi c\beta_2/\lambda^2$); and the fibre nonlinearity parameter $\gamma = 2.4\,\mathrm{W^{-1}/km}$. Using the same parameter values (RF frequencies, modulation formats, channel spacing, optical powers, fibre parameters for length, loss, dispersion and nonlinearity) as those for our analytical calculations, the

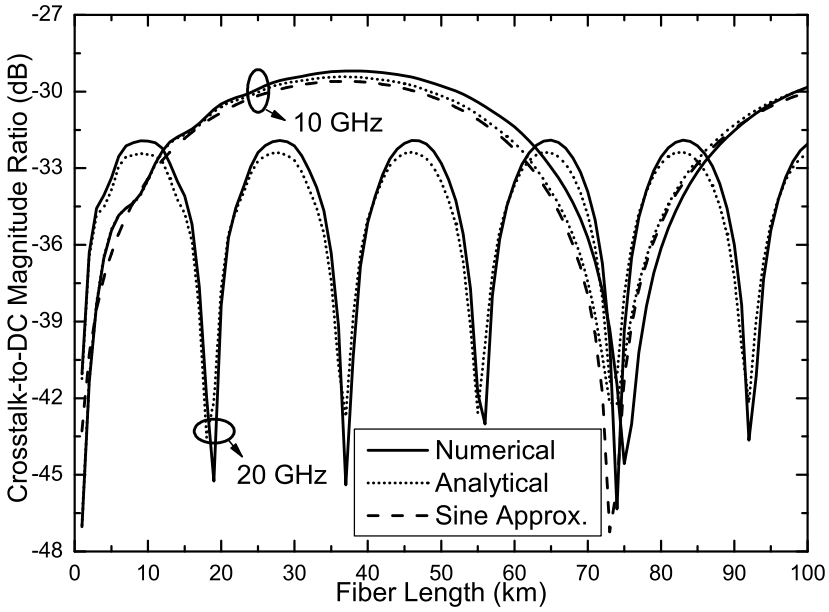

Figure 5.3: Calculated ratio of crosstalk to detected dc current level vs. fibre length. The solid lines and dotted lines are numerical and analytical calculation results, respectively. The dashed line is the sine approximation for the 10 GHz subcarrier.

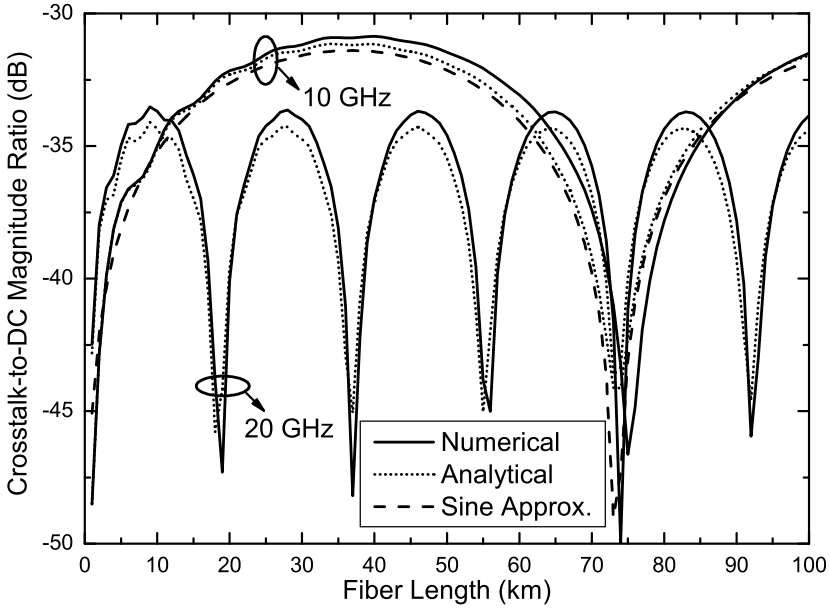

Figure 5.4: Calculated ratio of crosstalk to detected dc current level vs. fibre length. The solid lines and dotted lines are numerical and analytical calculation results, respectively. The dashed line is the sine approximation for the 10 GHz subcarrier.

numerical simulations shown as the solid curves in the figures are performed based on the split-step Fourier (SSF) method to verify our analytical results.

Figure 5.3 and Figure 5.4 show that the results calculated using our analytical model match those obtained by numerical simulation very well, even when the fibre length is quite long for such high frequency subcarrier cases. The results show that for WDM microwave fibre-optic links, the crosstalk level increases sharply at the beginning of the fibre and reaches its maximum value very soon. Hence the crosstalk may cause problem even for short fibre links. A noteworthy character of the crosstalk is its similarity to periodic power fading. It is very similar to the response of a dispersive link using phase modulation, which is characterized by $\sin(\kappa_2 z)$; this behaviour is shown by a dash curve for the 10 GHz subcarrier in Figure 5.3 and Figure 5.4 for comparison. Actually, although the crosstalk level can periodically drop to a very low level, it does not go to zero. However, given that Eq. (5.21) and Eq. (5.23) are quite complicated, the $\sin(\kappa_2 z)$ approximation lets us estimate the crosstalk evolution quickly.

Another interesting phenomenon observed in Figures 5.3 and 5.4 is that the maximum value of the crosstalk for the 20 GHz case is smaller than that for the 10 GHz case. It has been reported [43], [44] that a higher subcarrier frequency induces a higher crosstalk among channels through XPM. Indeed, this is true at the beginning of the fibre, which shows that the crosstalk in the 20 GHz case is higher and increases more sharply than that in the 10 GHz case. However, it is not true for the maximum crosstalk level. This interesting phenomenon means less nonlinear crosstalk problem for systems operating at higher microwave frequency. Hence, it is also important to get

a proper approximation to estimate the maximum crosstalk level quickly.

With the approximation $\sin(\kappa_2 z)$, we find that the maximum crosstalk occurs at $\kappa_2 z = \pm\pi/2$. Then we can find the following relationship for standard ODSB and OSSB modulation when $\kappa_2 z = \pm\pi/2$:

$$Cr|_{ODSB_{max}} = 4m\gamma\bar{P}_0\bar{P}_0' e^{-\alpha z} \cdot L_e(\mu_2)\frac{2\mu_2/L_e(\mu_2) + 4\kappa_2^2}{\mu_2^2 + 4\kappa_2^2} \tag{5.42a}$$

$$Cr|_{OSSB_{max}} = j2\sqrt{2}m\gamma\bar{P}_0\bar{P}_0' e^{-\alpha z} \times L_e(\mu_2)\frac{2/L_e(\mu_2) + j2\kappa_2}{\mu_2 + j2\kappa_2} \tag{5.42b}$$

where $L_e(\mu_2) = (1 - e^{-\mu_2 z})/\mu_2$. For large fibre lengths, $L_e(\mu_2) \to 1/\mu_2$ and Eq. (5.42) can be further simplified as:

$$Cr|_{ODSB_{max}} = 4m\gamma\bar{P}_0\bar{P}_0' e^{-\alpha z} \times L_e(\mu_2)\left[1 + \frac{1}{1 + (2\kappa_2/\mu_2)^2}\right] \tag{5.43a}$$

$$Cr|_{OSSB_{max}} = j2\sqrt{2}m\gamma\bar{P}_0\bar{P}_0' e^{-\alpha z} \times L_e(\mu_2)\left[1 + \frac{1}{1 + j(2\kappa_2/\mu_2)}\right] \tag{5.43b}$$

Because $2\kappa_2/\mu_2 \approx \omega_2/\Delta\omega$ which is typically very small, we can further approximate the two equations, Eq. (5.43) and Eq. (5.44), by a single relationship:

$$Cr|_{max} \propto 2m\gamma\bar{P}_0\bar{P}_0' L_e(\mu_2) \to \frac{2m\gamma\bar{P}_0\bar{P}_0'}{\mu_2} = \frac{2m\gamma\bar{P}_0\bar{P}_0'}{\sqrt{\alpha^2 + (\omega_2\beta_2\Delta\omega)^2}} e^{-j\arctan\left(\frac{\omega_2\beta_2\Delta\omega}{\alpha}\right)} \tag{5.44}$$

Eq. (5.44) shows that the maximum crosstalk level decreases as the channel spacing and modulating subcarrier frequency increase. Given that the

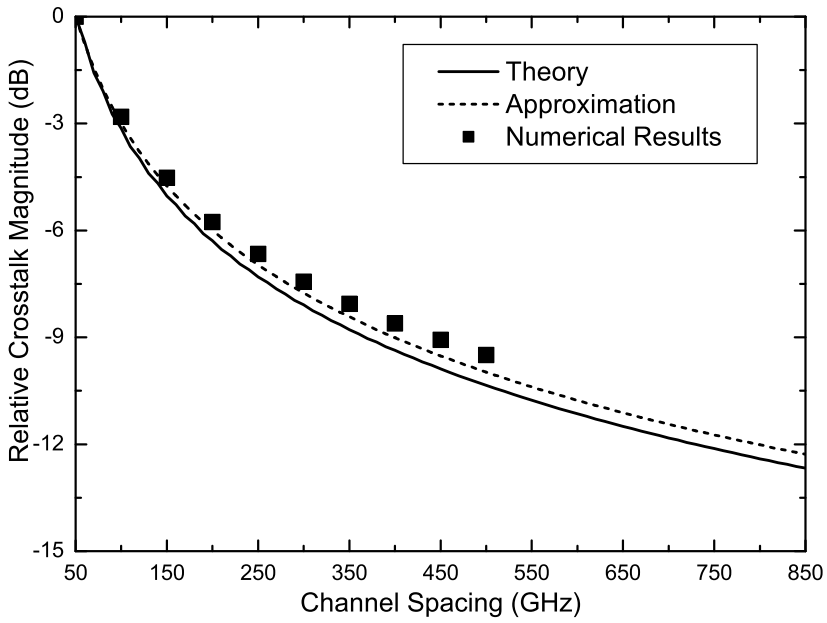

Figure 5.5: The relationship between the crosstalk magnitude and optical channel spacing. The results are normalized to the crosstalk magnitude at 50 GHz channel spacing. The solid line is the result by our analytical model; the short dash line is the result by our theoretical approximation; the square markers are numerical results.

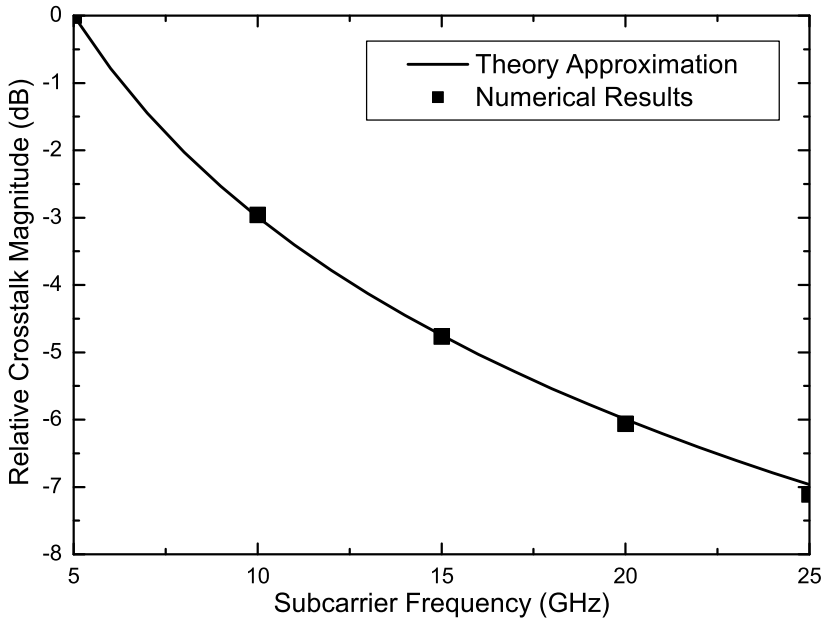

Figure 5.6: The relationship between the crosstalk magnitude and the modulating subcarrier frequency. The results are normalized to the crosstalk magnitude of the subcarrier at 5 GHz. The solid line is the result by our theoretical approximation; the square markers are the numerical simulation results.

crosstalk evolution can be approximated by $\sin(\kappa_2 z)$, the nonlinear crosstalk due to XPM can now be estimated quickly by using this simple expression. The solid curve in Figure 5.5 shows the calculated results according to our analytical model for a 37 km fibre link, for which case the crosstalk of the 10 GHz system reaches its maximum value. An approximation curve based on Eq. (5.44) is also shown as a short dash line, which is very close to the analytical model result. Both theory and approximation results match the numerical results based on SSF method very well. This figure shows that the crosstalk level drops gradually as the channel spacing increases, indicating that XPM typically affects the closest channels. The rate of drop also gradually slows down and can be quickly estimated from Eq. (5.44). Figure 5.6 shows the maximum crosstalk level versus the modulating subcarrier frequency for a 100 GHz optical channel spacing. Numerical results based on SSF method are gotten by finding the crosstalk level at $z = |\pi/(\beta_2\omega^2)|$. The solid curve is calculated from Eq. (5.44). The theoretical approximation matches the numerical results very well. The figure also shows that the maximum crosstalk level decrease as the modulating subcarrier frequency increases. Moreover, Figure 5.5 and Figure 5.6 show that the approximation in Eq. (5.44) is very good.

The NIMP evolutions along fibre length between two optical channels spaced at 100 GHz for several modulation settings are also calculated and shown in Figures 5.7 - 5.9. Other parameters are the same as those used in the previous figures. The match between the numerical results based on SSF method and the analytical results is still very good. NIMP shows similar characters as those of nonlinear crosstalk. However, the power fading period of NIMP is not determined by the NIMP frequency. It is determined by the

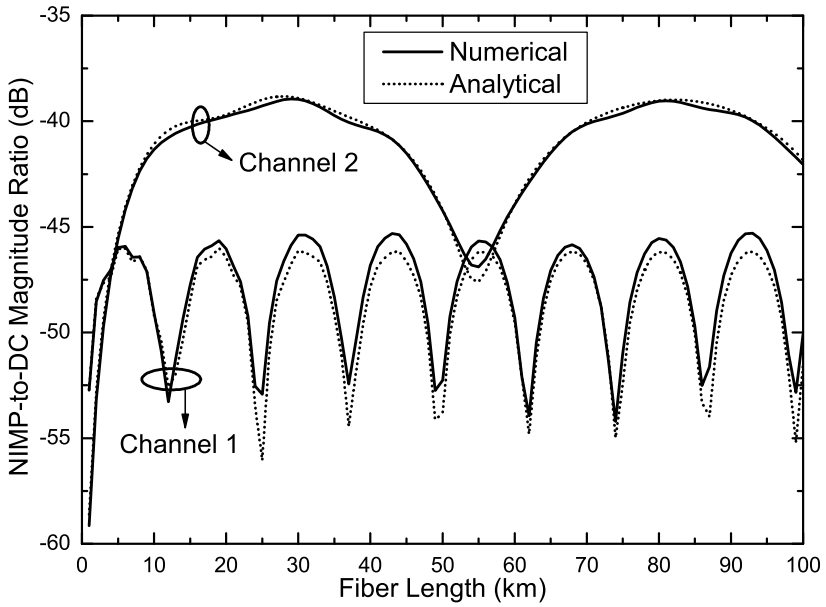

Figure 5.7: Calculated ratio of NIMP at 27 GHz to detected dc current level vs. fibre length for both channels. The solid lines and dotted lines are numerical and analytical calculation results, respectively. Channel 1 is OSSB modulated by a 5 GHz subcarrier while channel 2 is OSSB modulated by a 22 GHz subcarrier.

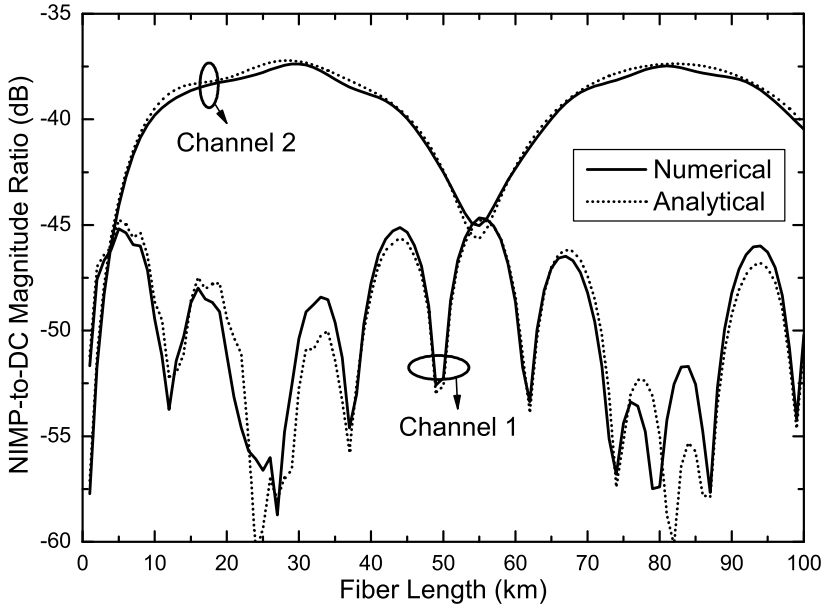

Figure 5.8: Calculated ratio of NIMP at 27 GHz to detected dc current level vs. fibre length for both channels. The solid lines and dotted lines are numerical and analytical calculation results, respectively. Channel 1 is ODSB modulated by a 5 GHz subcarrier while channel 2 is OSSB modulated by a 22 GHz subcarrier.

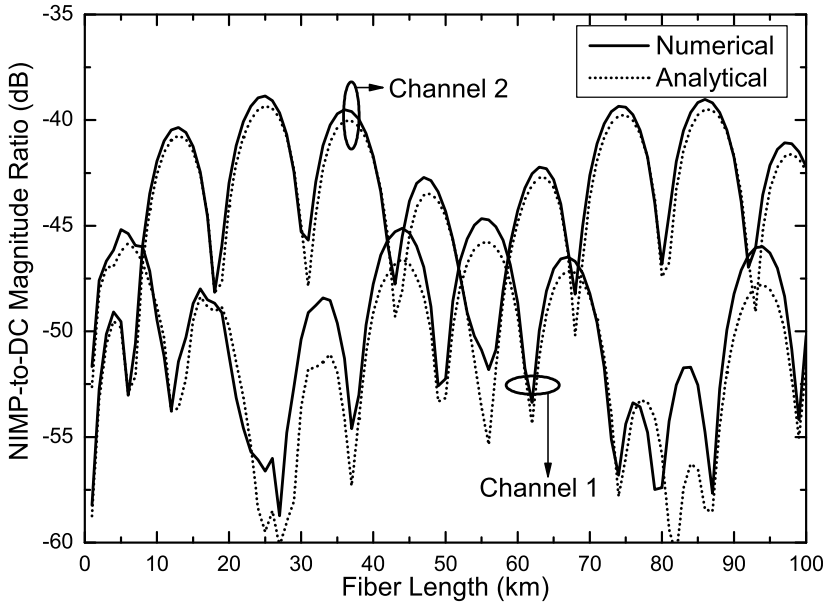

Figure 5.9: Calculated ratio of NIMP at 27 GHz to detected dc current level vs. fibre length for both channels. The solid lines and dotted lines are numerical and analytical calculation results, respectively. Channel 1 is ODSB modulated by a 5 GHz subcarrier while channel 2 is ODSB modulated by a 22 GHz subcarrier.

two subcarrier frequencies together which generate the NIMP.

Similar to the discussion of the approximation of the nonlinear crosstalk expressions, when the channel spacing $\Delta\omega$ is much larger than the subcarrier frequencies ω_1 and ω_2, all $L_e(x)$ in Eqs. (5.37) - (5.40) can be approximated as $L_e(\mu_2)$. Then, Eqs. (5.37) - (5.40) can be simplified further. When B_0 is OSSB modulated, then

$$\begin{aligned} NIMP|_{\omega_1+\omega_2} = -4m_1m_2\gamma\bar{P}_0\bar{P}_0' \exp(-\alpha z)L_e(\mu_2)\cdot \\ \exp\left[j\frac{\beta_2(\omega_1^2+\omega_1\omega_2)z}{2}\right]\cdot \\ \sin\left[\frac{\beta_2(\omega_2^2+\omega_1\omega_2)z}{2}\right] \end{aligned} \tag{5.45}$$

When B_0 is ODSB modulated, then

$$NIMP|_{\omega_1+\omega_2} = -8m_1m_2\gamma\bar{P}_0\bar{P}_0' \exp(-\alpha z)L_e(\mu_2)\cdot \cos\left[\frac{\beta_2(\omega_1^2+\omega_1\omega_2)z}{2}\right]\cdot \sin\left[\frac{\beta_2(\omega_2^2+\omega_1\omega_2)z}{2}\right] \tag{5.46}$$

It is seen that the NIMP evolution is decided only by the modulation format of B_0 and the modulation format of B_0' does not affect this evolution. Moreover, the power fading period of NIMPs is basically decided by $\omega_2^2+\omega_1\omega_2$. The power fading period of nonlinear crosstalk caused by ω_2 is actually a special case of NIMPs when $\omega_1 = 0$. Moreover, the sine approximation can be clearly identified in Eqs. (5.45) and (5.46).

For the maximum NIMP level, we can further approximate Eq. (5.45) and Eq. (5.46), resulting in a single relationship:

$$NIMP|_{\omega_1+\omega_2}^{max} \propto 2m_1m_2\gamma\bar{P}_0\bar{P}_0'L_e(\mu_2) \rightarrow \frac{2m_1m_2\gamma\bar{P}_0\bar{P}_0'}{\mu_2} = \frac{2m_1m_2\gamma\bar{P}_0\bar{P}_0'}{\sqrt{\alpha^2+(\omega_2\beta_2\Delta\omega)^2}}e^{-j\arctan\left(\frac{\omega_2\beta_2\Delta\omega}{\alpha}\right)} \tag{5.47}$$

5.4.2 Experiments

For experiments, the fibre length is 40 km. The fibre loss parameter $\alpha = 0.2\,\text{dB/km}$; the fibre dispersion parameter $D = 17\,\text{ps/nm}\cdot\text{km}$; and the fibre nonlinearity parameter $\gamma = 1\,\text{W}^{-1}/\text{km}$. One of the tuneable lasers is operating in CW mode at $\lambda_{cw} = 1553.33\,\text{nm}$. The other tuneable laser is operating at $\lambda_{mod} = 1552.52\,\text{nm}$ and is modulated by an RF tone which can be tuned from 1 GHz to 18 GHz. OSSB modulation is generated by using a DD-MZM and a 90° hybrid. The modulator shows a $V_\pi = 8.1\,\text{V}$ and OSSB modulation

is realized by biasing the modulator at 4.05 V. The launched optical power at λ_{mod} is -1.7 dBm and that of the CW channel is 5.75 dBm. No significant SBS is observed for both channels. Since OSSB modulation is used to avoid the power fading due to fibre dispersion, the crosstalk-to-subcarrier power ratio (CSR) is defined as the power ratio between the detected RF tone at λ_{cw} and that at λ_{mod}. The adjacent channel isolation of WDM is seen to be greater than 40 dB, resulting in a linear crosstalk well below noise floor.

5.4.2.1 Nonlinear Crosstalk due to XPM

In Fig. 5.10, two RF power levels, 15 dBm and 12 dBm, are used to study the nonlinear crosstalk response as a function of RF frequency. The figure shows that the results of our analytical model match very well the experiment results. Also, the figure confirms the 'periodic' nature of crosstalk level and that for a higher frequency, the maximum possible crosstalk level may not be higher than that at a lower frequency. Fig. 5.10 also shows that the CSR is independent of modulation index since both RF power levels produce the same CSR; this can also be deduced from our expressions easily. Note that due to the degraded response of the experiment link at high frequency, for 12 dBm RF source power the crosstalk level after 11 GHz is below noise level.

Even though the CSR is independent of the modulation index, the launched optical power has an impact on this ratio. From the expressions (e.g., Eq. (5.47)), every 1 dB increase of the launched optical power at both channels leads to 2 dB increase of the CSR. Figure 5.11 shows this tendency graphically by varying the launched optical power at λ_{cw} while keeping the

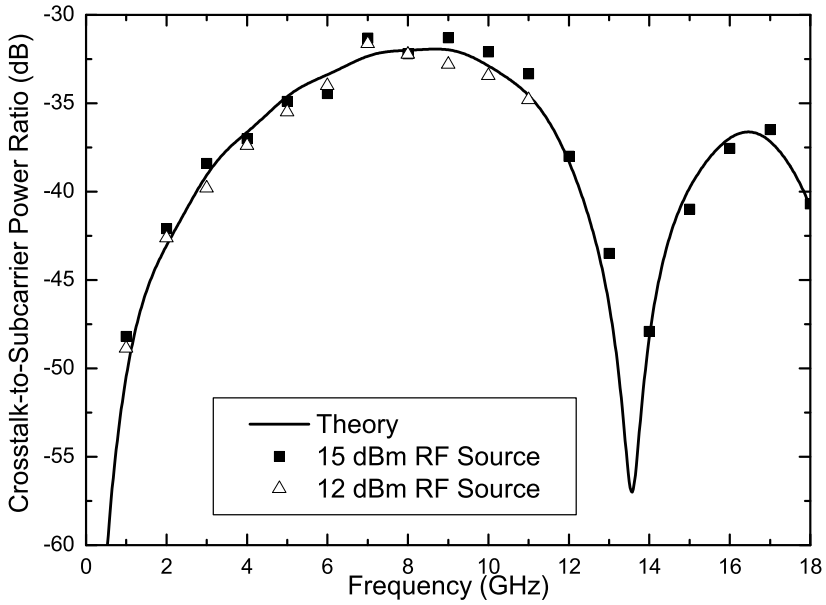

Figure 5.10: Simulation and experiment results of the nonlinear crosstalk due to XPM for a 40 km fibre. The solid line is of the results by analytical model; the square (15dBm RF source) and triangle markers (12 dBm RF source) are experiment results.

launched optical power at λ_{mod} constant at -1.7 dBm. The slope of the linear fit curves for 5 GHz and 10 GHz subcarrier are 1.97 and 2.22 respectively.

Given that the CSR is optical power intensity dependent but RF power independent, the nonlinear crosstalk due to XPM may impose stringent limits on the launched optical power if one wants to keep the nonlinear crosstalk well below noise level across the whole spurious free dynamic range (SFDR). Assuming both channels have the same average launched optical power ($\bar{P}_0 = \bar{P'}_0$), with Eqs. (5.43) and (5.44), the maximum CSR can be approximately written as:

$$CSR|_{max} \approx 16(\gamma \bar{P}_0)^2 |L_e(\mu_2)|^2 \rightarrow \frac{16(\gamma \bar{P}_0)^2}{\alpha^2 + (\omega_2 \beta_2 \Delta\omega)^2} \tag{5.48}$$

It is easy to find that Eq. (5.48) also holds for the maximum NIMP-to-subcarrier power ratio since both NIMPs and upconverted subcarriers are

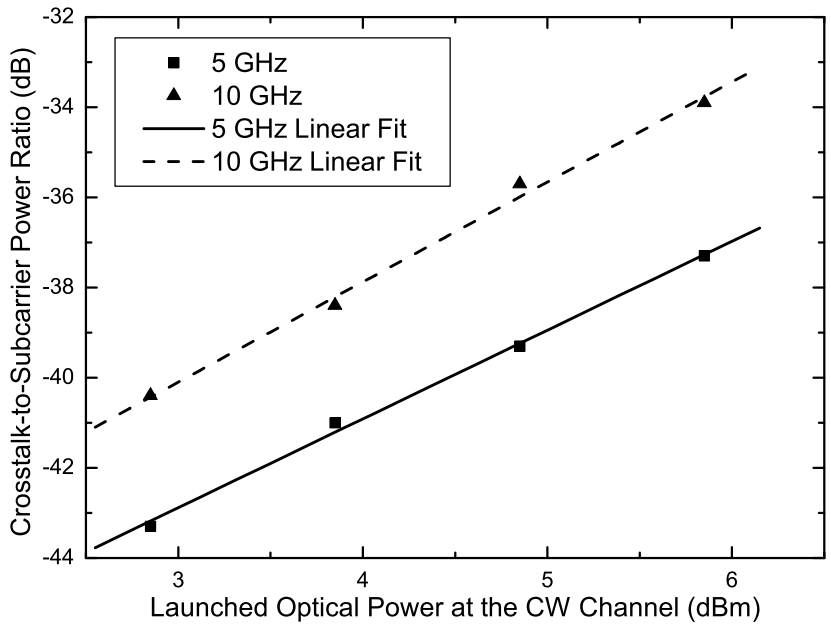

Figure 5.11: Measured and linear fitted CSR versus launched optical power at the CW channel for 5 GHz and 10 GHz subcarrier.

proportional to $m_1 m_2$. Moreover, for NIMPs, because ω_2 can be the intermediate frequency (IF) which is much lower than the subcarrier frequency at $\omega_1 + \omega_2$, the maximum NIMP-to-subcarrier power ratio is then about $(1 + \omega_1/\omega_2)^2$ times the maximum CSR. Therefore, the nonlinear distortion due to XPM can be more detrimental in electrooptical upconversion systems. For a fibre nonlinearity parameter $\gamma = 1\,W^{-1}/km$ and a launched optical power 0 dBm, Eq. (5.48) predicts that the CSR can be much greater than -60 dB for a practical system. For example, a 10 GHz microwave fibre-optic link with 100 GHz optical channel spacing results in this ratio as high as -46.6 dB. Typically, the SFDR requirement for a microwave fibre-optic links can be about $100\,\mathrm{dB}\cdot\mathrm{Hz}^{\frac{2}{3}}$, which means a 3rd-order-intermodulation-to-subcarrier power ratio smaller than -65 dB for a system with 200 kHz bandwidth. Hence the nonlinear crosstalk due to XPM can be an important interference source to limit the SFDR for a practical system; this is shown in Figure 5.12. To lower the nonlinear crosstalk level, according to Eq. (5.48),

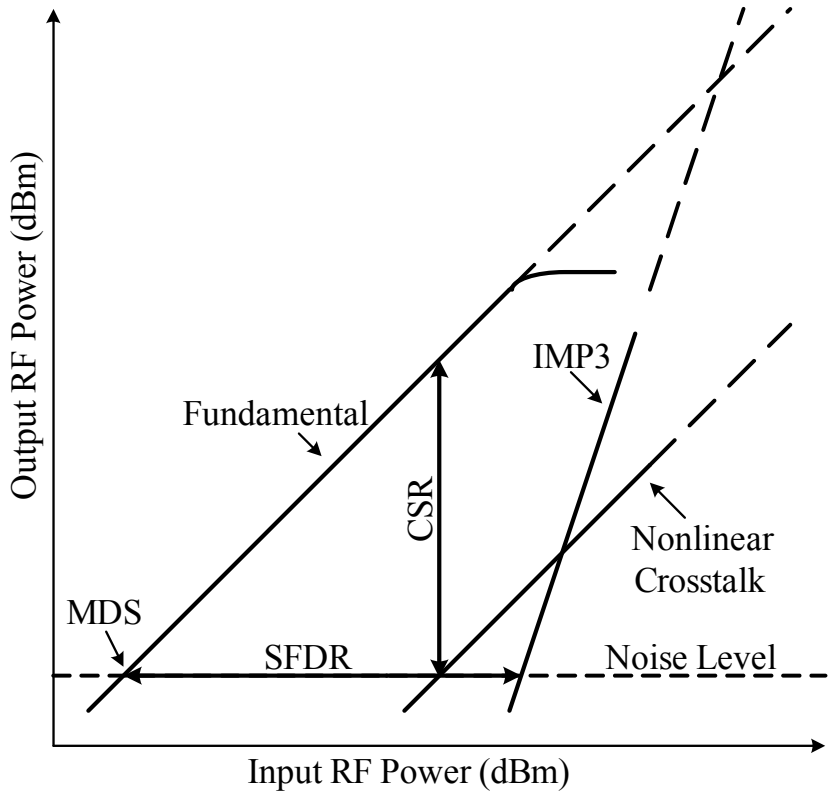

Figure 5.12: The impact of nonlinear crosstalk due to XPM on the SFDR of a microwave fibre-optic link. IMD3: the 3rd-order intermodulation; MDS: minimum discernible signal power.

one can either increase the channel spacing or operate the link at higher subcarrier frequency. The simplest way is just to lower the launched optical power. Lowering 1 dB launched optical power can improve CSR by 2 dB.

5.4.2.2 Effect of Optical Amplification

When one lowers the launched optical power to suppress the nonlinear crosstalk, the received SNR will also be degraded. Optical fibre amplification may then be used to restore this SNR, which may introduce extra nonlinear crosstalk. However, for a WDM microwave fibre-optic link, $|\omega_2\beta_2\Delta\omega|$ is typically much larger than $|\alpha|$ and hence Eq. (5.48) shows that α does

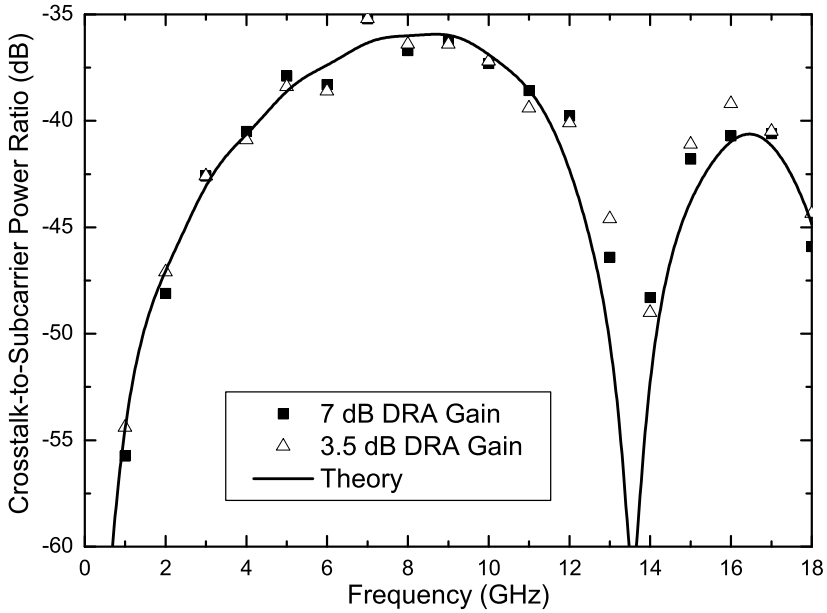

Figure 5.13: The crosstalk-to-subcarrier power ratio versus the modulating subcarrier frequency for a 40 km fibre with DRA. The solid line represents the results by our analytical model; the square makers and hollow triangle markers are the measured results for 7 dB and 3.5 dB gain of DRA respectively.

not have a significant influence on the nonlinear crosstalk level. For example, for a link with a 10 GHz subcarrier, 100 GHz optical channel spacing and using standard single mode fibre, $|\omega_2\beta_2\Delta\omega| \approx 0.86$ while for a standard single mode fibre $\alpha = 0.05\,\mathrm{km}^{-1}$ at $1.55\,\mu$m region. This is even true for practical systems with fibre amplification. For Erbium-doped fibre amplifier (EDFA), the length of EDF is very short and hence the very small accumulated dispersion in the EDF cannot lead to significant nonlinear crosstalk. For distributed Raman amplifier (DRA), the equivalent α after taking the Raman gain coefficient into account is still much smaller than 0.86 for a practical system.

Shown in Fig. 5.13 are the experiment results to study the influence of DRA on the nonlinear crosstalk due to XPM for a 100 GHz optical channel spacing WDM system with 40 km standard single mode fibre. The launched

optical power at λ_{mod} and at λ_{cw} is -0.65 dBm and 5.3 dBm respectively and the RF source power is 15 dBm. Cases with 7 dB and 3.5 dB DRA gain are studied. The measured results for both cases match with our analytical results without DRA very well. Note that at the high frequency region, the link response degrades and hence it is not surprising to see some relatively large measurement errors at this region for the case of 3.5 dB DRA gain. Therefore, the figure confirms that the DRA does not have significant impact on the nonlinear crosstalk level. The nonlinear crosstalk is mainly decided by the channel spacing, modulating subcarrier frequency, launched optical power, fibre dispersion and nonlinear parameter. Consequently, Eq. (5.48) can be used to estimate the maximum nonlinear distortion due to XPM in most practical WDM microwave fibre-optic links with and without fibre amplification quickly and accurately.

5.5 Summary and Conclusion

We have presented a new analytical model to study the nonlinear distortion due to XPM in dispersive WDM microwave fibre-optic links. The model is not based on the pump-probe approach and hence the results of our model can be used in systems such as electrooptical upconversion systems. Verified by simulations and experiments, our analytical model can predict this nonlinear distortion quite accurately even for very long fibre lengths and very high subcarrier frequencies.

Based on our model, two commonly used modulation methods, ODSB and OSSB, have been studied in detail and closed form expressions have been derived. The theoretical prediction matches numerical and experiment results very well. The studies show that a closer optical channel spacing

results in a higher nonlinear distortion level. Besides, the nonlinear distortion experiences a variation similar to power fading even when the original subcarrier does not experience power fading. Moreover, while higher subcarrier frequencies lead to sharper increase of nonlinear distortion level at the beginning of the fibre, a higher subcarrier frequency does not mean higher maximum nonlinear distortion level. Instead, the maximum nonlinear distortion level gradually drops as the subcarrier frequency increases. This behaviour has been confirmed by experiments as well as numerical simulations.

Further, very simple approximate expressions have been presented to estimate the nonlinear distortion quite accurately. These expressions make the physical mechanism of nonlinear crosstalk generation clearer. It is seen that the impact of fibre loss parameter on the nonlinear distortion level is negligible in dispersive WDM microwave fibre-optic links. The experiment results confirm this point.

In summary, the nonlinear distortion due to XPM in microwave fibre-optic links, especially in electrooptical upconversion systems, can be significant even when the launched optical power is very low and therefore should be considered carefully.

Chapter 6

Conclusion and Future Work

6.1 Conclusion

Subcarrier multiplexing (SCM) is a very promising technique to interface electronic communication systems with optical fibre communication systems, enabling us to utilize the huge bandwidth of optical fibre conveniently and efficiently. Therefore, it is widely used nowadays in broadband networks, especially in access networks. With the popularity of wireless communication and the proposals to exploit microwave and millimetre-wave bands for broadband communication, SCM has been gaining more and more attention in recent years.

The introduction of lightwave techniques as the transmission method leads to some additional nonlinear distortions to SCM signals even though they provide us very huge bandwidth. In this thesis, these nonlinear distortions have been studied in detail, leading to many new and useful results. The focus of these studies is SCM and SCM-WDM systems using microwave or millimetre-wave subcarriers. Moreover, emphasis has been placed on obtaining closed-form solutions of the nonlinear Schrödinger equation (NLSE)

that governs the propagation of lightwaves in dispersive, nonlinear optical fibres. These two aspects do not appear to have been fully investigated so far.

Optical modulators may be the most significant source of nonlinear distortion in SCM optical communication systems. We have studied the nonlinear distortion due to dual-drive Mach-Zehnder modulators (DD-MZM) with fibre dispersion in detail because of its wide usage in SCM optical communication systems. We have presented an exact analytical model to study the dispersive transmission of SCM fibre-optic links using DD-MZM. The model is very general and can take into account different operating conditions and drive levels for the DD-MZM. The model results in simple, new, closed form expressions for output power spectrum, permitting an accurate and fast analysis of such links. In general, for SCM links, the RF output of one subcarrier is not decided by its input solely. Instead, other RF inputs have significant impact on the output of the subcarrier. Moreover, the evolution of one subcarrier in a dispersive fibre link depends not only on the frequency itself but also on other subcarrier frequencies. Therefore, the subcarriers are actually coupled with each other. These phenomena can be analyzed quickly through our closed form expressions. Based on our model, we have studied two commonly used modulation methods, ODSB and OSSB, in detail. Some important system parameters have been derived for the first time. ODSB shows serious power fading under dispersive transmission while OSSB does not experience such power fading except some power fluctuation along fibre. However, OSSB does not show better linearity than ODSB. Instead, the linearity of OSSB may be even 3 dB worse than that of ODSB under dispersive transmission. For both modulation methods, at the same input RF power level, the output RF power level drops as the number of

multiplexing subcarriers increases. Hence, the capacity of a system using DD-MZM is actually limited by a bound, which has been given by our analysis.

Besides optical modulators, optical fibres are also an important source of nonlinearity. The first significant nonlinear distortion caused by the fibre is stimulated Brillouin scattering (SBS). SBS puts a very stringent upper limit on launched optical power, which in turn limits the system capacity seriously. When the launched optical power exceeds SBS threshold, significant amount of optical power is scattered back as Stokes wave with a frequency down shift of about 11 GHz. Besides power loss due to backward scattering, SBS also leads to strong optical power fluctuation and hence the fluctuation in the final detected RF power. The backward Stokes wave can also be scattered to forward direction by Rayleigh scattering and is shown as a strong source of interference at around 11 GHz after detection. Therefore, SBS should be avoided in SCM optical communication systems. To suppress SBS, phase dithering can be used to widen the laser linewidth by phase modulation of the laser output with PRBS signal to increase the SBS threshold. However, due to fibre dispersion, this random phase modulation can be converted to intensity noise after fibre transmission. Besides, our experiments show that there are also some spectral lines spaced at the PRBS data rate which may be undesired interference sources for some systems. The harmonics in the pulse pattern generator (PPG) output are one source of these spectral lines. Our theoretical study shows that the rising and falling edges of PRBS signal can also lead to these spectral lines. This point is confirmed by our experiments which show that the power of these spectral lines fluctuates randomly. Both types of spectral lines can be removed by low pass filtering the PPG

output. Our experiments also confirm this point.

Another type stimulated inelastic scattering, stimulated Raman scattering (SRS), can cause nonlinear crosstalk and nonlinear intermodulation product (NIMP) across optical channels. The most significant character of SRS is its low pass character. Therefore, the nonlinear distortion due to SRS is only significant for low frequency subcarriers such as those in hybrid fibre-coax (HFC) systems. Generally, the Raman-gain coefficient is larger at wider channel spacing. Therefore, more attention should be paid to the nonlinear distortion due to SRS for systems with wider channel spacing.

Nonlinear refraction is another important source of nonlinear distortion due to fibre in SCM-WDM optical fibre communication systems. A comprehensive analysis of such nonlinear distortion is presented in the thesis. The major difference in the analysis presented here and those available in the literature is that pump-probe approach is not used here. This makes the results of the present analysis applicable to systems such as those using electrooptical upconversion. We have first studied the nonlinear crosstalk and then have extended the analysis to cover nonlinear intermodulation. The analytical results match with the numerical analysis and experiments very well. The studies show that closer optical channel spacing results in higher nonlinear crosstalk level. Besides, the nonlinear distortion experiences power fading even when the original subcarrier does not experience power fading. Moreover, higher subcarrier frequencies lead to sharper increase of nonlinear crosstalk level at the beginning of fibre. However, the maximum nonlinear crosstalk level gradually drops as the subcarrier frequency increases. This point may be contrary to common thought but has

been confirmed by experiments as well as numerical simulations. Further studies enabled us to present a very simple approximate expression to estimate the nonlinear crosstalk quite accurately. It is also shown that the impact of fibre amplification on the nonlinear crosstalk level is negligible in microwave fibre-optic links. The experiment results confirm this point.

In summary, for SCM optical communication systems, the launched optical power should be well below SBS threshold. If phase dithering is used to increase the SBS threshold, the PRBS stream should be low pass filtered to remove the interference due to the spectral lines. For SCM-WDM optical communication systems, nonlinear crosstalk due to nonlinear refraction may impose more stringent limit on the launched optical power than SBS according to the nonlinear distortion requirement of the systems. Generally, nonlinear distortion level increases more sharply for higher frequency subcarriers than lower frequency subcarriers. However, the maximum nonlinear distortion level for higher frequency subcarriers is lower than that of lower frequency subcarriers. Besides these nonlinear distortion due to fibre, DD-MZM also leads to serious nonlinear distortion, imposing an upper limit on the system capacity.

6.2 Future Work

In this thesis, several new analytical models have been presented to analyze some major nonlinear distortions in SCM optical communication systems. Based on these models, some suggestions for further works are as follows:

- Optimizing the launched optical power level and the optical amplification scheme. The optical power distribution in fibre for

SCM optical communication systems should be carefully designed to maximize the performance and minimize the nonlinear distortion due to fibre as well. Both distributed Raman amplification and multi-span amplification using EDFA can be used to realize a certain power distribution. Therefore the optical amplification scheme may need optimization. The model presented here can be a basis for such optimization.

- Optimizing the frequency arrangement in SCM optical communication systems. As shown in the thesis, the nonlinear distortion generally depends on the subcarrier frequencies. Therefore, the subcarrier frequencies may need optimization to minimize the nonlinear distortion. For an optimum choice of subcarrier frequencies, the nonlinear distortion from different nonlinear processes may cancel each other.

- The nonlinear distortion due to electro-absorption external modulator (EAM) should be studied. EAM is also gaining wide use as an external modulator in SCM optical communication systems. Therefore, the nonlinear distortion due to EAM for dispersive transmission should be studied.

Bibliography

[1] G. P. Agrawal, *Fiber-Optic Communication Systems*, 3rd ed. Wiley-Interscience, 2002.

[2] W. I. Way, *Broadband Hybrid Fiber/Coax Access System Technologies*. Academic Press, 1995.

[3] B. Wilson, Z. Ghassemlooy, and I. Darwazeh, *Analogue Optical Fiber Communications*. the Institute of Electrical Engineers (IEE), 1995.

[4] W. I. Way, "Subcarrier multiplexed lightwave system design considerations for subscriber loop applications," *J. Lightwave Technol.*, vol. 7, no. 11, pp. 1806–1818, Nov. 1989.

[5] R. Hui, B. Zhu, R. Huang, C. T. Allen, K. R. Demarest, and D. Richards, "Subcarrier multiplexing for high-speed optical transmission," *J. Lightwave Technol.*, vol. 20, no. 3, pp. 417–427, Mar. 2002.

[6] H. Al-Raweshidy and S. Komaki, *Radio over Fiber Technologies for Mobile Communications Networks*. Artech House, 2002.

[7] E. J. Tyler, M. Webster, R. V. Penty, and I. H. White, "Penalty free subcarrier modulated multimode fiber links for datacomm applications

beyond the bandwidth limit," *IEEE Photon. Technol. Lett.*, vol. 14, no. 1, pp. 110–112, Jan. 2002.

[8] W.-P. Lin, M.-S. Kao, and S. Chi, "A reliable architecture for broadband fiber-wireless access networks," *IEEE Photon. Technol. Lett.*, vol. 15, no. 2, pp. 344–346, Feb. 2003.

[9] K. K. Y. Wong, M. E. Marhic, M.-C. Ho, and L. G. Kazovsky, "35-dB nonlinear crosstalk suppression in a WDM analog fiber system by complementary modulation of twin carriers," *IEEE Photon. Technol. Lett.*, vol. 14, no. 5, pp. 699–701, May 2002.

[10] T. Kuri, K. ichi Kitayama, and Y. Takahashi, "A single light-source configuration for full-duplex 60-GHz-band radio-on-fiber system," *IEEE Trans. Microwave Theory Tech.*, vol. 51, no. 2, Feb. 2003.

[11] A. B. Sahin, O. H. Adamczyk, and A. E. Willner, "Dispersion division multiplexing in subcarrier modulated data transmission using channel-specific RF fading," *IEEE Photon. Technol. Lett.*, vol. 14, no. 8, pp. 1190–1192, Aug. 2002.

[12] G. C. Wilson, J.-M. Delavaux, A. Srivastava, C. Hullin, C. McIntosh, C. G. Bethea, and C. Wolf, "Long-haul DWDM/SCM transmission of 64- and 256-QAM using electroabsorption modulated laser transmitters," *IEEE Photon. Technol. Lett.*, vol. 14, no. 8, pp. 1184–1186, Aug. 2002.

[13] C. Bisdikian, K. Maruyama, D. I. Seidman, and D. N. Serpanos, "Cable access beyond the hype: On residential broadband data services over HFC networks," *IEEE Commun. Mag.*, pp. 128–135, Nov. 1996.

[14] A. Kaszubowska, L.P.Barry, and P. Anandarajah, "Effects of intermodulation distortion on the performance of a hybrid radio/fiber system employing a self-pulsating laser diode transmitter," *IEEE Photon. Technol. Lett.*, vol. 15, no. 6, pp. 852–854, Jun. 2003.

[15] H.-H. Lu, S.-J. Tzeng, and Y.-L. Liu, "Intermodulation distortion suppression in a full-duplex radio-on-fiber ring network," *IEEE Photon. Technol. Lett.*, vol. 16, no. 2, pp. 602–604, Feb. 2004.

[16] G. J. Simonis and K. G. Purchase, "Optical generation, distribution, and control of microwave using laser heterodyne," *IEEE Trans. Microwave Theory Tech.*, vol. 38, no. 5, pp. 667–669, May 1990.

[17] Y. Wang and R. Baettig, "A microwave optical phase modulation system," *IEEE Photon. Technol. Lett.*, vol. 7, no. 5, pp. 570–572, May 1995.

[18] I. Seto, H. Shoki, and S. Ohshima, "Optical subcarrier multiplexing transmission for base station with adaptive array antenna," *IEEE Trans. Microwave Theory Tech.*, vol. 49, no. 10, pp. 2036–2041, Oct. 2001.

[19] L. A. Johansson and A. J. Seeds, "Generation and transmission of millimeter-wave data-modulated optical signals using an optical injection phase-lock loop," *J. Lightwave Technol.*, vol. 21, no. 2, pp. 511–520, Feb. 2003.

[20] S. Datta, S. Agashe, and S. R. Forrest, "A high bandwidth analog heterodyne rf optical link with high dynamic range and low noise figure," *IEEE Photon. Technol. Lett.*, vol. 16, no. 7, pp. 1733–1735, Jul. 2004.

[21] X. Lu, C. B. Su, R. B. Lauer, G. J. Meslener, and L. W. Ulbricht, "Analysis of relative intensity noise in semiconductor lasers and its effect on subcarrier multiplexed lightwave systems," *J. Lightwave Technol.*, vol. 12, no. 7, pp. 1159–1165, Jul. 1992.

[22] A. J. Rainal, "Laser intensity modulation as a clipped gaussian process," *IEEE Trans. Commun.*, vol. 43, no. 2/3/4, pp. 490–494, Feb./Mar./Apr. 1995.

[23] N. J. Frigo, "A model of intermodulation distortion in non-linear multicarrier systems," *IEEE Trans. Commun.*, vol. 42, no. 2/3/4, pp. 1216–1222, Feb./Mar./Apr. 1994.

[24] H.-T. Lin and Y.-H. Kao, "Nonlinear distortions and compensations of DFB laser diode in AM-VSB lightwave CATV applications," *J. Lightwave Technol.*, vol. 14, no. 11, pp. 2567–2574, Nov. 1996.

[25] W. B. Bridges and J. H. Schaffner, "Distortion in linearized electrooptic modulators," *IEEE Trans. Microwave Theory Tech.*, vol. 43, no. 9, pp. 2184–2197, Sep. 1995.

[26] G. P. Agrawal, *Nonlinear Fiber Optics*, 2nd ed. New York: Academic Press, 2001.

[27] M. Horowitz, A. r. chraplyvy, R. W. Tkach, and J. L. Zyskind, "Broadband transmitted intensity noise induced by stokes and anti-stokes brillouin scattering in single-mode fibers," *IEEE Photon. Technol. Lett.*, vol. 9, no. 1, pp. 124–126, Jan. 1997.

[28] A. V. T. Cartaxo, B. Wedding, and W. Idler, "Influence of fiber nonlinearity on the phase noise to intensity noise conversion in fiber transmission: Theoretical and experimental analysis," *J. Lightwave Technol.*, vol. 16, no. 7, pp. 1187–1194, Jul. 1998.

[29] Z. Jiang and C. Fan, "A comprehensive study on XPM- and SRS-induced noise in cascaded IM-DD optical fiber transmission systems," *J. Lightwave Technol.*, vol. 21, no. 4, pp. 953–960, Apr. 2003.

[30] M. Wu and W. I. Way, "Fiber nonlinearity limitations in ultra-dense WDM systems," *J. Lightwave Technol.*, vol. 22, no. 6, pp. 1483–1498, Jun. 2004.

[31] Z. Li, A. Nirmalathas, M. Bakaul, Y. J. Wen, L. Cheng, J. Chen, C. Lu, and S. Aditya, "Performance of wdm fiber-radio network using distributed raman amplifier," *IEEE Photon. Technol. Lett.*, vol. 18, no. 4, pp. 553–555, Feb. 2006.

[32] A. Carena, V. Curri, R. Gaudino, P. Poggioloini, and S. Benedetto, "New analytical results on fiber parametric gain and its effects on ase noise," *IEEE Photon. Technol. Lett.*, vol. 9, no. 4, pp. 535–537, Apr. 1997.

[33] ——, "System impact of fiber parametric gain in long-haul optical links," in *1998 IEEE International Conference on Communications*, vol. 2, Jun. 1998, pp. 906–910.

[34] A. Carena, V. Curri, R. Gaudino, P. Poggioloini, S. Benedetto, F. Bentivoglio, M. Frascolla, and C. Rocca, "Theoretical and experimental results on transmission penalty due to fiber parametric gain in normal

dispersion," in *1998 Optical Fiber Communication Conference and Exhibit*, Feb. 1998, pp. 394–396.

[35] J. L. Corral, J. Martí, and J. M. Fuster, "Optical up-conversion on continuously variable true time delay lines based on chirped fiber gratings for millimeter-wave optical beamforming networks," *IEEE Trans. Microwave Theory Tech.*, vol. 47, no. 7, pp. 1315–1320, Jul. 1999.

[36] K. Kojucharow, M. Sauer, and C. Schaffer, "Millimeter-wave signal properties resulting from electrooptical upconversion," *IEEE Trans. Microwave Theory Tech.*, vol. 49, no. 10, pp. 1977–1985, Oct. 2001.

[37] E. Hashimoto, A. Takada, and Y. Katagiri, "High-frequency synchronized signal generation using semiconductor lasers," *IEEE Trans. Microwave Theory Tech.*, vol. 47, no. 7, pp. 1206–1218, Jul. 1999.

[38] T. Kuri and K. ichi Kitayama, "Optical heterodyne detection technique for densely multiplexed millimeter-wave-band radio-on-fiber systems," *J. Lightwave Technol.*, vol. 21, no. 12, pp. 3167–3179, Dec. 2003.

[39] J.-H. Seo, C.-S. Choi, W.-Y. Choi, Y.-S. Kang, Y.-D. Chung, and J. Kim, "Remote optoelectronic frequency down-conversion using 60-ghz optical heterodyne signals and an electroabsorption modulator," *IEEE Photon. Technol. Lett.*, vol. 17, no. 5, pp. 1073–1075, May 2005.

[40] F. Devaux, Y. Sorel, and J. F. Kerdiles, "Simple measurement of fiber dispersion and of chirp parameter of intensity modulated light emitter," *J. Lightwave Technol.*, vol. 11, no. 12, pp. 1937–1940, Dec. 1993.

[41] M. Schiess and H. Carlden, "Evaluation of the chirp parameter of a

Mach-Zehnder intensity modulator," *Electron. Lett.*, vol. 30, no. 18, pp. 1524–1525, Sep. 1994.

[42] G. H. Smith, D. Novak, and Z. Ahmed, "Overcoming chromatic dispersion effects in fiber-wireless systems incorporating external modulators," *IEEE Trans. Microwave Theory Tech.*, vol. 45, no. 8, pp. 1410–1415, Oct. 1997.

[43] M. R. Phillips and D. M. Ott, "Crosstalk due to optical fiber nonlinearities in WDM CATV lightwave systems," *J. Lightwave Technol.*, vol. 17, no. 10, pp. 1782–1792, Oct. 1999.

[44] F. S. Yang, M. E. Marhic, and L. G. Kazovsky, "Nonlinear crosstalk and two countermeasures in SCM-WDM optical communication systems," *J. Lightwave Technol.*, vol. 18, no. 4, pp. 512–520, Apr. 2000.

[45] D. Marcuse, *Light Transmission Optics*. Van Nostrand Reinhold, 1982.

[46] A. W. Snyder and J. D. Love, *Optical Waveguide Theory*. Chapman and Hall, 1983.

[47] M. J. Adams, *An Introduction to Optical Waveguides*. Wiley, 1981.

[48] N. Bloembergen, *Nonlinear Optics*. Benjamin, Reading, 1977.

[49] Y. R. Shen, *Principles of Nonlinear Optics*. Wiley, 1984.

[50] P. N. Butcher and D. N. Cotter, *The Elements of Nonlinear Optics*. Cambridge University Press, 1990.

[51] R. W. Boyd, *Nonlinear Optics*. Academic Press, 1992.

[52] R. H. Stolen, E. P. Ippen, and A. R. Tynes, "Raman oscillation in glass optical waveguide," *Appl. Phys. Lett.*, vol. 20, no. 2, pp. 62–64, Jan. 1972.

[53] E. P. Ippen and R. H. Stolen, "Stimulated brillouin scattering in optical fibers," *Appl. Phys. Lett.*, vol. 21, no. 11, pp. 539–541, Dec. 1972.

[54] R. G. Smith, "Optical power handling capacity of low loss optical fibers as determined by stimulated raman and brillouin scattering," *Appl. Opt.*, vol. 11, no. 11, pp. 2489–2494, Nov. 1972.

[55] E. P. Ippen, *Laser Applications to Optics and Spectroscopy*, S. F. Jacobs, M. S. III, J. F. Scott, and M. O. Scully, Eds. Addison-Wesley, Reading, 1975, vol. 2.

[56] P. Diament, *Wave Transmission and Fiber Optics*. Macmillan, 1990.

[57] B. Jaskorzynska and D. Schadt, "All-fiber distributed compression of weak pulses in the regime of negative group-velocity dispersion," *IEEE J. Quantum Electron.*, vol. 24, no. 10, pp. 2117–2120, Oct. 1988.

[58] R. R. Alfano and P. P. Ho, "Self-, cross-, and induced-phase modulations of ultrashort laser pulse propagation," *IEEE J. Quantum Electron.*, vol. 24, no. 2, pp. 351–364, Feb. 1988.

[59] R. R. Alfano, Ed., *The Supercontinuum Laser Source*. Springer-Verlag, 1989.

[60] C. H. III and G. P. Agrawal, "Unified description of ultrafast stimulated raman scattering in optical fibers," *J. Opt. Soc. Am. B*, vol. 13, no. 10, pp. 2170–2177, Oct. 1996.

[61] R. A. Fisher and W. K. Bischel, "The role of linear dispersion in plane-wave self-phase modulation," *Appl. Phys. Lett.*, vol. 23, no. 12, pp. 661–663, Dec. 1973.

[62] ——, "Numerical studies of the interplay between self-phase modulation and dispersion for intense plane-wave laser pulses," *J. Appl. Phys.*, vol. 46, no. 11, pp. 4921–4934, Nov. 1975.

[63] P. M. Hill and R. Olshansky, "A 20-channel optical communication system using subcarrier multiplexing for the transmission of digital video signals," *J. Lightwave Technol.*, vol. 4, no. 10, pp. 554–556, Apr. 1990.

[64] C. Lim, A. Nirmalathas, M. Attygalle, D. Novak, and R. Waterhouse, "On the merging of millimeter-wave fiber-radio backbone with 25-GHz WDM ring networks," *J. Lightwave Technol.*, vol. 21, no. 10, pp. 2203–2210, Oct. 2003.

[65] W. H. Chen and W. I. Way, "Multichannel single-sideband SCM/DWDM transmission systems," *J. Lightwave Technol.*, vol. 22, no. 7, pp. 1679–1693, Jul. 2004.

[66] J. L. Corral, J. Martí, and J. M. Fuster, "General expressions for IM/DD dispersive analog optical links with external modulation or optical up-conversion in a Mach-Zehnder electrooptical modulator," *IEEE Trans. Microwave Theory Tech.*, vol. 49, no. 10, pp. 1968–1976, Oct. 2001.

[67] M. Bhattacharya, A. K. Saw, and T. Chattopadhyay, "Millimeter-wave generation through phase-locking of two modulation sidebands

of a pair of laser diodes," *IEEE Photon. Technol. Lett.*, vol. 16, no. 2, pp. 596–598, Feb. 2004.

[68] Y. Wu, X. B. Xie, J. H. Hodiak, S. M. Lord, and P. K. L. Yu, "Multioctave high dynamic range up-conversion optical-heterodyned microwave photonic link," *IEEE Photon. Technol. Lett.*, vol. 16, no. 10, pp. 2332–2334, Oct. 2004.

[69] H.-H. Lu, W.-S. Tsai, C.-Y. Chen, and H.-C. Peng, "CATV/radio-on-fiber transport systems based on EAM and optical SSB modulation technique," *IEEE Photon. Technol. Lett.*, vol. 16, no. 11, pp. 2565–2567, Nov. 2004.

[70] A. R. S. Bahai, M. Singh, A. J. Goldsmith, and B. R. Saltzberg, "A new approach for evaluating clipping distortion in multicarrier systems," *IEEE J. Select. Areas Commun.*, vol. 20, no. 5, pp. 1037–1045, Jun. 2002.

[71] S. L. Zhang and J. J. O'Reilly, "Effect of dynamic stimulated brillouin scattering on millimeter-wave fiber radio communication systems," *IEEE Photon. Technol. Lett.*, vol. 9, no. 3, pp. 395–397, Mar. 1997.

[72] M. Shtaif and M. Eiselt, "Analysis of intensity interference caused by cross-phase modulation in dispersive optical fibers," *IEEE Photon. Technol. Lett.*, vol. 10, no. 7, pp. 979–981, Jul. 1998.

[73] R. Hui, K. R. Demarest, and C. T. Allen, "Cross-phase modulation in multispan WDM optical fiber systems," *J. Lightwave Technol.*, vol. 17, no. 6, pp. 1018–1026, Jun. 1999.

[74] P. Mitra and J. B. Stark, "Nonlinear limits to the information capacity of optical fiber communications," *Nature*, vol. 411, pp. 1027–1029, Jun. 2001.

[75] S. L. Woodward and M. R. Phillips, "Optimizing subcarrier-multiplexed WDM transmission links," *J. Lightwave Technol.*, vol. 22, no. 3, pp. 773–778, Mar. 2004.

[76] N. Dagli, "Wide-bandwidth lasers and modulators for rf photonics," *IEEE Trans. Microwave Theory Tech.*, vol. 47, no. 7, pp. 1151–1171, Jul. 1999.

[77] A. J. Seeds, "Microwave photonics," *IEEE Trans. Microwave Theory Tech.*, vol. 50, no. 3, pp. 877–887, Mar. 2002.

[78] T. Ohno, K. Sato, S. Fukushima, Y. Doi, and Y. Matsuoka, "Application of DBR mode-locked lasers in millimeter-wave fiber-radio system," *J. Lightwave Technol.*, vol. 18, no. 1, pp. 301–307, Jan. 2000.

[79] V. Polo, F. Ramos, J. Martí, D. Moodie, and D. Wake, "Synthesis of photonic microwave filters based on external optical modulators and wide-band chirped fiber gratings," *J. Lightwave Technol.*, vol. 18, no. 2, pp. 213–220, Feb. 2000.

[80] K.-P. Ho and J. M. Kahn, "Spectrum of externally modulated optical signals," *J. Lightwave Technol.*, vol. 22, no. 2, pp. 658–663, Feb. 2004.

[81] B. Xu and M. B. Pearce, "Optical fibre parametric-gain-induced noise coloring and amplification by modulated signals," *J. Opt. Soc. Am. B*, vol. 21, pp. 499–513, 2004.

[82] K. V. Peddanarappagari and M. B. Pearce, "Volterra series approach

for optimizing fiber-optic communications systems designs," *J. Lightwave Technol.*, vol. 16, no. 11, pp. 2046–2055, Nov. 1998.

[83] B. Xu and M. B. Pearce, "Comparison of FWM- and XPM-induced crosstalk using the volterra series transfer function method," *J. Lightwave Technol.*, vol. 21, no. 1, pp. 40–53, Jan. 2003.

[84] M. R. Phillips, T. Darcie, D. Marcuse, G. Bodeep, and N. J. Frigo, "Nonlinear distortion generated by dispersive transmission of chirped intensity-modulated signals," *IEEE Photon. Technol. Lett.*, vol. 3, no. 5, pp. 481–483, May 1991.

[85] I. P. Kaminow and T. L. Koch, Eds., *Optical Fiber Telecommunications*, ser. III. Academic Press, 1997, vol. A.

[86] F. W. Willems, W. Muys, and J. C. van der Plaats, "Experimental verification of self-phase-modulation-induced nonlinear distortion in externally modulated AM-VSB lightwave systems," in *Tech. Digest, Conf. Optical Fiber Commun*, Feb 1996.

[87] Z. Wang, E. Bodtker, and G. Jacobsen, "Effects of cross-phase modulation in wavelength-multiplexed SCM video transmission systems," *Electron. Lett.*, vol. 31, pp. 1591–1592, Aug. 1995.

[88] F. Ramos and J. Martí, "Frequency transfer function of dispersive and nonlinear single-mode optical fibers in microwave optical systems," *IEEE Photon. Technol. Lett.*, vol. 12, no. 5, pp. 549–551, May 2000.

[89] E. L. Wooten, K. M. Kissa, A. Yi-Yan, E. J. Murphy, D. A. Lafaw, P. Hallemeier, D. Maack, D. V. Attanasio, D. J. Fritz, G. J. McBrien,

and D. E. Bossi, "A review of lithium niobate modulators for fiber-optic communications systems," *IEEE J. Select. Topics Quantum Electron.*, vol. 6, no. 1, pp. 69–82, 2000.

[90] G. L. Li and P. K. L. Yu, "Optical intensity modulators for digital and analog applications," *J. Lightwave Technol.*, vol. 21, no. 9, pp. 2010–2030, Sep. 2003.

[91] M. Abramowitz and I. A. Stegun, *Handbook of Mathematical Functions with Formulas, Graphs, and Mathematical Tables*, tenth printing ed. John Wiley & Sons, 1972.

[92] J. M. Fuster, J. Martí, J. L. Corral, V. Polo, and F. Ramos, "Generalized study of dispersion-induced power penalty mitigation techniques in millimeter-wave fiber-optic links," *J. Lightwave Technol.*, vol. 18, no. 7, pp. 933–940, Jul. 2000.

[93] V. J. Urick, J. X. Qiu, and F. Bucholtz, "Wide-band QAM-over-fiber using phase modulation and interferometric demodulation," *IEEE Photon. Technol. Lett.*, vol. 16, no. 10, pp. 2374–2376, Oct. 2004.

[94] A. V. T. Cartaxo, "Samll-signal analysis for nonlinear and dispersive optical fibers, and its application to design of dispersion supported transmission systems with optical dispersion compensation," *IEE Proc.-Optoelectron.*, vol. 146, no. 5, pp. 213–222, Oct. 1999.

[95] C. L. Tang, "Staruation and spectral characteristics of the stokes emission in the stimulated brillouin process," *J. Appl. Phys.*, vol. 37, no. 8, pp. 2945–2955, Jul. 1966.

[96] E. Lichtman, A. A. Friesem, R. G. Waarts, and H. H. Yaffe, "Stimulated brillouin scattering excited by two pump waves in single-mode fibers," *J. Opt. Soc. Am. B*, vol. 4, no. 9, pp. 1397–1403, Sep. 1987.

[97] A. Djupsjöbacka, G. Jacobsen, and B. Tromborg, "Dynamic stimulated brillouin scattering analysis," *J. Lightwave Technol.*, vol. 18, no. 3, pp. 416–424, Mar. 2000.

[98] R. H. Stolen and E. P. Ippen, "Raman gain in glass optical waveguide," *Appl. Phys. Lett.*, vol. 22, no. 6, pp. 276–278, Mar. 1973.

[99] L. Cheng, S. Aditya, and A. Nirmalathas, "An exact analytical model for dispersive transmission in microwave fiber-optic links using Mach-Zehnder external modulator," *IEEE Photon. Technol. Lett.*, vol. 17, no. 7, pp. 1525–1527, Jul. 2005.

[100] A. V. T. Cartaxo, "Cross-phase modulation in intensity modulation-direct detection wdm systems with multiple optical amplifiers and dispersion compensators," *J. Lightwave Technol.*, vol. 17, no. 2, pp. 178–190, Feb. 1999.

[101] S. Betti and M. Giaconi, "Analysis of the cross-phase modulation in dispersion compensated wdm optical fiber systems," *IEEE Photon. Technol. Lett.*, vol. 13, no. 12, pp. 1304–1306, Dec. 2001.

[102] Q. Lin and G. P. Agrawal, "Effects of polarization-mode dispersion on cross-phase modulation in dispersion-managed wavelength-division-multiplexed systems," *J. Lightwave Technol.*, vol. 22, no. 4, pp. 977–987, Apr. 2004.

[103] A. Vannucci, P. Serena, and A. Bononi, "The RP method: A new

tool for the iterative solution of the nonlinear schrödinger equation," *J. Lightwave Technol.*, vol. 20, no. 7, pp. 1102–1112, Jul. 2002.

Author's Publications

1. Linghao Cheng, Sheel Aditya, Zhaohui Li, Ampalavanapillai Nirmalathas, Arokiaswami Alphones and Ling Chuen Ong, "Nonlinear Distortion due to Cross-Phase Modulation in Microwave Fiber-Optic Links with Optical Single Sideband or Electrooptical Upconversion", accepted for publication in *IEEE Trans. on Microwave Theory and Techniques*.
2. Linghao Cheng, Sheel Aditya, Zhaohui Li and Ampalavanapillai Nirmalathas, "Generalized Analysis of Subcarrier Multiplexing in Dispersive Fiber-Optic Links Using Mach-Zehnder External Modulator", *IEEE/OSA J. Lightwave Technol.*, vol. 24, no. 6. Jun. 2006.
3. Linghao Cheng, Sheel Aditya, Zhaohui Li, Arokiaswami Alphones and L. C. Ong, "Nonlinear Distortion due to XPM in Electrooptical Upconversion WDM Microwave Fiber Optic Links", *2006 Asia-Pacific Microwave Photonics Conference (AP-MWP 2006)*, Kobe, Japan, 2006.
4. Linghao Cheng and Sheel Aditya, "Effect of nonlinearity and dispersion in microwave photonic subcarrier-multiplexed and access networks", *invited paper, International Conference on Optics & Optoelectronics (ICOL 2005)*, Dehradun, Uttaranchal, India, 2005.
5. Linghao Cheng, Sheel Aditya, Zhaohui Li, Arokiaswami Alphones and

L. C. Ong, "Nonlinear Distortion due to XPM in Dispersive WDM Microwave Fiber-Optic Links With Optical SSB Modulation", *2005 International Topical Meeting on Microwave Photonics (MWP 2005)*, Seoul, Korea, 2005.

6. Linghao Cheng, Sheel Aditya and Ampalavanapillai Nirmalathas,"An exact analytical model for dispersive transmission in microwave fiber-optic links using Mach-Zehnder external modulator", *IEEE Photon. Technol. Lett.*, vol. 17, no. 7, Jul. 2005.
7. Linghao Cheng and Sheel Aditya, "Noise due to Fiber Dispersion in Phase Dithered Microwave Fiber Optic Links", *2005 IEEE Sarnoff Symposium*, Princeton, New Jersey, USA, 2005.
8. Linghao Cheng and Sheel Aditya, "Analytical Estimate for Nonlinear Distortion due to Fiber in SCM-WDM Lightwave Systems", *Asia Pacific Microwave Conference 2004 (APMC 2004)*, New Delhi, India, 2004.
9. Linghao Cheng and Sheel Aditya, "Analytical Estimate for Nonlinear Distortion due to Fiber in SCM-WDM Lightwave System", *2004 Ninth Singapore International Conference on Communication Systems (ICCS 2004)*, Singapore, 2004.
10. Linghao Cheng and Sheel Aditya, "Nonlinear Distortion by XPM in SCM-WDM Systems: An Analytical Method", *Second International Conference on Optical Communications and Networks (ICOCN 2003)*, Bangalore, India, 2003.
11. Ning Liu, Wen-De Zhong, Yang Jing Wen, Chao Lu, Linghao Cheng and Yixin Wang,"PMD and Chirp Effects Suppression in RF Tone-Based Chromatic Dispersion Monitoring", *IEEE Photon. Technol. Lett.*, vol. 18, no. 5, Mar. 2006.

12. Zhaohui Li, Ampalavanapillai Nirmalathas, Masuduzzman Bakaul, Yang Jing Wen, Linghao Cheng, Jian Chen, Chao Lu and Sheel Aditya, "Performance of WDM Fiber-Radio Network Using Distributed Raman Amplifier", *IEEE Photon. Technol. Lett.*, vol. 18, no. 4, Feb. 2006.
13. Guoxiang Ning, Sheel Aditya, P. Shum, Linghao Cheng, Y. D. Gong and Chao Lu,"Tunable Photonic Microwave Bandpass Filter Using Phase Modulation and a Chirped Fiber Grating in a Sagnac Loop", *IEEE Photon. Technol. Lett.*, vol. 17, no. 9, Sep. 2005.

Appendix A

Addition Theorems of Bessel Functions

Let L denotes the Bessel functions of the first kind J, of the second kind Y (also called Weber's function) and of the third kind $H^{(1)}$, $H^{(2)}$ (also called the Hankel functions) or any linear combination of these functions.

A.1 Neumann's Addition Theorem

$$L_\nu(u+v) = \sum_{k=-\infty}^{\infty} L_{\nu\mp k}(u)J_k(v) \quad (|v| < |u|) \tag{A.1}$$

The restriction $|v| < |u|$ is unnecessary when $L = J$ and ν is an integer or zero. Special cases are

$$1 = J_0^2(z) + 2\sum_{k=1}^{\infty} J_k^2(z) \tag{A.2}$$

$$0 = \sum_{k=0}^{2n}(-1)^k J_k(z)J_{2n-k}(z) + 2\sum_{k=1}^{\infty} J_k(z)J_{2n+k}(z) \quad (n \geq 1) \tag{A.3}$$

$$J_n(2z) = \sum_{k=0}^{n} J_k(z)J_{n-k}(z) + 2\sum_{k=1}(-1)^k J_k(z)J_{n+k}(z) \tag{A.4}$$

A.2 Graf's Addition Theorem

$$L_\nu(w)\cos(\nu\chi) = \sum_{k=-\infty}^{\infty} L_{\nu+k}(u)J_k(v)\cos(k\alpha) \quad (|v\exp(\pm i\alpha)| < |u|) \tag{A.5}$$

$$L_\nu(w)\sin(\nu\chi) = \sum_{k=-\infty}^{\infty} L_{\nu+k}(u)J_k(v)\sin(k\alpha) \quad (|v\exp(\pm i\alpha)| < |u|) \tag{A.6}$$

A.3 Gegenbauer's Addition Theorem

$$\frac{L_\nu(w)}{w^\nu} = 2^\nu\Gamma(\nu)\sum_{k=0}^{\infty}(\nu+k)\frac{L_{\nu+k}(u)}{u^\nu}\frac{J_{\nu+k}(v)}{v^\nu}C_k^{(\nu)}(\cos\alpha)$$
$$(\nu \neq 0, \text{-}1, \ldots, |v\exp(\pm i\alpha| < |u|) \tag{A.7}$$

In Eqs. (A.6) and (A.7)

$$w = \sqrt{u^2 + v^2 - 2uv\cos\alpha} \tag{A.8a}$$

$$w\cos\chi = u - v\cos\alpha \tag{A.8b}$$

$$w\sin\chi = v\sin\alpha \tag{A.8c}$$

The branches being chosen so that $w \to u$ and $\chi \to 0$ as $v \to 0$. $C_k^{(\nu)}(\cos\alpha)$ is Gegenbauer's polynomial.

If u, v are real and positive and $0 \leq \alpha \leq \pi$, then w, χ are real and non-negative, and the geometrical relationship of the variables is shown in the Figure A.1.

The restrictions $|v\exp(\pm i\alpha| < |u|$ are unnecessary in Eq. (A.6) when

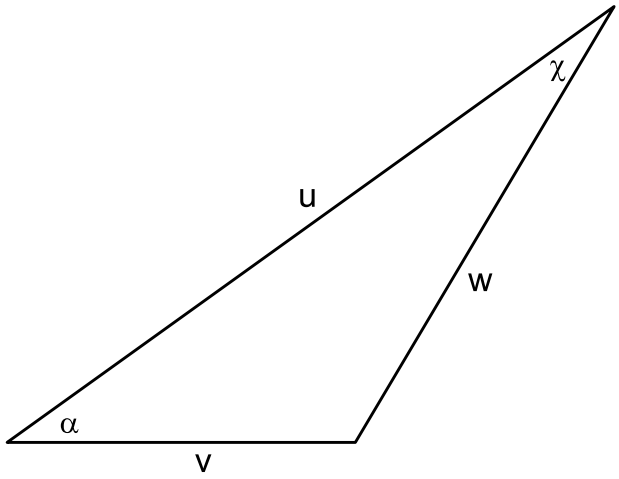

Figure A.1: Graf's and Gegenbauer's addition theorem.

$L = J$ and ν is an integer or zero, and in Eq. (A.7) when $L = J$.

Appendix B

MATLAB Programs

B.1 SSF Algorithm for Single Channel

```
function [to,fo] = sym_ssf(M,h,gamma,Dh,uf0)
%% Symmetrized Split-Step Fourier Algorithm
%%
%% ====================Inputs==============================
%% M = Simulation step number ( M*h = simulation distance )
%% h = Simulation step
%% gamma = Nonlinearity coefficient
%% Dh = Dispersion operator in frequency domain
%% uf0 = Input field in the frequency domain
%%
%% ====================Outputs=============================
%% to = Output field in the time domain
%% fo = Output field in the frequency domain
%%
%% written by Cheng Linghao
for k = 1:M
```

```
%%=======================================================
%% Prop. in the first half dispersion region, z to z+h/2
%%=======================================================
Hf = Dh.*uf0;
%%=======================================================
%% Initial est. of the nonlinear phase shift at z+(h/2)
%%=======================================================
%% Initial est. value
ht = ifft(Hf); % time signal after h/2 dispersion region
pq = ht.*conj(ht); % intensity in time
u2e = ht.*exp(h*i*gamma*pq); %Time signal
%%=======================================================
%% Prop. in the second Dispersion Region, z+(h/2) to z+h
%%=======================================================
u2ef = fft(u2e);
u3ef = u2ef.*Dh;
u3e = ifft(u3ef);
u3ei = u3e.*conj(u3e);
%%=======================================================
% %Iteration for the nonlinear phase shift(two iterations)
%%=======================================================
u2 = ht.*exp((h/2)*i*gamma*(pq+u3ei));
u2f = fft(u2) ;
u3f = u2f.* Dh;
u4 = ifft(u3f);
u4i = u4.*conj(u4);
u5 = ht.*exp((h/2)*i*gamma*(pq+u4i));
```

```
    u5f = fft(u5);
    uf0 = u5f.*Dh;
    u6 = ifft(uf0); u6i = u6.*conj(u6);
    %%=====================================================
    %% Maximum allowable tolerance after the two iterations
    etol = 1e-5;
    if abs(max(abs(u6i))-max(abs(u4i)))/max(abs(u6i)) > etol
    disp('Peak value is not converging! Reduce Step Size')
    break
    end
    %%=====================================================
end

to = u6; fo = uf0;
```

B.2 Soliton Propagation

```
%% This program simulates a soliton transmission in a
%% single-channel fiber transmission link using the
%% symmetrized split-step Fourier algorithm.
%%
%% written by Cheng Linghao
clear all
%%=============================================
%% Define Time Window and Frequency Window
%%=============================================
taum = 2000; % half of the time window
dtau = 2*taum/2^11; % resolution in time domain
```

```
tunit= 1e-12; % make time unit in psec
tau = (-taum:dtau:(taum-dtau))*tunit; % the full time window
fs = 1/(dtau*tunit); % sample freq. in time domain
tl = length(tau)/2;
w = 2*pi*fs*(-tl:(tl-1))/length(tau); % w=angular freq.
wst = w(2)-w(1); % resolution in freq. domain
%%=============================================
%% Define Physical Parameters
%%=============================================
c = 3e5; %[km/sec] speed of light
ram0 = 1.55e-9; %[km] center wavelength
k0 = 2*pi/ram0;
n2 = 6e-13 ; %[1/mW]
gamm = k0*n2 ; %[1/(km*mW)]
%alphaDB = 0.2 ; % [dB/km] Power Loss in dB
alphaDB = 0; % assuming no fiber loss for soliton trans.
alpha = alphaDB/(10*log10(exp(1))); %[1/km] Power Loss
%% Dispersion parameters
Dp = 1; % [ps/nm.km]
beta2 = -(ram0)^2*Dp/(2*pi*c); % [sec^2/km]
%%=============================================
%% Define Input Signal
%%=============================================
%% Two pulse shapes are listed here: Gaussian pulse
%%  and hyperbolic secant pulse (for soliton trans.)
t0 = 10e-12; %[sec] initial pulse width
%% choosing the initial peak power for soliton trans.
```

```
Po = abs(beta2)/(gamm*t0^2); % [mW] initial peak power
%%-----------------Gaussian Pulse--------------------------
% C = 0; % Chirping Parameter
% m = 1; % Super Gaussian parameter (m=1 ==> Gaussian)
%% Input field in the time domain
% at = sqrt(Po)*exp(-0.5*(1+i*C)*(tau./t0).^(2*m));
%%-------------------------------------------------------
%%
%%-----------------Hyperbolic Secant Pulse-----------------
at = sqrt(Po)*sech(tau/t0); % Input field in the time domain
a0 = fft(at);
af = fftshift(a0); % Input field in the frequency domain
%%-------------------------------------------------------
%%===============================================
%% Define Simulation Distance and Step Size
%%===============================================
LD=t0^2/abs(beta2);
zfinal = 150*LD; %[km] propagation distance
%% max allowable phase shift due to the nonlinear operator
pha_max = 0.01; %[rad]
% pha_max = h*gamma*Po (h = simulation step length)
h = pha_max/(gamm*Po); % [km] simulation step length
M = zfinal/h; % Partition Number
% Define Dispersion Exp. operator
Dh = exp((h/2)*(-alpha/2+(i/2)*beta2*w.^2)); %
%%===============================================
% %Propagation Through Fiber
```

```
%%================================================
%% Call the subroutine, sym_ssf.m for the
%% symmetrized split-step Fourier method
[bt,bf] = sym_ssf(M,h,gamm,Dh,af);
%% Preamplifier at the receiver
%% Optical amplifier is assumed ideal
GdB = alphaDB*zfinal; % [dB] optical amplifier power gain
gainA = sqrt(10^(GdB/10)); % field gain in linear scale
rt = gainA*bt;
%% plot the received power signal
figure(1)
semilogy(tau,abs(at).^2/Po,'b', 'LineWidth', 1);
hold on
semilogy(tau,abs(rt).^2/Po,'--r', 'LineWidth', 1);
legend('Input', 'Output');
title('Soliton Transmission');
xlabel('Time (s)');
```